

DISSERTATION

COOPERATIVE SENSING FOR TARGET ESTIMATION AND
TARGET LOCALIZATION

Submitted by

Wenshu Zhang

Department of Electrical and Computer Engineering

In partial fulfillment of the requirements

For the Degree of Doctor of Philosophy

Colorado State University

Fort Collins, Colorado

Fall 2011

Doctoral Committee:

Advisor: Liuqing Yang

Ali Pezeshki

J. Rockey Luo

Haonan Wang

Copyright by Wenshu Zhang 2011

All Rights Reserved

ABSTRACT

COOPERATIVE SENSING FOR TARGET ESTIMATION AND TARGET LOCALIZATION

As a novel sensing scheme, cooperative sensing has drawn great interests in recent years. By utilizing the concept of “cooperation”, which incorporates communications and information exchanges among multiple sensing devices, e.g. radar transceivers in radar systems, sensor nodes in wireless sensor networks, or mobile handsets in cellular systems, the sensing capability can achieve significant improvement compared to the conventional noncooperative mode in many aspects. For example, cooperative target estimation is inspired by the benefits of MIMO in communications, where multiple transmit and/or receive antennas can increase the diversity to combat channel fading for enhanced transmission reliability and increase the degrees of freedom for improved data rate. On the other hand, cooperative target localization is able to dramatically increase localization performance in terms of both accuracy and coverage.

From the perspective of cooperative target estimation, in this dissertation, we optimize waveforms from multiple cooperative transmitters to facilitate better target estimation in the presence of colored noise. We introduce the normalized MSE (NMSE) minimizing criterion for radar waveform designs. Not only is it more meaningful for parameter estimation problems, but it also exhibits more similar behaviors with the MI criterion than its MMSE counterpart. We also study the robust designs for both the probing waveforms at the transmitter and the estimator at the receiver

to address one type of *a priori* information uncertainties, i.e., in-band target and noise PSD uncertainties. The relationship between MI and MSEs is further investigated through analysis of the sensitivity of the optimum design to the out-band PSD uncertainties as known as the overestimation error.

From the perspective of cooperative target localization, in this dissertation, we study the two phases that comprise a localization process, i.e., the distance measurement phase and the location update phase. In the first distance measurement phase, thanks to UWB signals' many desirable features including high delay resolution and obstacle penetration capabilities, we adopt UWB technology for TOA estimation, and then translate the TOA estimate into distance given light propagation speed. We develop a practical data-aided ML timing algorithm and obtain its optimum training sequence. Based on this optimum sequence, the original ML algorithm can be simplified without affecting its optimality. In the second location update phase, we investigate secure cooperative target localization in the presence of malicious attacks, which consists of a fundamental issue in localization problems. We explicitly incorporate anchors' misplacements into distance measurement model and explore the pairwise sparse nature of the misplacements. We formulate the secure localization problem as an ℓ_1 -regularized least squares (LS) problem and establish the pairwise sparsity upper bound which defines the largest possible number of identifiable malicious anchors. Particularly, it is demonstrated that, with target cooperation, the capability of secure localization is improved in terms of misplacement estimation and target location estimation accuracy compared to the single target case.

ACKNOWLEDGMENTS

I would like to express my deepest gratitude to my advisor, Dr. Liuqing Yang. During my PhD study, Dr. Yang has been persistently guiding and encouraging me. She has taught me numerous skills and experience that are crucial to a researcher and influenced me in many aspects of my life. These experience and influence are the most valuable treasure for me that I can always benefit from in my future career, and entire life.

I would like to thank the members of my PhD dissertation committee, Dr. Haonan Wang, Dr. Ali Pezeshki and Dr. J. Rockey Luo for their time and effort to improve the quality of my research and supervise my proposal as well as the defense.

I would like to thank the professors in the Colorado State University and the University of Florida who have helped broaden my knowledge. These professors are: Dr. Jacob Hammer, Dr. John Shea, Dr. J. Cole Smith, Dr. Tan Wong, Dr. Jianbo Gao and Dr. James Hobert.

I want to thank my colleagues: Dr. Woong Cho, Dr. Fengzhong Qu, Rui Cao, Dongliang Duan, Siva Kumar Balaga, Bo Yu, Pan Deng, Wei Zang, Ning Wang, Xilin Cheng, Robert Griffin, Jian Dang, Dexin Wang and Luoyang Fang. Their friendliness and willingness to share their insights make our office an ideal place where I can read, think and work efficiently. I wish they all have a successful and happy career.

Also, I would like to thank all my friends in Gainesville, FL and Fort Collins, CO. I am always very pleased to travel, play table tennis, swim, chat and hang out with them.

Finally, I want to thank my husband Huilin Xu, our parents, and our grandparents for their patience and unconditional love that have supported me through the PhD study.

TABLE OF CONTENTS

Chapter	Page
ABSTRACT	ii
ACKNOWLEDGMENTS	iv
LIST OF FIGURES	viii
LIST OF TABLES	x
1 INTRODUCTION	1
1.1 Optimum and Robust Waveform Designs for Cooperative Target Estimation	1
1.2 ML TOA Estimation of IR UWB Signals for Target Localization	4
1.3 The ℓ_1 -Regularized LS Formulation for Cooperative Target Localization and Malicious Anchor Identification	6
1.4 Dissertation Organization	8
2 OPTIMUM AND ROBUST WAVEFORM DESIGNS FOR COOPERATIVE TARGET ESTIMATION	9
2.1 Motivation	10
2.2 Mixed MIMO Signal Model	13
2.3 Optimum Waveform Designs In Colored Noise	18
2.3.1 MI and MMSE Criteria	19
2.3.2 NMSE Criterion	22
2.4 Robust Joint Transceiver Designs	25
2.4.1 Robust Minimax Design Criteria	25
2.4.2 Joint Robust Designs	30
2.5 Sensitivity Analysis of the Optimum Designs	32
2.5.1 Waveform Design Sensitivity at the Transmitter	32
2.5.1.1 Strength Threshold Calculation	33
2.5.1.2 Strength Threshold Comparison	35
2.5.2 Estimation Performance Sensitivity at the Receiver	37
2.5.2.1 NMSE Performance Variation Calculation	38

2.5.2.2	NMSE Performance Variation Comparison	39
2.6	Simulations	40
2.6.1	Optimum Power Allocation in Colored Noise	40
2.6.2	Joint Estimator and Power Allocation Robust Design	43
2.6.3	Comparison of Sensitivity to the Overestimation Errors	47
2.7	Conclusions	50
3	ML TOA ESTIMATION OF IR UWB SIGNALS FOR TARGET LOCALIZATION	59
3.1	Motivation	59
3.2	Impulse-Radio (IR) UWB Signal Model	63
3.3	The ML Timing Algorithm	66
3.4	Training Sequence Design and The SML Algorithm	73
3.4.1	The Optimum Training Sequence Pattern	73
3.4.2	Simplified ML (SML) Algorithm	75
3.5	The Optimality of Data-Aided TDT in the ML Sense	78
3.6	Implementation Consideration	81
3.7	Simulations	83
3.8	Conclusions	88
4	THE ℓ_1 -REGULARIZED LEAST SQUARES FORMULATION FOR CO-OPERATIVE TARGET LOCALIZATION AND MALICIOUS ANCHOR IDENTIFICATION	95
4.1	Motivation	96
4.2	Sparse Reconstruction Preliminaries	98
4.3	Distance Measurement Model and Misplacement Sparsity	101
4.3.1	The $N_t = 1$ Single Target Case	102
4.3.2	The $N_t = 2$ Cooperative Targets Case	104
4.4	The Novel ℓ_1 -Regularized LS Formulation	105
4.4.1	Pairwise Sparsity Upper Bound	106
4.4.2	Misplacement Estimation Capability	109
4.4.3	Equivalence Condition	111
4.5	The Projected Gradient Search Algorithm	116
4.6	Simulations	119
4.7	Conclusions	126
5	CONCLUSIONS AND FUTURE WORKS	127
5.1	Conclusions	127
5.2	Future Works	129
	LIST OF REFERENCES	131

LIST OF FIGURES

Figure	Page
2.1 Illustration of the mixed MIMO structure.	16
2.2 Illustration of the band model for noise PSD: (a) normalized by target PSD; and (b) normalized by target PSD square.	32
2.3 (a) Target mode PSD; and (b) noise PSD.	40
2.4 Optimum power allocation schemes based on three criteria: MI, MMSE and NMSE.	41
2.5 MI performance of the optimum power allocation schemes.	41
2.6 MMSE performance of the optimum power allocation schemes.	42
2.7 NMSE performance of the optimum power allocation schemes.	42
2.8 Noise PSD uncertainty band model: (a) normalized by target PSD for the MI and NMSE criteria; and (b) normalized by target PSD square for the MMSE criterion.	44
2.9 MMSE performance for the robust designs.	45
2.10 NMSE performance for the robust designs.	45
2.11 MI performance for the robust designs.	46
2.12 Altered power allocation solutions: (a) $\lambda_e = 0.2$; and (b) $\lambda_e = 0.32$	48
2.13 The NMSE-based NMSE performance variation.	49
2.14 The MI-based NMSE performance variation.	49
2.15 The MMSE-based NMSE performance variation.	50
3.1 Illustration of the ML timing algorithm, $T_s = 3T_f$, $K = 2$	69
3.2 Illustration of the TDT timing algorithm, $T_s = 3T_f$, $K = 2$	80
3.3 The noise-free part of the SML (TDT) objective function, $K = 8$ and $n_0 = 534$	82
3.4 P_d for various sequences, $\mathcal{E}/N_0 = 1dB$	84
3.5 Objective function magnitude for the ML, SML and TDT algorithms, $\mathcal{E}/N_0 = 5dB$, $K = 8$ and $n_0 = 15$	84
3.6 P_d and the lower bounds for the SML and TDT algorithms, coarse timing.	86
3.7 Normalized MSE for the SML and TDT algorithms, coarse timing.	87
3.8 Average BER for the SML and TDT algorithms, coarse timing.	87
3.9 Normalized MSE versus differential step wT_c under various \mathcal{E}/N_0	88
3.10 Normalized MSE for the SML and TDT algorithms, fine timing.	89

4.1	Illustration of a wireless sensor network in the presence of malicious anchors.	102
4.2	Illustration of anchor location estimation ambiguity regions for (a) a single target case and (b) two cooperative targets case.	110
4.3	Noiseless convergence path for the single target location estimation in the presence of two malicious anchors.	120
4.4	Noiseless convergence path for the single target location estimation in the presence of three malicious anchors.	122
4.5	Noiseless convergence paths for two cooperative targets location estimation in the presence of two malicious anchors.	124
4.6	Noiseless convergence paths for two cooperative targets location estimation in the presence of three malicious anchors.	124

LIST OF TABLES

<u>Table</u>	<u>Page</u>
4.1 Identification probability and target location mean absolute error, a single target, two colluding malicious anchors	121
4.2 Identification probability and target location mean absolute error, a single target, three colluding malicious anchors	123
4.3 Identification probability and target location mean absolute error, two colluding malicious anchors	125
4.4 Identification probability and target location mean absolute error, three colluding malicious anchors	125

CHAPTER 1

INTRODUCTION

By utilizing the concept of “cooperation”, which incorporates communications and information exchanges among multiple sensing devices, e.g. radar transceivers in radar systems, sensor nodes in wireless sensor networks, or mobile handsets in cellular systems, the sensing capability can achieve significant improvement compared to the conventional noncooperative mode in many aspects. In this dissertation, we will exploit the benefits of cooperative sensing from two perspectives, namely, cooperative target estimation and cooperative target localization.

1.1 Optimum and Robust Waveform Designs for Cooperative Target Estimation

In multi-input multi-output (MIMO) communication systems, multiple transmit and/or receive antennas can increase the diversity to combat channel fading for enhanced transmission reliability and increase the degrees of freedom for improved data rate. Partly inspired by these benefits, MIMO sensing has drawn great interests in recent years (see e.g., [2, 6, 4, 10, 11, 17, 20, 21, 25]). In such systems, a particularly critical issue is the waveform optimization. Bell’s 1993 paper first used the mutual information (MI) to design radar waveforms for the estimation of an extended target [4]. His MI-based water-filling approach has been extended by several recent works.

The MI is an essential measure in the field of communications. However, its role in sensing is not yet clear. In an attempt to link the MI criterion with more

direct performance indicators in sensing, and particularly target parameter estimation applications, Yang and Blum studied the extended target estimation problem in a widely separated MIMO radar scenario. In [65], it is shown that the MI and the minimum mean square error (MMSE) criteria lead to the same optimum water-filling strategy, assuming perfectly known target and white noise power spectral densities (PSDs). These waveform designs were then extended in [66] to account for bounded uncertainty in the target PSD. In contrast to [65], [66] shows that the MI and MMSE criteria result in distinct waveform designs.

Though the results in [65] and [66] shed some light on the possible connection between the MI and MMSE measures, they are based on limiting assumptions such as white noise and perfectly known noise PSD. In this dissertation, we will further these existing works and reveal more intrinsic connections between the MI and MSE measures in a sensing setup.

Our contributions are three-fold. First, we take into consideration the more general and practical colored Gaussian noise that can emerge in various situations. For example, the received signal may be affected by unwanted interferences including jammers. The noise spectrum might also be shaped by the antenna and RF filters [55]. It turns out that in the presence of colored Gaussian noise, the equivalence between the MI and MMSE design criteria established in [65] does not hold, even when the target and noise PSDs are both perfectly known. Secondly, we introduce the normalized MSE (NMSE) minimizing criterion for radar waveform designs. Not only is it more meaningful for parameter estimation problems, but it also exhibits more similar behaviors with the MI criterion than its MMSE counterpart, especially in robust designs. Last but not least, we provide joint robust designs for both the probing waveforms at the transmitter and the estimator at the receiver under various uncertainty models. Compared with [66], our improvements include: i) we consider

colored noise instead of white noise; ii) we jointly optimize both the transmitter (waveforms) and the receiver (estimator) instead of limiting only to the transmitter side; and iii) we account for the uncertainty for both target and noise PSDs instead of assuming perfectly known noise PSD. Results show that the MI- and NMSE-based robust designs are built on an identical least favorable set (LFS), which differs from the LFS of the MMSE-based designs.

Since the optimum waveform design relies on an ideal assumption of known target and noise PSDs, a small PSD estimation error might introduce considerable impact on the designed waveform. Besides the target and noise's in-band PSD uncertainty addressed in joint robust designs, there is another type of PSD uncertainty, namely the overestimation error. In case that additional error modes appear, the original optimum waveform solution for the nominal modes may be altered, which will induce estimation performance degradation. Therefore, the sensitivity analysis of the optimum designs consists of an intriguing task. Furthermore, the study of the sensitivity comparison among the MI, MMSE and NMSE criteria can help further our understanding on the relationship linking the three criteria.

To focus on our main objective, only a single error mode will be considered in this dissertation. We perform the sensitivity analysis not only at the transmitter, but also at the receiver. At the transmitter side, for each criterion we derive the explicit formula of the error mode strength threshold. When the error mode strength exceeds the threshold, it will consume nonzero transmit power and the original optimum solution for the nominal modes will be inevitably altered. The design scheme which has the highest strength threshold is the least sensitive to the overestimation error. At the receiver side, the normalized NMSE indicator of the estimation performance variation is calculated and then compared among the three criteria. Both analytical and numerical results show that all three criteria do not exhibit significant performance

deterioration. Particularly, the NMSE-based design has lower strength threshold, experiences worse performance variation, and therefore is more vulnerable than the MI-based design. Due to their very different strength structures, however, there does not exist a universal relationship between the former two criteria and MMSE.

1.2 ML TOA Estimation of IR UWB Signals for Target Localization

UWB technology exhibits prominent features in many wireless communications, networking and localization applications. Since the ultrashort pulse waveform is transmitted at very low power in UWB systems [63, 58], accurate and rapid timing estimation becomes one of the most critical challenges.

Without invoking impractical assumptions as in several UWB timing research (see e.g., [22, 29, 38]) such as known multipath propagation, timing with dirty templates (TDT) algorithms developed in [64] are feasible for realistic UWB settings. The most attractive merits of TDT include its low complexity and applicability in narrowband and wideband systems with a single user or multiple ones as long as the intersymbol interference (ISI) is absent or avoided. The training sequence used in [64] for data-aided TDT has a repeated pattern $\{+1, +1, -1, -1\}$, with which the data-aided TDT can achieve very rapid acquisition by using as few as four training symbols. More recently, its digital counterparts are investigated in [61], which shows that the digital TDT algorithms remain effective even with very-low-resolution digital UWB receivers. Despite all these appealing advantages, the optimality issue of TDT has never been thoroughly explored.

To address this issue, we establish a data-aided maximum likelihood (ML) timing algorithm. Based on the ML criterion, the estimation of all multipath gains and delays was pursued in [43] and the estimation performance was analyzed in [13]. However, [43] is based on an unrealistic multipath channel model which assumes no

inter-path overlapping. The real channel with a large number of dense taps would make this method impossible to implement. Unlike [43], we focus on the estimation of a single parameter, namely, the delay of the first arriving path, without invoking any unrealistic channel model assumption. We will show that although our ML estimator does not explicitly involve the channel information, it is able to collect multipath energy without channel estimation.

Considering the ML acquisition performance in terms of the probability of detection, we obtain the *unique* optimum training pattern in the sense of acquisition speed and consistency. By using this optimum training sequence, the ML algorithm can be simplified. Interestingly, we will show that the simplified ML (SML) and TDT estimators share the identical optimum training sequence and estimation operations. Furthermore, it can be proved that the criterion and performance of the TDT algorithm are essentially the same as those of the SML algorithm. These lead to the conclusion that the data-aided TDT algorithm is ML optimum.

Fine timing with high accuracy is not only desired in communications [54], but also critical to localization with UWB technology [27, 28, 16]. While the data-aided SML and TDT estimators can theoretically achieve any resolution level, from the consideration of practical environment, they may suffer from the ambiguity induced by the weak tail of the multipath channel and the extent of the noise-only region between consecutive symbols. To circumvent the ambiguity, we complement the SML and TDT algorithms with one more step by searching the peak of the first-order difference of the objective functions, which facilitates the SML and TDT comparison at the chip-level fine timing.

1.3 The ℓ_1 -Regularized LS Formulation for Cooperative Target Localization and Malicious Anchor Identification

Secure target localization in the presence of malicious anchors is a fundamental and intriguing problem in wireless sensor networks (WSNs) [45]. When targets are deployed in hostile environments, attackers may disturb the localization process and make the location estimation unreliable. Unreliable target locations lead to severe consequences, e.g., wrong military decisions on the battlefield or mistakenly granting access rights to people [67]. Localization attacks can be launched in either the network layer or the physical layer. We focus on the physical layer attack which can be classified into simple attacks and complicated attacks [67]. In a simple attack, an attacker may fake the distance measurement between the target and a compromised anchor by reporting fake self location or manipulating the transmission power [68]. A complicated attack involves multiple compromised anchors which can either independently broadcast fake information or collaborate to mislead the target to the same false location [67]. The former is referred to as an uncoordinated attack and the latter is often termed as a collusion attack. A collusion attack is usually much more powerful than an uncoordinated one.

The presence of malicious anchors induces discrepancy, or inconsistency, between the measured distance obtained from the first phase and the calculated distance from second phase target location estimate. Based on this, malicious anchors can be filtered out such that the remaining anchors yield more consistent estimate [40, 41, 35]. Reference [35] starts from a randomly picked subset of size 3 and make an LS estimation of the target location. It then accumulates the number of the remaining anchors which have the consistent distance measurements with this estimate. If the consistency number is beyond a certain predetermined threshold, then the estimate

is regarded as correct and the algorithm stops; otherwise, it randomly picks another subset to repeat the consistency check procedure until a correct estimate can be obtained. The problem with this method is that, without knowledge of the number of malicious anchors, it is hard to choose the consistency threshold. Reference [41] adopts a suboptimal searching method. Unlike [35], it starts from the entire available anchor set and deletes one malicious anchor which induces the largest inconsistency at each stage, until all malicious anchors are removed. Reference [40] tries to identify the outliers by minimizing the median of the squared distance measurement errors. These methods are straightforward and easy to implement. However, they do not directly tackle the false location information. The optimal estimation can only be achieved by enumerating all possible attack scenarios.

To address this problem, we explicitly incorporate anchors' misplacements, i.e., location errors, into the distance measurement model to locate the target and identify malicious anchors simultaneously. By exploring the pairwise sparse nature inherent in the misplacements, we are able to formulate secure target localization as an ℓ_1 -regularized LS problem. Under this problem formulation, we establish the pairwise sparsity threshold, which defines the largest possible number of identifiable malicious anchors. We then propose a simple projected gradient search algorithm to solve the ℓ_1 -regularized LS problem in WSNs.

Particularly, we consider two scenarios for the secure localization problem, namely, a single target noncooperative localization and two-target cooperative localization. While single target localization is a typical scenario in the field of secure localization as in [45, 68, 41, 37, 40, 41], to the authors' knowledge, we are the first to incorporate target cooperation into this area. With the proposed ℓ_1 -regularized LS formulation, we recognize the misplacement estimation limitation in the single target case; that is, solving the ℓ_1 -regularized LS problem can only identify the malicious anchors but fails

to yield correct misplacement estimates. It is demonstrated that the misplacement estimation can be enhanced by incorporating target cooperation. Certainly, due to cooperation, target location estimation accuracy can be improved as well.

1.4 Dissertation Organization

The organization of this dissertation is as follows. The optimum and robust waveform designs for cooperative target estimation are introduced in Chapter 2. Chapter 2 also performs the sensitivity analysis for the optimum designs to the overestimation errors. In Chapter 3, TOA estimation of IR UWB signals is investigated for the first phase of distance measurement in a localization process. Provided the distance measurements, in Chapter 4, secure localization with target cooperation is studied in the presence of malicious anchors. Summarizing remarks and future works are given in Chapter 5.

CHAPTER 2

OPTIMUM AND ROBUST WAVEFORM DESIGNS FOR COOPERATIVE TARGET ESTIMATION

Information theory, and particularly the mutual information (MI), has provided fundamental guidance for communications research. In Bell's 1993 paper, the MI was first applied to radar waveform design. Similar to its communications counterpart, the solution comes in a water-filling form. However, the practical meaning of MI in the sensing context remains unclear to date. Recently, Yang and Blum's 2007 paper shows that under the white noise assumption, the optimum water-filling scheme simultaneously maximizes the MI and minimizes the estimation minimum mean square error (MMSE). Such an equivalence, however, does not hold when the target parameter statistics are not perfectly known as shown in Yang and Blum's subsequent work. To further the understanding of the practical meaning of MI and to establish a connection between the MI and commonly adopted MSE measures for sensing, we take a fresh look at the target estimation problem. We consider the general colored noise, incorporate the normalized MSE (NMSE), and develop joint robust designs for both the transmitter (waveforms) and the receiver (estimator) under various target and noise uncertainty models. Our results show that: i) the optimum waveform designs resulted from the MI, MMSE and NMSE criteria are all different; and ii) compared to MMSE, the NMSE-based designs share more similarities with the MI-based ones, especially when the target and noise statistics are not perfectly known.

We then further investigate this relationship by analyzing the sensitivity of the

optimum design to the overestimation error. For each of the three criteria, we derive the explicit formula for the error mode strength threshold, above which the error mode would consume nonzero transmit power and the original waveform design will be inevitably altered. We also develop a normalized NMSE indicator to measure the estimation performance variation induced by the error mode. Both analytical and numerical results confirm that the optimum waveform designs based on the three criteria do not show significant performance deterioration. While the NMSE-based optimum solution is always more sensitive to the overestimation error than the MI-based one, there is no universal relationship between these two criteria and MMSE.

2.1 Motivation

In multi-input multi-output (MIMO) communication systems, multiple transmit and/or receive antennas can increase the diversity to combat channel fading for enhanced transmission reliability and increase the degrees of freedom for improved data rate. Partly inspired by these benefits, MIMO sensing has drawn great interests in recent years (see e.g., [2, 6, 4, 10, 11, 17, 20, 21, 25]). In such systems, a particularly critical issue is the waveform optimization. Solutions to this problem mainly fall into two categories, the space-time correlation optimization of the transmitted waveforms (see e.g., [4, 39, 44]), and the specific time-domain signal design given the desired space-time correlation properties (see e.g., [17]). In this chapter, we focus on the former. Bell's 1993 paper first used the mutual information (MI) to design radar waveforms for the estimation of an extended target [4]. His MI-based water-filling approach has been extended by several recent works. In particular, [39] deals with multiple extended targets using a large coherent phased array, and [44] considers the detection of an extended target. Both of them adopt the MI as the optimization criterion.

The MI is an essential measure in the field of communications. However, its role in sensing is not yet clear. In an attempt to link the MI criterion with more direct performance indicators in sensing, and particularly target parameter estimation applications, Yang and Blum studied the extended target estimation problem in a widely separated MIMO radar scenario. In [65], it is shown that the MI and the minimum mean square error (MMSE) criteria lead to the same optimum water-filling strategy, assuming perfectly known target and white noise power spectral densities (PSDs). These waveform designs were then extended in [66] to account for bounded uncertainty in the target PSD. In contrast to [65], [66] shows that the MI and MMSE criteria result in distinct waveform designs.

Though the results in [65] and [66] shed some light on the possible connection between the MI and MMSE measures, they are based on limiting assumptions such as white noise and perfectly known noise PSD. In this chapter, we will further these existing works and reveal more intrinsic connections between the MI and MSE measures in a sensing setup.

For comparison convenience, we will consider a MIMO radar setup as in [65] and [66]. However, rather than the widely separated MIMO radar, we employ a mixed MIMO structure with widely separated transmit array elements and closely spaced receive array elements. This is due to the inherent identifiability issue associated with the former setup as will be detailed in Section 2.2.

Our contributions are three-fold. First, we take into consideration the more general and practical colored Gaussian noise that can emerge in various situations. For example, the received signal may be affected by unwanted interferences including jammers. The noise spectrum might also be shaped by the antenna and RF filters [55]. It turns out that in the presence of colored Gaussian noise, the equivalence between the MI and MMSE design criteria established in [65] does not hold, even

when the target and noise PSDs are both perfectly known. Secondly, we introduce the normalized MSE (NMSE) minimizing criterion for radar waveform designs. Not only is it more meaningful for parameter estimation problems, but it also exhibits more similar behaviors with the MI criterion than its MMSE counterpart, especially in robust designs. Last but not least, we provide joint robust designs for both the probing waveforms at the transmitter and the estimator at the receiver under various uncertainty models. Compared with [66], our improvements include: i) we consider colored noise instead of white noise; ii) we jointly optimize both the transmitter (waveforms) and the receiver (estimator) instead of limiting only to the transmitter side; and iii) we account for the uncertainty for both target and noise PSDs instead of assuming perfectly known noise PSD. Results show that the MI- and NMSE-based robust designs are built on an identical least favorable set (LFS), which differs from the LFS of the MMSE-based designs.

Since the optimum waveform design relies on an ideal assumption of known target and noise PSDs, a small PSD estimation error might introduce considerable impact on the designed waveform. Besides the target and noise's in-band PSD uncertainty addressed in joint robust designs, there is another type of PSD uncertainty, namely the overestimation error. In case that additional error modes appear, the original optimum waveform solution for the nominal modes may be altered, which will induce estimation performance degradation. Therefore, the sensitivity analysis of the optimum designs consists of an intriguing task. Furthermore, the study of the sensitivity comparison among the MI, MMSE and NMSE criteria can help further our understanding on the relationship linking the three criteria.

To focus on our main objective, only a single error mode will be considered in this chapter. We perform the sensitivity analysis not only at the transmitter, but also at the receiver. At the transmitter side, for each criterion we derive the explicit formula

of the error mode strength threshold. When the error mode strength exceeds the threshold, it will consume nonzero transmit power and the original optimum solution for the nominal modes will be inevitably altered. The design scheme which has the highest strength threshold is the least sensitive to the overestimation error. At the receiver side, the normalized NMSE indicator of the estimation performance variation is calculated and then compared among the three criteria. Both analytical and numerical results show that all three criteria do not exhibit significant performance deterioration. Particularly, the NMSE-based design has lower strength threshold, experiences worse performance variation, and therefore is more vulnerable than the MI-based design. Due to their very different strength structures, however, there does not exist a universal relationship between the former two criteria and MMSE.

The organization of this chapter is as follows. The system model is given in Section 2.2. Three design criteria (MI, MMSE and NMSE) and their corresponding optimum waveform designs in the presence of colored noise are introduced in Section 2.3. The joint estimator and power loading robust designs are discussed in Section 2.4 for all three criteria. Further analysis for the sensitivity of the optimum waveform design to the overestimation error for all three criteria is performed in Section 2.5. Numerical results are given in Section 2.6, followed by the concluding remarks in Section 2.7.

2.2 Mixed MIMO Signal Model

Despite the many similarities between MIMO communications and MIMO radar, they have some fundamental differences. Take the transmitted signal optimization as an example, where we consider a simple setup of $M = 2$ transmit antennas and $N = 2$ receive antennas.

In communications, the objective is to optimize the transmitted signals for better estimation of themselves. Assume that the duration of the transmitted signals is

L , length of the channel delay is K , and the white noise $\boldsymbol{\xi}$ is zero-mean Gaussian distributed. The system representation can be expressed as:

$$\begin{bmatrix} \mathbf{r}_1 \\ \mathbf{r}_2 \end{bmatrix} = \mathbf{H} \begin{bmatrix} \mathbf{x}_1 \\ \mathbf{x}_2 \end{bmatrix} + \boldsymbol{\xi} = \begin{bmatrix} \mathbf{H}_{1,1} & \mathbf{H}_{1,2} \\ \mathbf{H}_{2,1} & \mathbf{H}_{2,2} \end{bmatrix} \begin{bmatrix} \mathbf{x}_1 \\ \mathbf{x}_2 \end{bmatrix} + \boldsymbol{\xi} \quad (2.1)$$

where \mathbf{x}_i is the $L \times 1$ transmitted signal vector emitted from the i th transmitter, \mathbf{r}_j is the $L \times 1$ received signal vector at the j th receiver, and the $L \times L$ Toeplitz matrix $\mathbf{H}_{j,i}$ represents the channel response from the i th transmitter to the j th receiver. Denote the covariance matrices as $\boldsymbol{\Sigma}_x$ for the transmitted signals, and $\boldsymbol{\Sigma}_\xi = \sigma_\xi^2 \mathbf{I}$ for the white noise. Then the mutual information (MI) between the transmitted and received signals is:

$$\text{MI} = \log \left| \sigma_\xi^{-2} \boldsymbol{\Sigma}_x \mathbf{H}^H \mathbf{H} + \mathbf{I}_{2L} \right| \quad (2.2)$$

and the resultant MMSE after the MMSE estimator is

$$\text{MMSE} = \text{tr} \left\{ (\sigma_\xi^{-2} \mathbf{H}^H \mathbf{H} + \boldsymbol{\Sigma}_x^{-1})^{-1} \right\} . \quad (2.3)$$

In communications, the classical optimum transmitted signal design maximizing the MI or minimizing the MMSE is achieved when $(\sigma_\xi^{-2} \boldsymbol{\Sigma}_x \mathbf{H}^H \mathbf{H} + \mathbf{I}_{2L})$ or $(\sigma_\xi^{-2} \mathbf{H}^H \mathbf{H} + \boldsymbol{\Sigma}_x^{-1})$ is a diagonal matrix (see e.g., [48, 49, 50, 53]). The $2L$ eigenvalues of $\boldsymbol{\Sigma}_x$ are allocated according to the strength of the corresponding channel eigenvalues of $\mathbf{H}^H \mathbf{H}$.

On the other hand, for a 2×2 radar system with widely separated transmit and receive array elements, the total $M \times N = 4$ viewing aspects of the target can be

acquired, and the signal model is given by [65]:

$$\begin{bmatrix} \mathbf{r}_1 \\ \mathbf{r}_2 \end{bmatrix} = \begin{bmatrix} \mathbf{X} & \mathbf{0}_{L \times 2K} \\ \mathbf{0}_{L \times 2K} & \mathbf{X} \end{bmatrix} \begin{bmatrix} \mathbf{g}_1 \\ \mathbf{g}_2 \end{bmatrix} + \boldsymbol{\xi} \quad (2.4)$$

where $\mathbf{X} = [\mathbf{X}_1 \ \mathbf{X}_2]$ and \mathbf{X}_i is the $L \times K$ Toeplitz signal matrix emitted from the i th transmit antenna, \mathbf{r}_j is the $L \times 1$ signal vector at the j th receive antenna, and $\mathbf{g}_j = [\mathbf{g}_{j,1}^T \ \mathbf{g}_{j,2}^T]^T$ with $\mathbf{g}_{j,i}$ being the $K \times 1$ target viewing aspect from the i th transmit antenna to the j th receive antenna. Accordingly, the MI between the target response and the received signal is:

$$\text{MI} = \log \left| \sigma_\xi^{-2} \boldsymbol{\Sigma}_g (\mathbf{I}_2 \otimes \mathbf{X}^H \mathbf{X}) + \mathbf{I}_{4K} \right| \quad (2.5)$$

where $\boldsymbol{\Sigma}_g$ is the covariance matrix of the target response, and the resulting MMSE after the MMSE estimator is:

$$\text{MMSE} = \text{tr} \left\{ \left(\sigma_\xi^{-2} (\mathbf{I}_2 \otimes \mathbf{X}^H \mathbf{X}) + \boldsymbol{\Sigma}_g^{-1} \right)^{-1} \right\} . \quad (2.6)$$

In order to maximize the MI or minimize the MMSE, the optimum strategy again requires $(\sigma_\xi^{-2} \boldsymbol{\Sigma}_g (\mathbf{I}_2 \otimes \mathbf{X}^H \mathbf{X}) + \mathbf{I}_{4K})$ or $(\sigma_\xi^{-2} (\mathbf{I}_2 \otimes \mathbf{X}^H \mathbf{X}) + \boldsymbol{\Sigma}_g^{-1})$ to be an optimum diagonal matrix, as detailed in [65]. However, unlike the communications case, the special repeated structure of $\mathbf{I}_2 \otimes \mathbf{X}^H \mathbf{X}$ makes such a condition impossible. In other words, one *cannot* design the 2 transmitted signals such that the estimation of 4 viewing aspects (namely g_{11} , g_{12} , g_{21} and g_{22}) are optimized simultaneously – there is simply a lack of sufficient degrees of freedom.

This simple comparison suggests that the transmitted signal optimization problem is ill-formulated for the widely separated MIMO radar setup in [65]. To avoid this

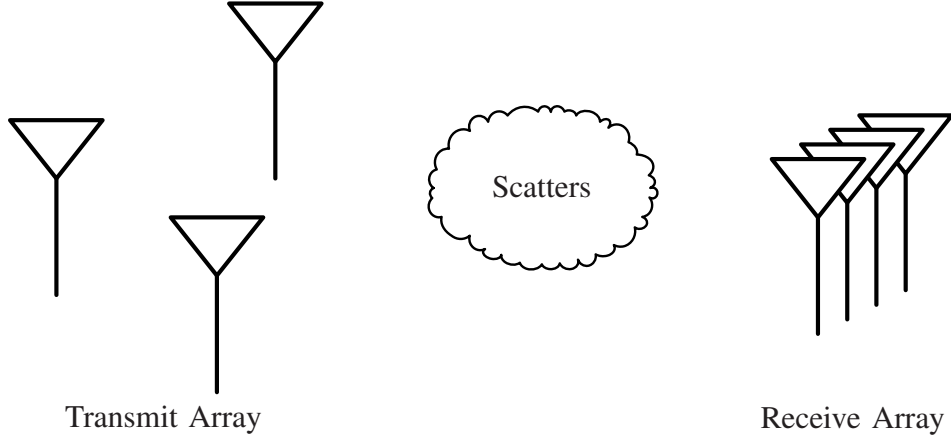


Figure 2.1: Illustration of the mixed MIMO structure.

problem, we consider a mixed MIMO structure (see Fig. 2.1), which is equipped with a widely separated M -element transmit array and a closely spaced N -element receive array. For an extended target of interest, the M transmitted waveforms can impinge distinct scatterers from different angles. On the other hand, for each of the M reflected signals, the receiver acquires N coherent returns, the only difference among which is a phase shift. One can then combine them coherently to obtain a processing gain of N . As a result, the target response is captured by the mixed MIMO setup from totally M viewing aspects. Having M transmitted signals to design, this mixed MIMO setup provides sufficient degrees of freedom for the signal design optimizing the estimation of all M viewing aspects.

Bearing the goal of comparing the MI- and MSE-based radar waveform designs, we will borrow the “mode” space signal model from [65]. Though originally developed for the widely separated MIMO radar, it can be readily modified for our mixed MIMO setup. The coherent combining of the arrival signals at the closely spaced receive array is rather straightforward. Hence we set $N = 1$ here without loss of generality.

As a result, the received waveform can be expressed as

$$\mathbf{r}_1 = \mathbf{X}\mathbf{g} + \boldsymbol{\xi} \quad (2.7)$$

where $\mathbf{X} = [\mathbf{X}_1, \dots, \mathbf{X}_M]$, $\mathbf{g} = [\mathbf{g}_1^T, \dots, \mathbf{g}_M^T]^T$, \mathbf{r}_1 is the $L \times 1$ signal vector at the receive antenna, and $\boldsymbol{\xi}$ the $L \times 1$ zero-mean Gaussian noise vector. To facilitate the target response estimation, it is required that L cannot be less than MK . We set $L = MK$ in our signal model.

While the target response is assumed to be Gaussian distributed with full rank covariance matrix $\boldsymbol{\Sigma}_g$ [65], the zero-mean non-white Gaussian noise has covariance matrix $\boldsymbol{\Sigma}_\xi$. Through eigenvalue decomposition, $\boldsymbol{\Sigma}_g$ and $\boldsymbol{\Sigma}_\xi$ can be diagonalized as

$$\boldsymbol{\Sigma}_g = \mathbf{U}_g \boldsymbol{\Lambda}_g \mathbf{U}_g^H, \quad \boldsymbol{\Sigma}_\xi = \mathbf{U}_\xi \boldsymbol{\Lambda}_\xi \mathbf{U}_\xi^H$$

where the entries of the diagonal matrices $\boldsymbol{\Lambda}_g$ and $\boldsymbol{\Lambda}_\xi$ can be regarded as their corresponding PSD samples [65], respectively. In [65], the maximum MI or minimum MMSE is achieved when $\mathbf{X} = \boldsymbol{\Psi} \mathbf{D}^{\frac{1}{2}} \mathbf{U}_g^H$, with $\boldsymbol{\Psi}$ being an $L \times MK$ matrix with orthonormal columns and \mathbf{D} a diagonal matrix. Having $L = MK$, we can generalize this result to the colored noise case by constraining the arbitrary matrix $\boldsymbol{\Psi}$ as \mathbf{U}_ξ , namely $\mathbf{X} = \mathbf{U}_\xi \mathbf{D}^{\frac{1}{2}} \mathbf{U}_g^H$, which gives rise to the ‘‘mode’’ space system representation:

$$\mathbf{y} = \mathbf{D}^{\frac{1}{2}} \mathbf{h} + \boldsymbol{\eta} \quad (2.8)$$

where $\mathbf{y} \doteq \mathbf{U}_\xi^H \mathbf{r}_1$ is defined as the $MK \times 1$ observed signal in the mode space, $\mathbf{h} \doteq \mathbf{U}_g^H \mathbf{g}$ is the $MK \times 1$ ‘‘mode’’ vector capturing the response of the extended target, and $\boldsymbol{\eta} \doteq \mathbf{U}_\xi^H \boldsymbol{\xi}$ the $MK \times 1$ Gaussian noise vector in the mode space. Clearly, the covariance matrices for \mathbf{h} and $\boldsymbol{\eta}$ are $\boldsymbol{\Lambda} = \boldsymbol{\Lambda}_g$ and $\boldsymbol{\Sigma}_\eta = \boldsymbol{\Lambda}_\xi$ diagonal matrices,

respectively. $\mathbf{D} = \text{diag}\{d_1, \dots, d_{MK}\}$ is the power allocation matrix with transmit power d_i allocated to the corresponding mode space waveform, subject to the total transmit power constraint $\sum_{i=1}^{MK} d_i = \mathcal{P}_0$.

With this representation, the waveform design problem simplifies to a power allocation problem, where the total power will be optimally assigned to MK orthogonal waveforms in the mode space. It is worth noting that, though we adopt the mode space representation in [65] for comparison with the results therein, this model is actually very general. Our model and the results hereafter can be readily generalized to cover “MIMO” radar systems resulted not only from multiple spatial viewing aspects, but also by alternative means such as frequency agility. Additionally, various receiver beamforming techniques (conventional [36], minimum variance distortionless response (MVDR) [15], and other adaptive algorithms [56]) can also be readily accommodated.

2.3 Optimum Waveform Designs In Colored Noise

The optimum power allocation problem has been studied in [65], under the white Gaussian noise assumption for which $\mathbf{\Sigma}_\eta = \sigma_\eta^2 \mathbf{I}_{MK}$. In a sensing scenario, however, unwanted interferences including jammers and antenna effects are often inevitable, suggesting the necessity of incorporating more general colored noise. Throughout our analysis, we will consider colored Gaussian noise with zero-mean and covariance matrix $\mathbf{\Sigma}_\eta = \text{diag}\{\sigma_{\eta_1}^2, \dots, \sigma_{\eta_{MK}}^2\}$, where the diagonal elements can be different.

In this section, we assume that both the target and noise PSDs are known exactly at both the transmitter and the receiver. This assumption will be relaxed in the next section, where uncertainty of such knowledge will be taken into account.

2.3.1 MI and MMSE Criteria

The MI between the observed signal \mathbf{y} and the target mode response \mathbf{h} given power allocation matrix \mathbf{D} is:

$$I(\mathbf{y}; \mathbf{h} | \mathbf{D}) = \log |\mathbf{\Lambda} \mathbf{D} \mathbf{\Sigma}_\eta^{-1} + \mathbf{I}_{MK}| = \sum_{i=1}^{MK} \log (\sigma_{\eta_i}^{-2} \lambda_i d_i + 1) . \quad (2.9)$$

The logarithm is base-2 unless otherwise indicated, and the unit for MI is bit. Note that, instead of the white noise with a flat PSD in [65], we consider non-flat colored noise here.

Proposition 2.1 (MI-based Optimum Power Allocation): *The optimum power allocation maximizing the MI in the presence of colored Gaussian noise has the following water-filling form:*

$$d_i|_{MI} = \left[\gamma_{MI} - \frac{\sigma_{\eta_i}^2}{\lambda_i} \right]^+ , \text{ for } i = 1, \dots, MK \quad (2.10)$$

where γ_{MI} is a constant satisfying the total power constraint $\sum_{i=1}^{MK} d_i|_{MI} = \mathcal{P}_0$.

Proof. The problem of optimum power allocation for maximizing the MI in (2.9) subject to the total power constraint can be formulated as:

$$\begin{aligned} & \max_{\{d_i\}} \sum_{i=1}^{MK} \log (\sigma_{\eta_i}^{-2} \lambda_i d_i + 1) , \\ & \text{subject to } \sum_{i=1}^{MK} d_i = \mathcal{P}_0, \text{ and } d_i \geq 0, \text{ for } i = 1, \dots, MK . \end{aligned} \quad (2.11)$$

This constrained optimization problem can be solved by the Lagrange multiplier

method. Specifically, we first construct the objective function:

$$J_{\text{MI}} = \sum_{i=1}^{MK} \log(\sigma_{\eta_i}^{-2} \lambda_i d_i + 1) + \gamma'_{\text{MI}} \left(\sum_{i=1}^{MK} d_i - \mathcal{P}_0 \right) \quad (2.12)$$

and then differentiate it with respect to d_i and set it to zero. As a result, we get:

$$d_i|_{\text{MI}} = \left[\gamma_{\text{MI}} - \frac{\sigma_{\eta_i}^2}{\lambda_i} \right]^+, \text{ for } i = 1, \dots, MK \quad (2.13)$$

where the notation $[a]^+ \doteq \max\{0, a\}$, and the water level

$$\gamma_{\text{MI}} = -1/\gamma'_{\text{MI}} = \frac{\mathcal{P}_0 + \sum_{i \in \mathcal{S}_{\text{MI}}} \frac{\sigma_{\eta_i}^2}{\lambda_i}}{\|\mathcal{S}_{\text{MI}}\|} \quad (2.14)$$

is a constant determined by the total power constraint $\sum_{i=1}^{MK} d_i|_{\text{MI}} = \mathcal{P}_0$. The mode index set $\mathcal{S}_{\text{MI}} \doteq \{i : d_i|_{\text{MI}} > 0\}$, and the set length $\|\cdot\|$ is defined as the number of elements belonging to the set. ■

In the MI-based water-filling scheme, the mode strength is described by the target-to-noise power ratio. Note that the MI-based scheme inclines to discard the weakest modes.

For the MSE-based designs, one needs to first specify the MMSE estimator, denoted by Φ , as follows:

$$\hat{\mathbf{h}} = \Phi \mathbf{y} = (\mathbf{D} \Sigma_{\eta}^{-1} + \mathbf{\Lambda}^{-1})^{-1} \mathbf{D}^{\frac{1}{2}} \Sigma_{\eta}^{-1} \mathbf{y}. \quad (2.15)$$

Accordingly, the MMSE is given by

$$\text{MMSE} = \text{tr} \left\{ \text{E} \left\{ \left(\mathbf{h} - \hat{\mathbf{h}} \right) \left(\mathbf{h} - \hat{\mathbf{h}} \right)^{\mathcal{H}} \right\} \right\} = \text{tr} \left\{ \left(\Sigma_{\eta}^{-1} \mathbf{D} + \mathbf{\Lambda}^{-1} \right)^{-1} \right\} = \sum_{i=1}^{MK} \frac{\lambda_i}{\sigma_{\eta_i}^{-2} \lambda_i d_i + 1}. \quad (2.16)$$

Proposition 2.2 (MMSE-based Optimum Power Allocation): *The optimum power allocation minimizing the MMSE in the presence of colored Gaussian noise has the following form:*

$$d_i|_{\text{MMSE}} = \lambda_i \left[\gamma_{\text{MMSE}} \sqrt{\frac{\sigma_{\eta_i}^2}{\lambda_i^2}} - \frac{\sigma_{\eta_i}^2}{\lambda_i^2} \right]^+, \text{ for } i = 1, \dots, MK \quad (2.17)$$

where γ_{MMSE} is a constant ensuring the total power constraint.

Proof. The problem of optimum power allocation for minimizing the MMSE in (2.16) subject to the total power constraint can be formulated as:

$$\begin{aligned} \min_{\{d_i\}} \quad & \sum_{i=1}^{MK} \frac{\lambda_i}{\sigma_{\eta_i}^{-2} \lambda_i d_i + 1}, \\ \text{subject to} \quad & \sum_{i=1}^{MK} d_i = \mathcal{P}_0, \text{ and } d_i \geq 0, \text{ for } i = 1, \dots, MK. \end{aligned} \quad (2.18)$$

Using the Lagrange multiplier method, by differentiating the following cost function with respect to d_i :

$$J_{\text{MMSE}} = \sum_{i=1}^{MK} \frac{\lambda_i}{\sigma_{\eta_i}^{-2} \lambda_i d_i + 1} + \gamma'_{\text{MMSE}} \left(\sum_{i=1}^{MK} d_i - \mathcal{P}_0 \right) \quad (2.19)$$

and then setting it to zero, we get:

$$d_i|_{\text{MMSE}} = \left[\gamma_{\text{MMSE}} \sqrt{\sigma_{\eta_i}^2} - \frac{\sigma_{\eta_i}^2}{\lambda_i} \right]^+ = \lambda_i \left[\gamma_{\text{MMSE}} \sqrt{\frac{\sigma_{\eta_i}^2}{\lambda_i^2}} - \frac{\sigma_{\eta_i}^2}{\lambda_i^2} \right]^+, \forall i \quad (2.20)$$

where

$$\gamma_{\text{MMSE}} = \sqrt{\frac{1}{\gamma'_{\text{MMSE}}}} = \frac{\mathcal{P}_0 + \sum_{i \in \mathcal{S}_{\text{MMSE}}} \frac{\sigma_{\eta_i}^2}{\lambda_i}}{\sum_{i \in \mathcal{S}_{\text{MMSE}}} \sqrt{\sigma_{\eta_i}^2}} \quad (2.21)$$

is a constant ensuring the total power constraint and the mode index set $\mathcal{S}_{\text{MMSE}} \doteq$

$\{i : d_i|_{\text{MMSE}} > 0\}$. ■

To facilitate a water-filling interpretation, we can rewrite the allocation solution in a weighted form [42] as:

$$\frac{d_i|_{\text{MMSE}}}{\sqrt{\sigma_{\eta_i}^2}} = \left[\gamma_{\text{MMSE}} - \frac{\sqrt{\sigma_{\eta_i}^2}}{\lambda_i} \right]^+, \text{ for } i = 1, \dots, MK \quad (2.22)$$

where γ_{MMSE} can be regarded as the water level. The mode strength here is measured by the target-to-square-root-of-noise ratio. If a mode is weaker than the water level, it will be simply ignored.

From Propositions 2.1 and 2.2, we see that in the presence of colored Gaussian noise, the MMSE criterion does *not* lead to the water-filling solution as in [65]. In other words, the MI and MMSE criteria now are *not* equivalent as observed in [65], when the additive noise is colored.

2.3.2 NMSE Criterion

While the MMSE design minimizes the sum of the target mode estimation errors, there is no guarantee on the MSEs of individual modes. Additionally, it is possible for the weakest modes to be discarded due to the total power constraint. In a radar problem, however, these weak modes may assume significant information useful in describing the target [4]. A natural amendment to this problem is to introduce the normalized MSE (NMSE) criterion, which is a common exercise in various estimation problems (see e.g., [30, 46, 57]).

Specifically, normalizing the individual MSEs with respect to their average strength,

we obtain the following expression:

$$\begin{aligned} \text{NMSE} &\doteq \text{tr} \left\{ \mathbf{E} \left\{ \boldsymbol{\Lambda}^{-\frac{1}{2}} (\mathbf{h} - \hat{\mathbf{h}}) (\mathbf{h} - \hat{\mathbf{h}})^{\mathcal{H}} \boldsymbol{\Lambda}^{-\frac{1}{2}} \right\} \right\} = \text{tr} \left\{ (\boldsymbol{\Sigma}_{\eta}^{-1} \boldsymbol{\Lambda} \mathbf{D} + \mathbf{I}_{MK})^{-1} \right\} \\ &= \sum_{i=1}^{MK} \frac{1}{\sigma_{\eta_i}^{-2} \lambda_i d_i + 1}. \end{aligned} \quad (2.23)$$

Proposition 2.3 (NMSE-based Optimum Power Allocation): *The optimum power allocation minimizing the NMSE in the presence of colored Gaussian noise has the following form:*

$$d_i|_{\text{NMSE}} = \left[\gamma_{\text{NMSE}} \sqrt{\frac{\sigma_{\eta_i}^2}{\lambda_i} - \frac{\sigma_{\eta_i}^2}{\lambda_i}} \right]^+, \text{ for } i = 1, \dots, MK \quad (2.24)$$

where γ_{NMSE} is a constant ensuring the total power constraint.

Proof. The problem of optimum power allocation based on the NMSE criterion under a total power constraint can be formulated as:

$$\begin{aligned} \min_{\{d_i\}} \quad & \sum_{i=1}^{MK} \frac{1}{\sigma_{\eta_i}^{-2} \lambda_i d_i + 1}, \\ \text{subject to} \quad & \sum_{i=1}^{MK} d_i = \mathcal{P}_0, \text{ and } d_i \geq 0, \text{ for } i = 1, \dots, MK. \end{aligned} \quad (2.25)$$

As in proofs of Propositions 2.1 and 2.2, we construct the cost function:

$$J_{\text{NMSE}} = \sum_{i=1}^{MK} \frac{1}{\sigma_{\eta_i}^{-2} \lambda_i d_i + 1} + \gamma'_{\text{NMSE}} \left(\sum_{i=1}^{MK} d_i - \mathcal{P}_0 \right) \quad (2.26)$$

and differentiate it to obtain:

$$d_i|_{\text{NMSE}} = \left[\gamma_{\text{NMSE}} \sqrt{\frac{\sigma_{\eta_i}^2}{\lambda_i} - \frac{\sigma_{\eta_i}^2}{\lambda_i}} \right]^+, \quad \forall i \quad (2.27)$$

where

$$\gamma_{\text{NMSE}} = \sqrt{\frac{1}{\gamma'_{\text{NMSE}}}} = \frac{\mathcal{P}_0 + \sum_{i \in \mathcal{S}_{\text{NMSE}}} \frac{\sigma_{\eta_i}^2}{\lambda_i}}{\sum_{i \in \mathcal{S}_{\text{NMSE}}} \sqrt{\frac{\sigma_{\eta_i}^2}{\lambda_i}}} \quad (2.28)$$

is a constant ensuring the total power constraint and $\mathcal{S}_{\text{NMSE}} \doteq \{i : d_i|_{\text{NMSE}} > 0\}$. ■

We re-express the solution as

$$\frac{d_i|_{\text{NMSE}}}{\sqrt{\sigma_{\eta_i}^2/\lambda_i}} = \left[\gamma_{\text{NMSE}} - \sqrt{\frac{\sigma_{\eta_i}^2}{\lambda_i}} \right]^+, \text{ for } i = 1, \dots, MK \quad (2.29)$$

where γ_{NMSE} is the water level, and the mode strength is subject to the target-to-noise power ratio, as in the MI-based scheme.

Results summarized in Propositions 2.1–2.3 show that the optimum power allocation obtained via maximizing the MI differs from those by minimizing the MMSE or NMSE, when colored noise is taken into account. While the MI-based water-filling solution tends to ignore the weakest modes, the MMSE- and NMSE-based solutions put more weights on the relatively weak modes which may assume significant information in describing/characterizing the target [4]. The three mode index sets \mathcal{S}_{MI} , $\mathcal{S}_{\text{MMSE}}$ and $\mathcal{S}_{\text{NMSE}}$ may be different from each other. Clearly, these index sets differ only in a few weakest modes and the difference vanishes when the total power \mathcal{P}_0 is sufficiently high.

These results are based on the exact knowledge of both the target and noise PSDs. In practice, however, this knowledge can only be acquired with some uncertainty. In the subsequent sections, we will investigate behaviors of the MI-, MMSE- and NMSE-based designs under in-band and out-band uncertainty models, respectively.

2.4 Robust Joint Transceiver Designs

We first consider in-band PSD uncertainty in the section. When the PSDs of the target and the colored noise are not precisely available, some robust approaches need to be utilized to design the probing waveforms at the transmitter, as well as the estimator at the receiver. [66] adopted the *minimax* approach to address the bounded target PSD uncertainty, while assuming that the white noise PSD is perfectly known. Here, we not only consider a colored noise PSD which includes unwanted interferences such as jamming signals often encountered by a sensing system, but also allow for various uncertainty levels in the noise PSD. Another significant difference from [66] is: [66] focuses only on the robust design for the transmitted waveforms while assuming that the exact target PSD is available at the receiver; whereas we *jointly* design the transmitted waveforms and the MMSE estimator via a robust procedure.

2.4.1 Robust Minimax Design Criteria

In our *minimax* problem formulation, the estimator and the power allocation are jointly designed to: i) provide the optimum performance for the least favorable set (LFS) of the target and noise PSDs; and ii) provide equivalent or better performance for all other possible sets within the uncertainty regions. Mathematically, we jointly design the MMSE estimator matrix Φ and the power allocation matrix \mathbf{D} such that [31, 32]:

$$\begin{aligned}
 & \max_D \left\{ \inf_{\Lambda, \Sigma_\eta} \text{MI}(\Lambda, \Sigma_\eta; \mathbf{D}) \right\}, & \text{MI-based,} \\
 & \min_{\Phi, \mathbf{D}} \left\{ \sup_{\Lambda, \Sigma_\eta} \text{MMSE}(\Lambda, \Sigma_\eta; \Phi, \mathbf{D}) \right\}, & \text{MMSE-based,} \\
 & \min_{\Phi, \mathbf{D}} \left\{ \sup_{\Lambda, \Sigma_\eta} \text{NMSE}(\Lambda, \Sigma_\eta; \Phi, \mathbf{D}) \right\}, & \text{NMSE-based.}
 \end{aligned} \tag{2.30}$$

To solve the above problems, we will look for a saddle point for each criterion by finding the LFS ($\mathbf{\Lambda}^R = \text{diag}\{\lambda_1^R, \dots, \lambda_{MK}^R\}$, $\mathbf{\Sigma}_\eta^R = \text{diag}\{\sigma_{\eta_1}^{2R}, \dots, \sigma_{\eta_{MK}}^{2R}\}$), the robust estimator $\mathbf{\Phi}^R$ and the robust power allocation matrix $\mathbf{D}^R = \text{diag}\{d_1^R, \dots, d_{MK}^R\}$ satisfying:

$$\min_{\mathbf{\Lambda}, \mathbf{\Sigma}_\eta} \text{MI}(\mathbf{\Lambda}, \mathbf{\Sigma}_\eta; \mathbf{D}^R) = \text{MI}(\mathbf{\Lambda}^R, \mathbf{\Sigma}_\eta^R; \mathbf{D}^R) = \max_D \text{MI}(\mathbf{\Lambda}^R, \mathbf{\Sigma}_\eta^R; \mathbf{D}) ,$$

$$\max_{\mathbf{\Lambda}, \mathbf{\Sigma}_\eta} \text{MMSE}(\mathbf{\Lambda}, \mathbf{\Sigma}_\eta; \mathbf{\Phi}^R, \mathbf{D}^R) = \text{MMSE}(\mathbf{\Lambda}^R, \mathbf{\Sigma}_\eta^R; \mathbf{\Phi}^R, \mathbf{D}^R) = \min_{\mathbf{\Phi}, \mathbf{D}} \text{MMSE}(\mathbf{\Lambda}^R, \mathbf{\Sigma}_\eta^R; \mathbf{\Phi}, \mathbf{D}) ,$$

$$\max_{\mathbf{\Lambda}, \mathbf{\Sigma}_\eta} \text{NMSE}(\mathbf{\Lambda}, \mathbf{\Sigma}_\eta; \mathbf{\Phi}^R, \mathbf{D}^R) = \text{NMSE}(\mathbf{\Lambda}^R, \mathbf{\Sigma}_\eta^R; \mathbf{\Phi}^R, \mathbf{D}^R) = \min_{\mathbf{\Phi}, \mathbf{D}} \text{NMSE}(\mathbf{\Lambda}^R, \mathbf{\Sigma}_\eta^R; \mathbf{\Phi}, \mathbf{D}) .$$

Note that once the LFSs $\mathbf{\Lambda}^R$ and $\mathbf{\Sigma}_\eta^R$ are determined, the second equalities in the above saddle point condition can be easily achieved through the optimum design that has been introduced in Section 2.3. So the *minimax* robust procedure will focus on the first equalities only, resulting in an equivalent saddle point condition:

$$\begin{aligned} \text{MI}(\mathbf{\Lambda}, \mathbf{\Sigma}_\eta; \mathbf{D}^R) - \text{MI}(\mathbf{\Lambda}^R, \mathbf{\Sigma}_\eta^R; \mathbf{D}^R) &\geq 0 , \\ \text{MMSE}(\mathbf{\Lambda}, \mathbf{\Sigma}_\eta; \mathbf{\Phi}^R, \mathbf{D}^R) - \text{MMSE}(\mathbf{\Lambda}^R, \mathbf{\Sigma}_\eta^R; \mathbf{\Phi}^R, \mathbf{D}^R) &\leq 0 , \\ \text{NMSE}(\mathbf{\Lambda}, \mathbf{\Sigma}_\eta; \mathbf{\Phi}^R, \mathbf{D}^R) - \text{NMSE}(\mathbf{\Lambda}^R, \mathbf{\Sigma}_\eta^R; \mathbf{\Phi}^R, \mathbf{D}^R) &\leq 0 . \end{aligned} \quad (2.31)$$

Next, the explicit expressions of the differences on the left hand sides of (2.31) will be derived for the MI, MMSE and NMSE criteria to facilitate the identification of their respective LFSs.

MI-based:

As defined in (2.9), the MI formula has nothing to do with the receiver design.

To calculate the MI difference in (2.31), one can substitute with (2.9) as follows:

$$\begin{aligned}
& \text{MI}(\mathbf{\Lambda}, \mathbf{\Sigma}_\eta; \mathbf{D}^R) - \text{MI}(\mathbf{\Lambda}^R, \mathbf{\Sigma}_\eta^R; \mathbf{D}^R) \\
&= \sum_{i=1}^{MK} \log(\sigma_{\eta_i}^{-2} \lambda_i d_i^R + 1) - \sum_{i=1}^{MK} \log(\sigma_{\eta_i}^{-2R} \lambda_i^R d_i^R + 1) \\
&= \sum_{i=1}^{MK} \log \frac{\frac{\lambda_i}{\sigma_{\eta_i}^2} d_i^R + 1}{\frac{\lambda_i^R}{\sigma_{\eta_i}^{2R}} d_i^R + 1} \tag{2.32}
\end{aligned}$$

where the robust power allocation \mathbf{D}^R is simply the optimum one for the LFS [c.f. (2.10)]:

$$d_i^R = \left[\gamma_{\text{MI}}^R - \frac{\sigma_{\eta_i}^{2R}}{\lambda_i^R} \right]^+, \quad \forall i. \tag{2.33}$$

In Section 2.4.2, we will find the LFS for MI using (2.32) and (2.33).

MMSE-based:

Calculation of the MMSE difference is more complicated than the MI case, because one now needs to jointly consider the power allocation \mathbf{D}^R and the estimator $\mathbf{\Phi}^R$.

As mentioned before, the robust power allocation matrix \mathbf{D}^R is optimum for the LFS; that is [c.f. (2.17)]:

$$d_i^R = \lambda_i^R \left[\gamma_{\text{MMSE}}^R \sqrt{\frac{\sigma_{\eta_i}^{2R}}{(\lambda_i^R)^2} - \frac{\sigma_{\eta_i}^{2R}}{(\lambda_i^R)^2}} \right]^+, \quad \forall i. \tag{2.34}$$

Likewise, the robust estimator $\mathbf{\Phi}^R$ is also optimum (MSE-minimizing) for the LFS.

From (2.15), we have:

$$\mathbf{\Phi}^R = \left(\mathbf{D}^R (\mathbf{\Sigma}_\eta^R)^{-1} + (\mathbf{\Lambda}^R)^{-1} \right)^{-1} (\mathbf{D}^R)^{\frac{1}{2}} (\mathbf{\Sigma}_\eta^R)^{-1} \tag{2.35}$$

which results in the MMSE for the LFS [c.f. (2.16)]:

$$\begin{aligned}
& \text{MMSE}(\mathbf{\Lambda}^R, \mathbf{\Sigma}_\eta^R; \mathbf{\Phi}^R, \mathbf{D}^R) \\
&= \sum_{i=1}^{MK} \frac{\lambda_i^R}{\sigma_{\eta_i}^{-2R} \lambda_i^R d_i^R + 1} \\
&= \sum_{i=1}^{MK} \left(\frac{1}{(\sigma_{\eta_i}^{-2R} \lambda_i^R d_i^R + 1)^2} \lambda_i^R + \frac{(\sigma_{\eta_i}^{-2R} \lambda_i^R)^2 d_i^R}{(\sigma_{\eta_i}^{-2R} \lambda_i^R d_i^R + 1)^2 \sigma_{\eta_i}^{2R}} \right) \quad (2.36)
\end{aligned}$$

where the last equality seems redundant but will make our later computations easier.

In the lack of exact knowledge of the true target and noise PSDs, one should always use the robust power allocation design \mathbf{D}^R at the transmitter, and the robust estimator design $\mathbf{\Phi}^R$ at the receiver. Accordingly, for target response \mathbf{h} with arbitrary PSD $\mathbf{\Lambda}$ and noise $\boldsymbol{\eta}$ with $\mathbf{\Sigma}_\eta$, we have:

$$\begin{aligned}
& \text{MMSE}(\mathbf{\Lambda}, \mathbf{\Sigma}_\eta; \mathbf{\Phi}^R, \mathbf{D}^R) \\
&= \text{tr} \left\{ \mathbb{E} \left\{ \left(\mathbf{h} - \hat{\mathbf{h}} \right) \left(\mathbf{h} - \hat{\mathbf{h}} \right)^{\mathcal{H}} \right\} \right\} \\
&= \text{tr} \left\{ \mathbb{E} \left\{ \left(\mathbf{h} - \mathbf{\Phi}^R(\mathbf{D}^R \mathbf{h} + \boldsymbol{\eta}) \right) \left(\mathbf{h} - \mathbf{\Phi}^R(\mathbf{D}^R \mathbf{h} + \boldsymbol{\eta}) \right)^{\mathcal{H}} \right\} \right\} \\
&= \sum_{i=1}^{MK} \left(\frac{1}{(\sigma_{\eta_i}^{-2R} \lambda_i^R d_i^R + 1)^2} \lambda_i + \frac{(\sigma_{\eta_i}^{-2R} \lambda_i^R)^2 d_i^R}{(\sigma_{\eta_i}^{-2R} \lambda_i^R d_i^R + 1)^2 \sigma_{\eta_i}^2} \right). \quad (2.37)
\end{aligned}$$

Subtracting (2.36) from (2.37), we obtain the MMSE difference in (2.31) as:

$$\begin{aligned}
& \text{MMSE}(\mathbf{\Lambda}, \mathbf{\Sigma}_\eta; \mathbf{\Phi}^R, \mathbf{D}^R) - \text{MMSE}(\mathbf{\Lambda}^R, \mathbf{\Sigma}_\eta^R; \mathbf{\Phi}^R, \mathbf{D}^R) \\
&= \sum_{i=1}^{MK} \left(\frac{1}{(\sigma_{\eta_i}^{-2R} \lambda_i^R d_i^R + 1)^2} (\lambda_i - \lambda_i^R) + \frac{(\sigma_{\eta_i}^{-2R} \lambda_i^R)^2 d_i^R}{(\sigma_{\eta_i}^{-2R} \lambda_i^R d_i^R + 1)^2} (\sigma_{\eta_i}^2 - \sigma_{\eta_i}^{2R}) \right). \quad (2.38)
\end{aligned}$$

NMSE-based:

Using the robust MMSE estimator $\mathbf{\Phi}^R$, we obtain the NMSE for the LFS as [c.f.

(2.23)]:

$$\begin{aligned}
& \text{NMSE}(\mathbf{\Lambda}^R, \mathbf{\Sigma}_\eta^R; \mathbf{\Phi}^R, \mathbf{D}^R) \\
&= \text{tr} \left\{ \mathbb{E} \left\{ (\mathbf{\Lambda}^R)^{-\frac{1}{2}} (\mathbf{h} - \hat{\mathbf{h}}) (\mathbf{h} - \hat{\mathbf{h}})^{\mathcal{H}} (\mathbf{\Lambda}^R)^{-\frac{1}{2}} \right\} \right\} \\
&= \sum_{i=1}^{MK} \frac{1}{\sigma_{\eta_i}^{-2R} \lambda_i^R d_i^R + 1} \\
&= \sum_{i=1}^{MK} \left(\frac{1}{(\sigma_{\eta_i}^{-2R} \lambda_i^R d_i^R + 1)^2} + \frac{(\sigma_{\eta_i}^{-2R} \lambda_i^R)^2 d_i^R}{(\sigma_{\eta_i}^{-2R} \lambda_i^R d_i^R + 1)^2} \frac{\sigma_{\eta_i}^{2R}}{\lambda_i^R} \right) \tag{2.39}
\end{aligned}$$

where d_i^R s come from the optimum NMSE-based power allocation matrix \mathbf{D}^R for the LFS [c.f. (2.24)]:

$$d_i^R = \left[\gamma_{\text{NMSE}}^R \sqrt{\frac{\sigma_{\eta_i}^{2R}}{\lambda_i^R}} - \frac{\sigma_{\eta_i}^{2R}}{\lambda_i^R} \right]^+, \quad \forall i. \tag{2.40}$$

For target response and noise with arbitrary PSDs, we have:

$$\begin{aligned}
& \text{NMSE}(\mathbf{\Lambda}, \mathbf{\Sigma}_\eta; \mathbf{\Phi}^R, \mathbf{D}^R) \\
&= \text{tr} \left\{ \mathbb{E} \left\{ \mathbf{\Lambda}^{-\frac{1}{2}} (\mathbf{h} - \hat{\mathbf{h}}) (\mathbf{h} - \hat{\mathbf{h}})^{\mathcal{H}} \mathbf{\Lambda}^{-\frac{1}{2}} \right\} \right\} \\
&= \sum_{i=1}^{MK} \left(\frac{1}{(\sigma_{\eta_i}^{-2R} \lambda_i^R d_i^R + 1)^2} + \frac{(\sigma_{\eta_i}^{-2R} \lambda_i^R)^2 d_i^R}{(\sigma_{\eta_i}^{-2R} \lambda_i^R d_i^R + 1)^2} \frac{\sigma_{\eta_i}^2}{\lambda_i} \right). \tag{2.41}
\end{aligned}$$

As a result, the NMSE difference is given by:

$$\begin{aligned}
& \text{NMSE}(\mathbf{\Lambda}, \mathbf{\Sigma}_\eta; \mathbf{\Phi}^R, \mathbf{D}^R) - \text{NMSE}(\mathbf{\Lambda}^R, \mathbf{\Sigma}_\eta^R; \mathbf{\Phi}^R, \mathbf{D}^R) \\
&= \sum_{i=1}^{MK} \frac{(\sigma_{\eta_i}^{-2R} \lambda_i^R)^2 d_i^R}{(\sigma_{\eta_i}^{-2R} \lambda_i^R d_i^R + 1)^2} \left(\frac{\sigma_{\eta_i}^2}{\lambda_i} - \frac{\sigma_{\eta_i}^{2R}}{\lambda_i^R} \right). \tag{2.42}
\end{aligned}$$

Recall that our robust *minimax* designs based on MI, MMSE and NMSE criteria are described by the three inequalities in (2.31), respectively. Now with the specific expressions available in (2.32), (2.38) and (2.56), we will next find the LFS $(\mathbf{\Lambda}^R, \mathbf{\Sigma}_\eta^R)$

satisfying these inequalities.

2.4.2 Joint Robust Designs

We have seen in the preceding subsection that the robust transmitter and receiver designs \mathbf{D}^R and $\mathbf{\Phi}^R$ will be uniquely specified once the LFS is determined. The LFS is not only determined by the inequalities in (2.31), but also heavily dependent on the uncertainty model. In this subsection, we will consider separately two models allowing for uncertainty in both target and noise PSDs.

Uncertainty Model I:

In [66], a banded uncertainty model for the target PSD is considered: the exact target PSD is unknown, but lies within a band whose upper and lower bounds are known. Here, we adopt this model for both the target and noise; that is,

$$\lambda_i^L \leq \lambda_i \leq \lambda_i^U, \sigma_{\eta_i}^{2L} \leq \sigma_{\eta_i}^2 \leq \sigma_{\eta_i}^{2U}, \forall i. \quad (2.43)$$

Proposition 2.4 (LFS for Uncertainty Model I): *When the uncertain target and noise PSDs fall within the banded regions with known upper and lower limits and with no other constraint, the LFS for the joint robust designs consists of:*

- $\left(\{ \lambda_i^L \}_{i=1}^{MK}, \{ \sigma_{\eta_i}^{2U} \}_{i=1}^{MK} \right)$ for MI criterion;
- $\left(\{ \lambda_i^U \}_{i=1}^{MK}, \{ \sigma_{\eta_i}^{2U} \}_{i=1}^{MK} \right)$ for MMSE criterion; and
- $\left(\{ \lambda_i^L \}_{i=1}^{MK}, \{ \sigma_{\eta_i}^{2U} \}_{i=1}^{MK} \right)$ for NMSE criterion.

Proof. See Appendix 2-I. ■

We notice that the LFS for MI- and NMSE-based designs is identical, but differs from that of the MMSE-based design.

Uncertainty Model II:

In this model, we assume that the target PSD is known for simplicity and incorporate an average power ratio constraint on the noise PSD uncertainty; that is,

$$\sigma_{\eta_i}^{2L} \leq \sigma_{\eta_i}^2 \leq \sigma_{\eta_i}^{2U}, \quad \forall i, \quad \text{and} \quad \frac{1}{MK} \sum_i \frac{\sigma_{\eta_i}^2}{\lambda_i} = \rho. \quad (2.44)$$

Proposition 2.5 (LFS for Uncertainty Model II): *When the uncertain noise PSD falls within the banded region with known upper and lower limits under the average power ratio constraint, the LFS is given as follows:*

$$\sigma_{\eta_i}^{2R} = \begin{cases} \sigma_{\eta_i}^{2L}, & \text{if } \sigma_{\eta_i}^{2L} > k_n \lambda_i \\ \sigma_{\eta_i}^{2U}, & \text{if } \sigma_{\eta_i}^{2U} < k_n \lambda_i \\ k_n \lambda_i, & \text{otherwise} \end{cases} \quad (2.45)$$

for MI and NMSE criteria, and

$$\sigma_{\eta_i}^{2R} = \begin{cases} \sigma_{\eta_i}^{2L}, & \text{if } \sigma_{\eta_i}^{2L} > k_m \lambda_i^2 \\ \sigma_{\eta_i}^{2U}, & \text{if } \sigma_{\eta_i}^{2U} < k_m \lambda_i^2 \\ k_m \lambda_i^2, & \text{otherwise} \end{cases} \quad (2.46)$$

for MMSE criterion, where k_n and k_m (typically $k_n \neq k_m$) are constants ensuring the average power ratio constraint and the target PSD is assumed to be known.

Proof. See Appendix 2-II. ■

Proposition 2.5 is illustrated in Fig. 2.2. Under the average power ratio constraint, the MI and NMSE criteria again give rise to the same LFS. In fact, the LFS given by (2.45) is one where $\{\sigma_{\eta_i}^2/\lambda_i\}_i$ is made as flat as possible. This result is very intuitive since the worst interference PSD is the one that perfectly matches the target PSD.

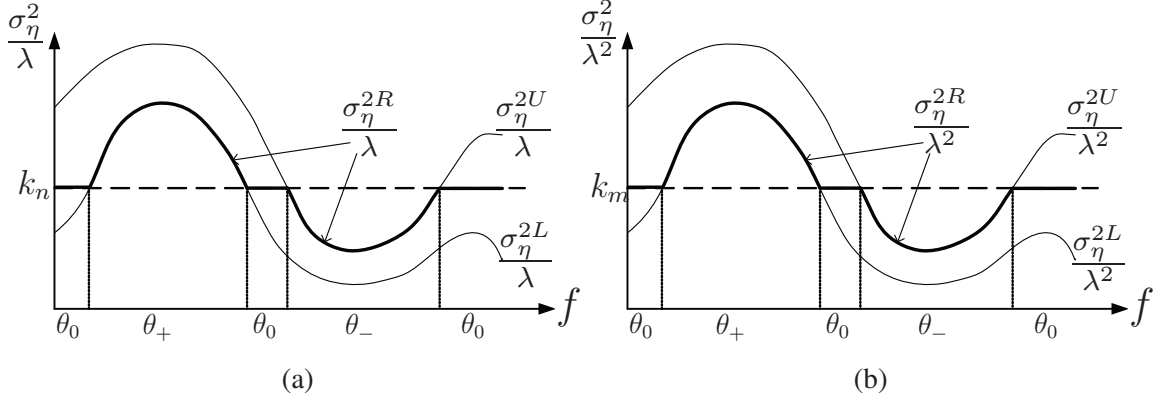


Figure 2.2: Illustration of the band model for noise PSD: (a) normalized by target PSD; and (b) normalized by target PSD square.

On the other hand, MMSE-based design suggests a different LFS where the noise PSD is maximumly matched to the target PSD square. This result is consistent with the NMSE-based one, considering that the latter is obtained by normalizing the MSE with respect to the target PSD.

2.5 Sensitivity Analysis of the Optimum Designs

Since the optimum waveform solutions rely on the perfect target and noise PSD knowledge assumption, a small target overestimation error may introduce considerable impact to the optimum designs. In order to address the robustness issue, the error sensitivity analysis needs to be performed not only at the transmitter in terms of the waveform design sensitivity, but also at the receiver in terms of the estimation performance sensitivity.

2.5.1 Waveform Design Sensitivity at the Transmitter

A single error mode accounting for the small overestimation error is considered in addition to the nominal modes. We have learnt from the Section 2.3 that the

weakest modes will be discarded due to the total power limit. Therefore, the strength ratio $\lambda_e/\sigma_{\eta_e}^2$ (for MI and NMSE) or $\lambda_e/\sqrt{\sigma_{\eta_e}^2}$ (for MMSE) of the overestimation error mode is a key parameter in the sensitivity analysis. If the error mode is so weak that the original optimum power allocation solution is not altered at all, then the estimation performance would not be affected either; otherwise, the performance will be degraded. We define the strength ratio $(\lambda_e/\sigma_{\eta_e}^2)_t$ or $(\lambda_e/\sqrt{\sigma_{\eta_e}^2})_t$ as the error mode strength threshold, above which the error mode is allocated certain transmit power. The power associated with the error mode is denoted as d_e .

Problem 2.1 *Suppose that an overestimation error mode with target strength λ_e and noise strength $\sigma_{\eta_e}^2$ appears in addition to the nominal modes. The waveform design sensitivity is measured by the strength threshold $(\lambda_e/\sigma_{\eta_e}^2)_t$ (for MI and NMSE) or $(\lambda_e/\sqrt{\sigma_{\eta_e}^2})_t$ (for MMSE), above which the original optimum power allocation solution for the nominal modes will be altered and $d_e > 0$. Then, for each criterion, one needs to find the highest tolerable strength of the error mode; that is, $(\lambda_e/\sigma_{\eta_e}^2)_t = \max \lambda_e/\sigma_{\eta_e}^2$ or $(\lambda_e/\sqrt{\sigma_{\eta_e}^2})_t = \max \lambda_e/\sqrt{\sigma_{\eta_e}^2}$, subject to $d_e = 0$.*

Next, the strength threshold will be computed for the MI, MMSE, and NMSE criteria, respectively, followed by the sensitivity comparison among the three criteria in terms of their strength thresholds.

2.5.1.1 Strength Threshold Calculation

MI-based: Suppose that the target is overestimated by an error mode with strength $\lambda_e/\sigma_{\eta_e}^2$. The transmit power allocated to the error mode can be *attemptedly* expressed as $d_e|_{\text{MI}} = \gamma_{\text{MI}}^e - \frac{\sigma_{\eta_e}^2}{\lambda_e}$ (c.f. (2.10)) with the altered water level (c.f. (2.14)):

$$\gamma_{\text{MI}}^e = \frac{\mathcal{P}_0 + \sum_{i \in \mathcal{S}_{\text{MI}}} \frac{\sigma_{\eta_i}^2}{\lambda_i} + \frac{\sigma_{\eta_e}^2}{\lambda_e}}{\|\mathcal{S}_{\text{MI}}\| + 1}. \quad (2.47)$$

According to Problem 2.1, one needs to find the largest power ratio $\lambda_e/\sigma_{\eta_e}^2$ such that $d_e = 0$, which gives rise to the condition

$$\frac{\mathcal{P}_0 + \sum_{i \in \mathcal{S}_{\text{MI}}} \frac{\sigma_{\eta_i}^2}{\lambda_i} + \frac{\sigma_{\eta_e}^2}{\lambda_e}}{\|\mathcal{S}_{\text{MI}}\| + 1} - \frac{\sigma_{\eta_e}^2}{\lambda_e} \leq 0.$$

After calculation, one can easily obtain $\lambda_e/\sigma_{\eta_e}^2 \leq 1/\gamma_{\text{MI}}$ and therefore the strength threshold:

$$\left(\lambda_e/\sigma_{\eta_e}^2\right)_t \Big|_{\text{MI}} = \frac{1}{\gamma_{\text{MI}}} \quad (2.48)$$

where γ_{MI} is the water level of the original optimum design given in (2.14).

MMSE-based: Likewise, the transmit power *potentially* allocated to the error mode based on the MMSE criterion can be written as $d_e|_{\text{MMSE}} = \gamma_{\text{MMSE}}^e \sqrt{\sigma_{\eta_e}^2} - \frac{\sigma_{\eta_e}^2}{\lambda_e}$ (c.f. (2.17)) with its altered water level (c.f. (2.21)):

$$\gamma_{\text{MMSE}}^e = \frac{\mathcal{P}_0 + \sum_{i \in \mathcal{S}_{\text{MMSE}}} \frac{\sigma_{\eta_i}^2}{\lambda_i} + \frac{\sigma_{\eta_e}^2}{\lambda_e}}{\sum_{i \in \mathcal{S}_{\text{MMSE}}} \sqrt{\sigma_{\eta_i}^2} + \sqrt{\sigma_{\eta_e}^2}}. \quad (2.49)$$

To ensure the requirement in Problem 2.1, i.e., $\frac{\mathcal{P}_0 + \sum_{i \in \mathcal{S}_{\text{MMSE}}} \frac{\sigma_{\eta_i}^2}{\lambda_i} + \frac{\sigma_{\eta_e}^2}{\lambda_e}}{\sum_{i \in \mathcal{S}_{\text{MMSE}}} \sqrt{\sigma_{\eta_i}^2} + \sqrt{\sigma_{\eta_e}^2}} \sqrt{\sigma_{\eta_e}^2} - \frac{\sigma_{\eta_e}^2}{\lambda_e} \leq 0$, the error mode strength should satisfy the condition of $\lambda_e/\sqrt{\sigma_{\eta_e}^2} \leq 1/\gamma_{\text{MMSE}}$ with the strength threshold

$$\left(\lambda_e/\sqrt{\sigma_{\eta_e}^2}\right)_t \Big|_{\text{MMSE}} = \frac{1}{\gamma_{\text{MMSE}}} \quad (2.50)$$

where γ_{MMSE} is the water level of the original optimum design given in (2.21).

NMSE-based: The allocated power to the error mode based on the NMSE criterion follows the structure $d_e|_{\text{NMSE}} = \gamma_{\text{NMSE}}^e \sqrt{\frac{\sigma_{\eta_e}^2}{\lambda_e}} - \frac{\sigma_{\eta_e}^2}{\lambda_e}$ (c.f. (2.24)) where the altered power allocation level can be expressed as (c.f. (2.28)):

$$\gamma_{\text{NMSE}}^e = \frac{\mathcal{P}_0 + \sum_{i \in \mathcal{S}_{\text{NMSE}}} \frac{\sigma_{\eta_i}^2}{\lambda_i} + \frac{\sigma_{\eta_e}^2}{\lambda_e}}{\sum_{i \in \mathcal{S}_{\text{NMSE}}} \sqrt{\frac{\sigma_{\eta_i}^2}{\lambda_i}} + \sqrt{\frac{\sigma_{\eta_e}^2}{\lambda_e}}}. \quad (2.51)$$

Then the error mode strength that is not sufficiently strong to acquire positive power allocation, i.e., $\frac{\mathcal{P}_0 + \sum_{i \in \mathcal{S}_{\text{NMSE}}} \frac{\sigma_{\eta_i}^2}{\lambda_i} + \frac{\sigma_{\eta_e}^2}{\lambda_e}}{\sum_{i \in \mathcal{S}_{\text{NMSE}}} \sqrt{\frac{\sigma_{\eta_i}^2}{\lambda_i}} + \sqrt{\frac{\sigma_{\eta_e}^2}{\lambda_e}}} \sqrt{\frac{\sigma_{\eta_e}^2}{\lambda_e}} - \frac{\sigma_{\eta_e}^2}{\lambda_e} \leq 0$, falls into the range $\lambda_e/\sigma_{\eta_e}^2 \leq 1/\gamma_{\text{NMSE}}^2$ with the error mode strength threshold:

$$(\lambda_e/\sigma_{\eta_e}^2)_t \Big|_{\text{NMSE}} = \frac{1}{\gamma_{\text{NMSE}}^2} \quad (2.52)$$

where γ_{NMSE} is the water level of the original NMSE-based optimum design given in (2.28) for the nominal modes.

Remarks: The error mode strength thresholds for the three criteria are all exclusively associated with their corresponding optimum water levels, which is quite reasonable. The physical interpretation of the water level is a means to prevent wasting power on the weakest modes given the total power constraint. As a result, only the error mode which is stronger than the original allocation level will be allocated nonzero power and change the original solution (and therefore the estimation performance for sure).

2.5.1.2 Strength Threshold Comparison

The relative magnitude of the error mode strength thresholds suggests the sensitivity comparison among the three criteria. The criterion which has the largest threshold is the one least sensitive to the overestimation error. Clearly, the three criteria exhibit different levels of sensitivity. In order to make a comparison, let us revisit the NMSE-based strength threshold, which can be explicitly written as:

$$\begin{aligned}
\left(\frac{\lambda_e}{\sigma_{\eta_e}^2}\right)_t \Big|_{\text{NMSE}} &= \frac{1}{\gamma_{\text{NMSE}}^2} = \left(\frac{\sum_{i \in \mathcal{S}_{\text{NMSE}}} \sqrt{\frac{\sigma_{\eta_i}^2}{\lambda_i}}}{\mathcal{P}_0 + \sum_{i \in \mathcal{S}_{\text{NMSE}}} \frac{\sigma_{\eta_i}^2}{\lambda_i}}\right)^2 \\
&\leq \frac{\sum_{i \in \mathcal{S}_{\text{NMSE}}} \sqrt{\frac{\sigma_{\eta_i}^2}{\lambda_i}}}{\mathcal{P}_0 + \sum_{i \in \mathcal{S}_{\text{NMSE}}} \frac{\sigma_{\eta_i}^2}{\lambda_i}} \leq \frac{\|\mathcal{S}_{\text{NMSE}}\|}{\mathcal{P}_0 + \sum_{i \in \mathcal{S}_{\text{NMSE}}} \frac{\sigma_{\eta_i}^2}{\lambda_i}} \approx \left(\frac{\lambda_e}{\sigma_{\eta_e}^2}\right)_t \Big|_{\text{MI}}
\end{aligned} \tag{2.53}$$

where the first inequality follows the straightforward fact that $\frac{\sum_{i \in \mathcal{S}_{\text{NMSE}}} \sqrt{\frac{\sigma_{\eta_i}^2}{\lambda_i}}}{\mathcal{P}_0 + \sum_{i \in \mathcal{S}_{\text{NMSE}}} \frac{\sigma_{\eta_i}^2}{\lambda_i}} < 1$, and the second inequality comes from that the average target-to-noise power ratio is typically no less than 1. As detailed in Section 2.3, although the power allocation solutions are implemented in distinct fashions, the difference of the mode index sets for the three criteria can be negligible, especially when the total available power is sufficiently high. Specifically, \mathcal{S}_{MI} and $\mathcal{S}_{\text{NMSE}}$ are almost the same except that $\mathcal{S}_{\text{NMSE}}$ may contain a few more weak modes, which establishes the last approximation in (2.53). Then, it can be easily deduced from (2.53) that in general the NMSE-based strength threshold is lower than the MI-based threshold, and therefore the NMSE-based optimum design is more vulnerable to the overestimation error compared to the MI-based one. This conclusion can also be appreciated from the optimization ideas behind these criteria. Since the NMSE criterion puts more effort (weights) than the MI to those weak modes, it is intuitively more apt to be affected by the weak error mode than the MI.

Since the MMSE-based strength threshold is expressed in a ratio form different from the MI- and NMSE-based thresholds, one cannot directly compare the ratios unless the specific error mode strength is known. A special case of interest can be obtained by normalizing the error noise mode to 1, and then compare the error target mode thresholds. Moreover, in the white noise case, it can be readily verified that the MMSE-based target strength threshold is the same as the MI-based one. Further

numerical comparison will be given in Section 2.6.

2.5.2 Estimation Performance Sensitivity at the Receiver

The explicit strength threshold formulae for the waveform design at the transmitter have been derived in the preceding subsection. A natural question now is how the estimation performance at the receiver would be affected once the error mode strength exceeds the threshold.

For comparison convenience and fairness, here we select the NMSE, denoted by ε , as the common performance indicator for all three criteria. One could also resort to MI or MMSE as the common indicator which will lead to the same results. We have the original NMSE performance (c.f. (2.23)):

$$\begin{aligned}
\varepsilon_{\text{MI}} &= \sum_{i=1}^{MK} \frac{1}{\sigma_{\eta_i}^{-2} \lambda_i [\gamma_{\text{MI}} - \frac{\sigma_{\eta_i}^2}{\lambda_i}] + 1} = \frac{1}{\gamma_{\text{MI}}} \sum_{i \in \mathcal{S}_{\text{MI}}} \frac{\sigma_{\eta_i}^2}{\lambda_i} + \|\bar{\mathcal{S}}_{\text{MI}}\|, \\
\varepsilon_{\text{MMSE}} &= \frac{1}{\gamma_{\text{MMSE}}} \sum_{i \in \mathcal{S}_{\text{MMSE}}} \frac{\sqrt{\sigma_{\eta_i}^2}}{\lambda_i} + \|\bar{\mathcal{S}}_{\text{MMSE}}\|, \\
\varepsilon_{\text{NMSE}} &= \frac{1}{\gamma_{\text{NMSE}}} \sum_{i \in \mathcal{S}_{\text{NMSE}}} \sqrt{\frac{\sigma_{\eta_i}^2}{\lambda_i}} + \|\bar{\mathcal{S}}_{\text{NMSE}}\|,
\end{aligned} \tag{2.54}$$

and the corresponding altered NMSE due to the error mode:

$$\begin{aligned}
\varepsilon_{\text{MI}}^e &= \frac{1}{\gamma_{\text{MI}}^e} \sum_{i \in \mathcal{S}_{\text{MI}}} \frac{\sigma_{\eta_i}^2}{\lambda_i} + \|\bar{\mathcal{S}}_{\text{MI}}\|, \\
\varepsilon_{\text{MMSE}}^e &= \frac{1}{\gamma_{\text{MMSE}}^e} \sum_{i \in \mathcal{S}_{\text{MMSE}}} \frac{\sqrt{\sigma_{\eta_i}^2}}{\lambda_i} + \|\bar{\mathcal{S}}_{\text{MMSE}}\|, \\
\varepsilon_{\text{NMSE}}^e &= \frac{1}{\gamma_{\text{NMSE}}^e} \sum_{i \in \mathcal{S}_{\text{NMSE}}} \sqrt{\frac{\sigma_{\eta_i}^2}{\lambda_i}} + \|\bar{\mathcal{S}}_{\text{NMSE}}\|.
\end{aligned} \tag{2.55}$$

It should be stressed that we are interested in the small overestimation disturbance to the optimum waveform design and it is thus sufficient to take into account only the

weak error mode which cannot alter the mode index sets. As a result, for a particular criterion, the original and altered NMSEs are only different in the water level terms.

Remarks: Consider the altered water levels given in (2.47), (2.49) and (2.51) for the MI, MMSE and NMSE criteria, respectively. We notice that the water levels are affected the most around the strength thresholds, and interestingly, the effect is diminishing along with the increase of the error mode strength. Accordingly, the NMSE variation, namely the difference between the altered and original NMSEs, will be reduced in the presence of relatively strong error mode.

As the second terms in (2.54) and (2.55) are the same for a specific criterion, it is convenient to measure the variation of the NMSE performance by the normalized difference of the first terms in (2.55) and (2.54), i.e.,

$$\Delta\varepsilon_i = \frac{\varepsilon_i^e(1) - \varepsilon_i(1)}{\varepsilon_i(1)} = \frac{\gamma_i - \gamma_i^e}{\gamma_i^e}, i \in \{\text{MI, MMSE, NMSE}\}. \quad (2.56)$$

In simulations we will still use both terms in (2.55) for the NMSE performance comparison to corroborate the validity of the $\Delta\varepsilon_i$ measure.

Problem 2.2 *Suppose that there is an error mode whose strength exceeds the strength threshold given either in (2.48), (2.50) or (2.52), for the MI, MMSE, or NMSE criterion, respectively. The problem is to calculate $\Delta\varepsilon_i$ defined in (2.56) for each criterion and use this measure to compare the performance sensitivity among the three criteria.*

2.5.2.1 NMSE Performance Variation Calculation

MI-based: With γ_{MI} given in (2.14) and γ_{MI}^e given in (2.47), we can evaluate (2.56) for the MI criterion:

$$\Delta\varepsilon_{\text{MI}} = \frac{\frac{1}{\|\mathcal{S}_{\text{MI}}\|} \left(\mathcal{P}_0 + \sum_{i \in \mathcal{S}_{\text{MI}}} \frac{\sigma_{\eta_i}^2}{\lambda_i} \right) - \frac{\sigma_{\eta_e}^2}{\lambda_e}}{\mathcal{P}_0 + \sum_{i \in \mathcal{S}_{\text{MI}}} \frac{\sigma_{\eta_i}^2}{\lambda_i} + \frac{\sigma_{\eta_e}^2}{\lambda_e}}. \quad (2.57)$$

MMSE-based: With γ_{MMSE} given in (2.21) and γ_{MMSE}^e given in (2.49), the MMSE-based NMSE variation measure is:

$$\Delta\epsilon_{\text{MMSE}} = \frac{\frac{1}{\sum_{i \in \mathcal{S}_{\text{MMSE}}} \sqrt{\sigma_{\eta_i}^2 / \sigma_{\eta_e}^2}} \left(\mathcal{P}_0 + \sum_{i \in \mathcal{S}_{\text{MMSE}}} \frac{\sigma_{\eta_i}^2}{\lambda_i} \right) - \frac{\sigma_{\eta_e}^2}{\lambda_e}}{\mathcal{P}_0 + \sum_{i \in \mathcal{S}_{\text{MMSE}}} \frac{\sigma_{\eta_i}^2}{\lambda_i} + \frac{\sigma_{\eta_e}^2}{\lambda_e}}. \quad (2.58)$$

NMSE-based: Likewise, the NMSE variation measure for the NMSE criterion given γ_{NMSE} in (2.28) and γ_{NMSE}^e in (2.51) has the following form:

$$\Delta\epsilon_{\text{NMSE}} = \frac{\frac{1}{\sum_{i \in \mathcal{S}_{\text{NMSE}}} \sqrt{\frac{\lambda_e}{\sigma_{\eta_e}^2} / \frac{\lambda_i}{\sigma_{\eta_i}^2}}} \left(\mathcal{P}_0 + \sum_{i \in \mathcal{S}_{\text{NMSE}}} \frac{\sigma_{\eta_i}^2}{\lambda_i} \right) - \frac{\sigma_{\eta_e}^2}{\lambda_e}}{\mathcal{P}_0 + \sum_{i \in \mathcal{S}_{\text{NMSE}}} \frac{\sigma_{\eta_i}^2}{\lambda_i} + \frac{\sigma_{\eta_e}^2}{\lambda_e}}. \quad (2.59)$$

2.5.2.2 NMSE Performance Variation Comparison

Now we are ready to compare the NMSE performance sensitivity in terms of $\Delta\epsilon_i$ among the three criteria. Again, the mode index set difference is negligible. The major difference among (2.57), (2.58) and (2.59) lies in the first fractions in the numerators. Therefore, the performance sensitivity analysis amounts to the comparison of these fractions.

The three fractions are all different, suggesting that the sensitivity levels of the three criteria are different. The fraction for the MI is a constant irrelevant to the error mode strength, whereas the NMSE-based fraction is decided by the average strength ratio between the error mode and the nominal modes. Specifically, since we only care about small disturbances, the error mode strength $\lambda_e / \sigma_{\eta_e}^2$ for NMSE is typically smaller than the average nominal mode strength. Therefore, the denominator of the first fraction in the numerator of (2.59) satisfies $\sum_{i \in \mathcal{S}_{\text{NMSE}}} \sqrt{\frac{\lambda_e}{\sigma_{\eta_e}^2} / \frac{\lambda_i}{\sigma_{\eta_i}^2}} < \|\mathcal{S}_{\text{NMSE}}\| \approx \|\mathcal{S}_{\text{MI}}\|$, resulting in $\Delta\epsilon_{\text{NMSE}} > \Delta\epsilon_{\text{MI}}$. This means that the NMSE-based design would experience more performance variation than the MI-based one. As the error mode

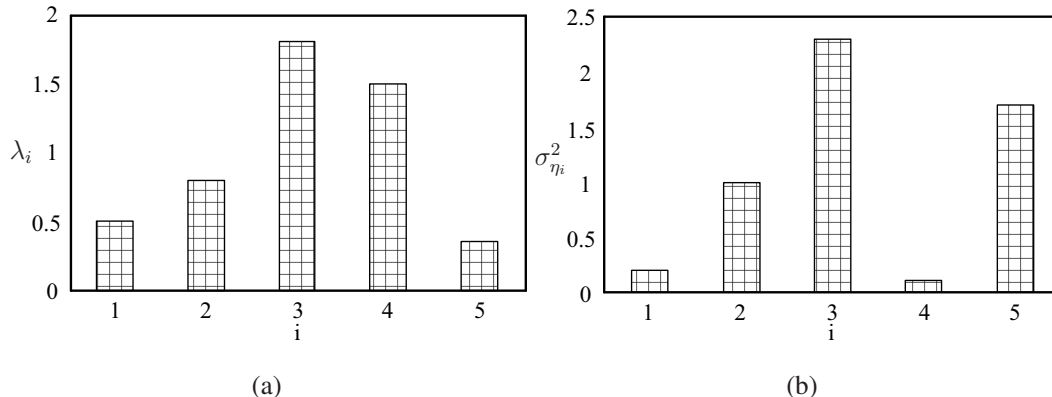


Figure 2.3: (a) Target mode PSD; and (b) noise PSD.

grows, however, $\sum_{i \in \mathcal{S}_{\text{NMSE}}} \sqrt{\frac{\lambda_e}{\sigma_{\eta_e}^2} / \frac{\lambda_i}{\sigma_{\eta_i}^2}}$ approaches $\|\mathcal{S}_{\text{NMSE}}\|$ and the variation difference shrinks. The MMSE-based performance variation relies on the average ratio of the error to nominal noise modes. Some special cases may provide more insights of the comparison. For instance, in the white noise case, the MI and MMSE would have the same sensitivity level, and the NMSE is relatively more sensitive to the error.

2.6 Simulations

In this section, we provide simulation results to verify our analytical conclusions and to provide further comparisons among the MI, MMSE and NMSE criteria.

2.6.1 Optimum Power Allocation in Colored Noise

In this simulation, we consider an extended target described by five modes. Fig. 2.3 gives the target and noise PSDs $\{\lambda_i\}$ and $\{\sigma_{\eta_i}^2\}$, for $i = 1, \dots, 5$. The total power constraint is $\mathcal{P}_0 = 10$ dB. Fig. 2.4 shows the optimum power allocation schemes for all three criteria in the presence of colored noise. Recall that under the assumption of white Gaussian noise, the MMSE and MI criteria lead to the same water-filling power

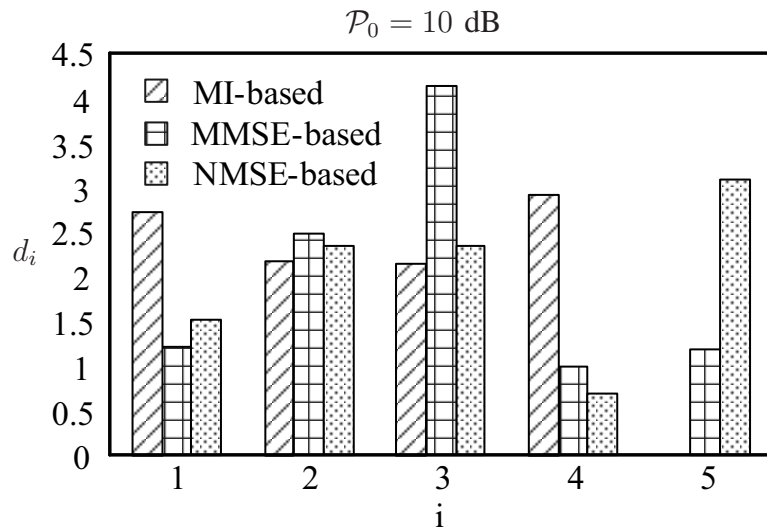


Figure 2.4: Optimum power allocation schemes based on three criteria: MI, MMSE and NMSE.

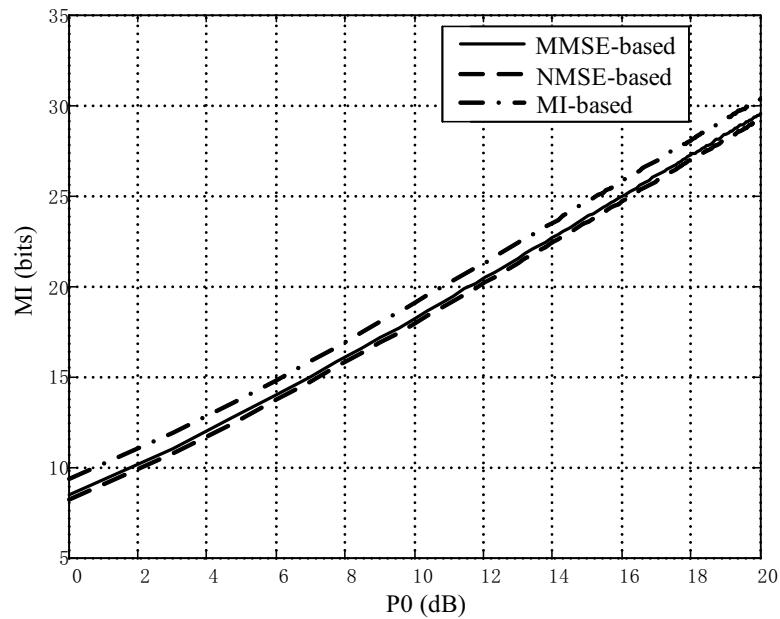


Figure 2.5: MI performance of the optimum power allocation schemes.

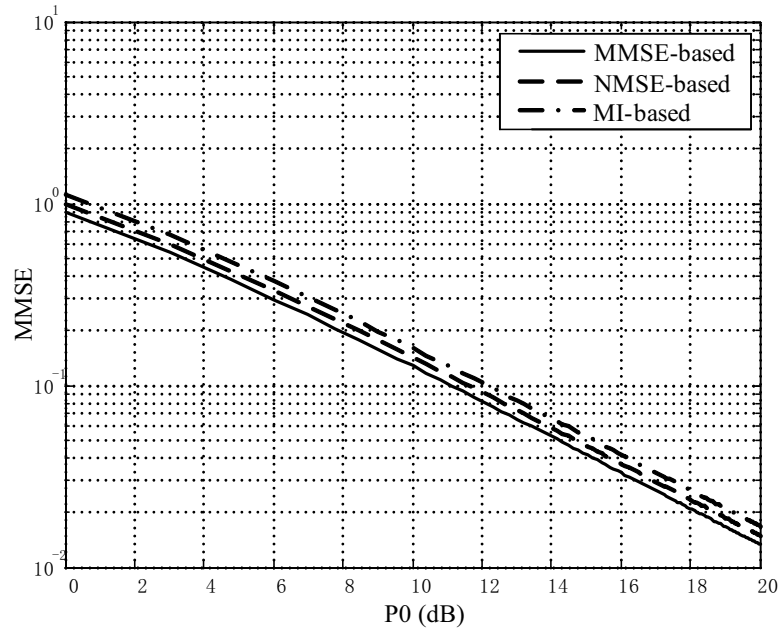


Figure 2.6: MMSE performance of the optimum power allocation schemes.

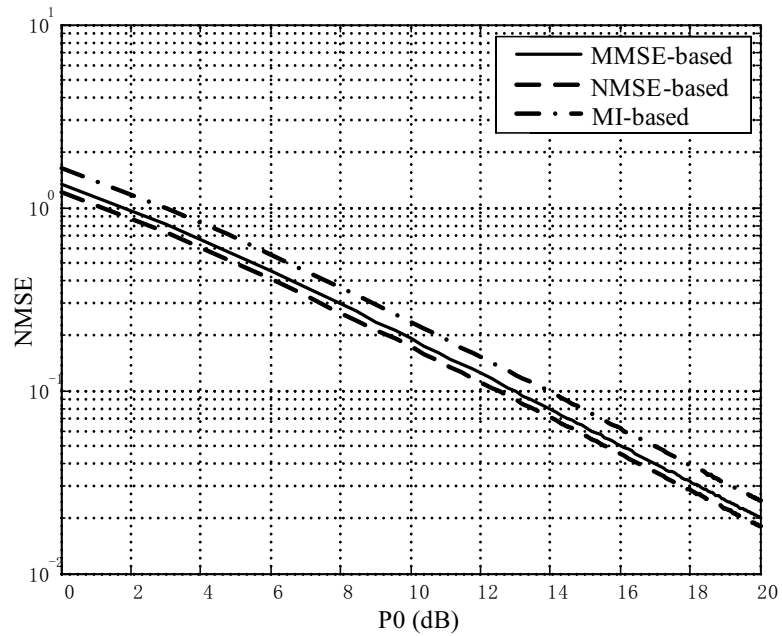


Figure 2.7: NMSE performance of the optimum power allocation schemes.

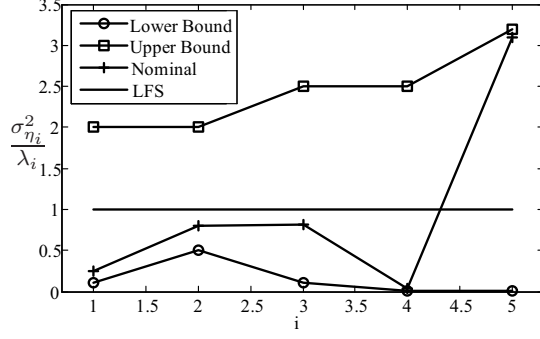
allocation [65]. In colored noise, however, we can see from the figure that while the MI-based solution remains water-filling, the MMSE-based is not. In addition, they are both different from the NMSE-based solution. In terms of the optimum power allocation under the colored noise, no connection between the MSEs and the MI is observed.

The performance curves are plotted in Figs. 2.5, 2.6 and 2.7 for the three merits (MI, MMSE, and NMSE) based on the three criteria. Evidently, in terms of MI performance, the MI-based design is optimum, while the MMSE- and NMSE- based designs both exhibit performance losses. Similar observations can be made for the MMSE and NMSE performance. These results agree well with our analysis that all the criteria are different in the presence of colored noise.

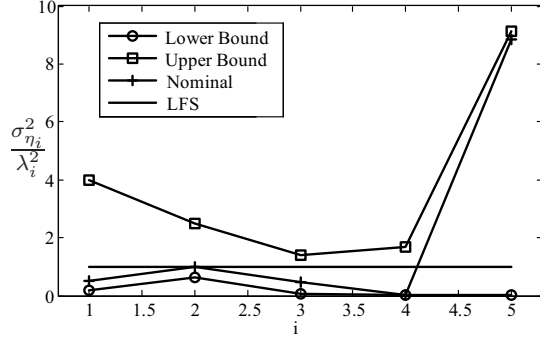
2.6.2 Joint Estimator and Power Allocation Robust Design

Since the LFS for the robust design with uncertainty model I is straightforward, here we will only verify the case with uncertainty model II. The target PSD is assumed to be available as shown in Fig. 2.3(a). Uncertainty in the colored noise normalized by target PSD $\{\lambda_i\}_i$ is modeled as in Fig. 2.8(a), which has upper bound $\{\sigma_{\eta_i}^{2U}/\lambda_i\}_i$ and lower bound $\{\sigma_{\eta_i}^{2L}/\lambda_i\}_i$ subject to the average power ratio constraint $\rho = 1$. The same noise uncertainty normalized by target PSD square $\{\lambda_i^2\}_i$ is given in Fig. 2.8(b). A set of arbitrary nominal values is randomly chosen to make performance comparisons.

The MI and NMSE criteria share the identical normalized noise LFS, which is supposed to be as flat as possible. In Fig. 2.8(a), when the constant $k_n = 1$, the straight line lies between the upper and lower bounds. According to the MI and NMSE criteria, the normalized noise LFS which satisfies the average power ratio constraint should be $\sigma_{\eta_i}^{2R}/\lambda_i = 1, \forall i$. For MMSE criterion, on the other hand, the straight line $k_m = 5\rho \sum_i \lambda_i = 1.0101$ is lying between its corresponding upper and



(a)



(b)

Figure 2.8: Noise PSD uncertainty band model: (a) normalized by target PSD for the MI and NMSE criteria; and (b) normalized by target PSD square for the MMSE criterion.

lower bounds in Fig. 2.8(b). Therefore the noise LFS for the MMSE criterion is $\sigma_{\eta_i}^{2R}/\lambda_i^2 = 1.0101, \forall i$.

We plot the MMSE, NMSE and MI curves in Figs. 2.9, 2.10 and 2.11, respectively, to show how the robust design optimizes the worst case scenario. There are four curves for each case: A) nominal PSD with nominal design, which is the best achievable performance if there is no uncertainty; B) LFS PSD with nominal design, which is the case when one assumes the nominal PSD in design but encounters the LFS scenario; C) LFS PSD with robust design, which indicates the worst-case performance for the robust design; and D) nominal PSD with robust design, which corresponds to the actual performance when the nominal PSD is applied but the robust design is used. For MMSE and NMSE criteria, large gaps between B (LFS PSD with nominal

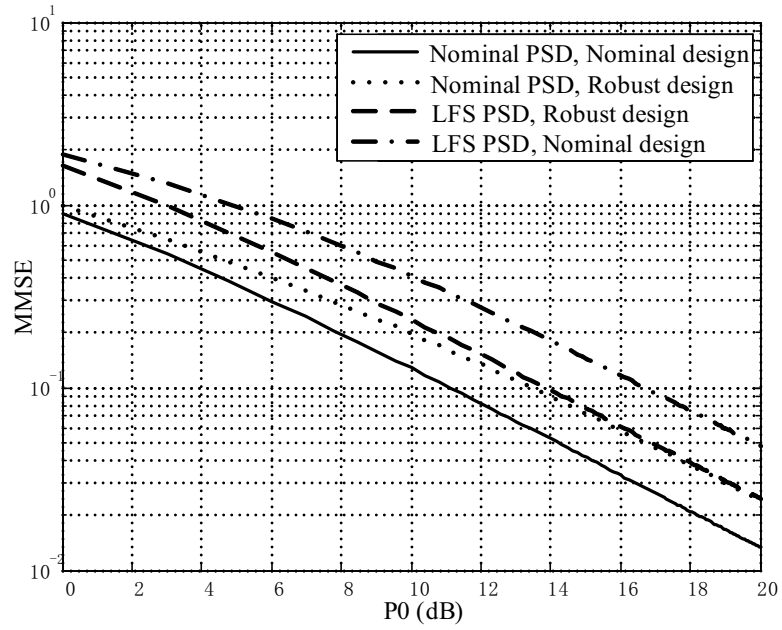


Figure 2.9: MMSE performance for the robust designs.

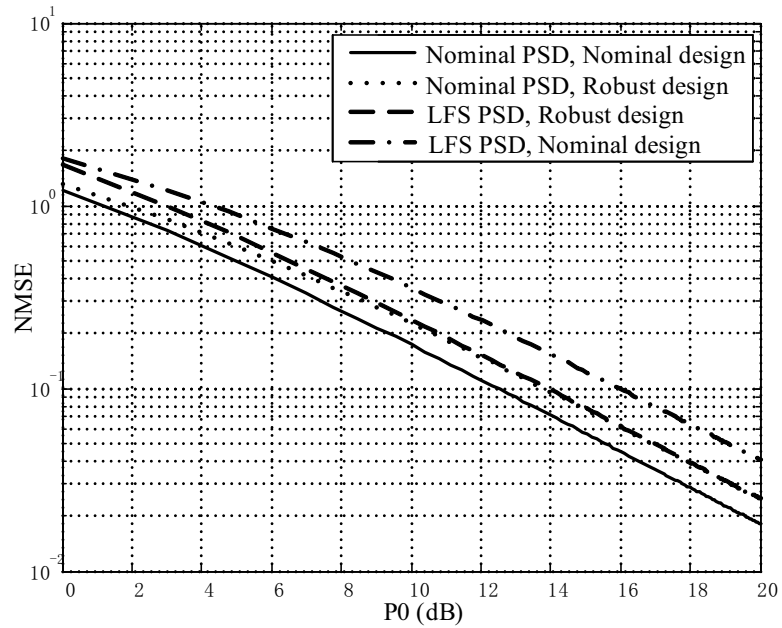


Figure 2.10: NMSE performance for the robust designs.

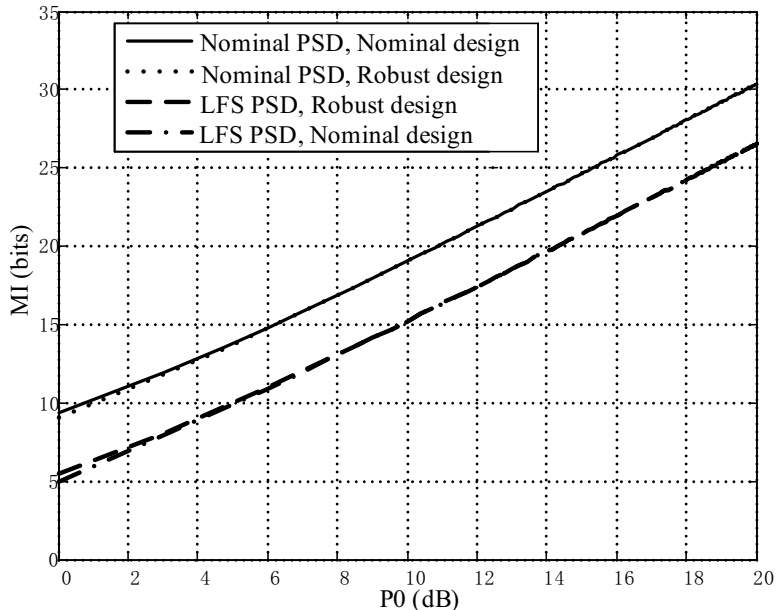


Figure 2.11: MI performance for the robust designs.

design) curves and C (LFS PSD with robust design) curves illustrate the significant improvement provided by the robust design for the worst case. This “best worst case” performance provides a performance lower bound. That is, for any PSD within the uncertainty region, the performance cannot be worse than this lower bound. This is evidenced by the D (nominal PSD with robust design) curves, which are bounded by C (LFS PSD with robust design) curves. For the MI-based design, we see that the performance is mainly determined by the actual PSD (nominal or LFS) but hardly affected by the power allocation design (nominal or robust), especially at high SNR. To find an explanation for this, let us go back to the power allocation scheme $d_i = \left[\gamma_{\text{MI}} - \frac{\sigma_{n_i}^2}{\lambda_i} \right]^+$ [c.f. (2.10)]. Subject to the average power ratio constraint ρ , the water-filling level $\gamma_{\text{MI}} = \frac{\mathcal{P}_0 + MK\rho}{MK}$ is the same for any possible PSD. Especially when \mathcal{P}_0 is large, d_i is dominated by γ_{MI} and remains pretty much the same for both nominal and robust designs. That is the reason why the difference of the MI performance comes mainly from the different PSDs, but not from the different designs. We can remark that the robust design does not help much in this case. Despite the small

quantitative improvement, Fig. 2.11 confirms that the robust design does improve the LFS performance as well as push up the MI lower bound.

2.6.3 Comparison of Sensitivity to the Overestimation Errors

In this section, we provide the numerical results to verify our sensitivity analysis and to provide further comparisons among the MI, MMSE and NMSE criteria.

We consider the same extended target described by five modes as Section 2.6.1, with the nominal target PSD $\{\lambda_i\}_i = \{0.5, 0.8, 1.8, 1.5, 0.35\}$ and noise PSD $\{\sigma_{\eta_i}^2\}_i = \{0.2, 1, 2.3, 0.1, 1.7\}$. The total power constraint is $\mathcal{P}_0 = 10$ dB. Fig. 2.4 shows the optimum power allocation solutions for all three criteria. It can be observed that the 5th mode is discarded by the MI-based scheme, preserved by the MMSE-based scheme, but emphasized by the NMSE-based one. The mode index sets $\mathcal{S}_{\text{MI}} = \{1, 2, 3, 4\}$ and $\mathcal{S}_{\text{MMSE}} = \mathcal{S}_{\text{NMSE}} = \{1, 2, 3, 4, 5\}$. If the error noise mode strength is normalized to 1, we can calculate the error target mode strength thresholds from (2.48), (2.50) and (2.52) for the MI, MMSE and NMSE criteria, respectively; that is, $\lambda_{e_t}|_{\text{MI}} = 1/\gamma_{\text{MI}} = 0.3078$, $\lambda_{e_t}|_{\text{MMSE}} = 1/\gamma_{\text{MMSE}} = 0.2568$, and $\lambda_{e_t}|_{\text{NMSE}} = 1/\gamma_{\text{NMSE}}^2 = 0.0896$. Obviously, the NMSE-based threshold is much lower than the MI-based one, which confirms that the NMSE-based waveform design is more sensitive to the overestimation error. In this example, the MMSE-based design is less sensitive than NMSE but not as robust as the MI. The validity of the strength thresholds can be further verified in Fig. 2.12, where the error target mode strength is 0.2 within the range of $(\lambda_{e_t}|_{\text{NMSE}}, \lambda_{e_t}|_{\text{MMSE}})$ in (a) and 0.32 larger than $\lambda_{e_t}|_{\text{MI}}$ in (b). As a result, only the most sensitive NMSE-based solution allocates nonzero power to the error mode in (a), while all three solutions allocate nonzero power to the error mode in (b).

The NMSE performance variation is also compared among the three criteria in Figs. 2.13 – 2.15, where the error noise mode strength is normalized to 1. For

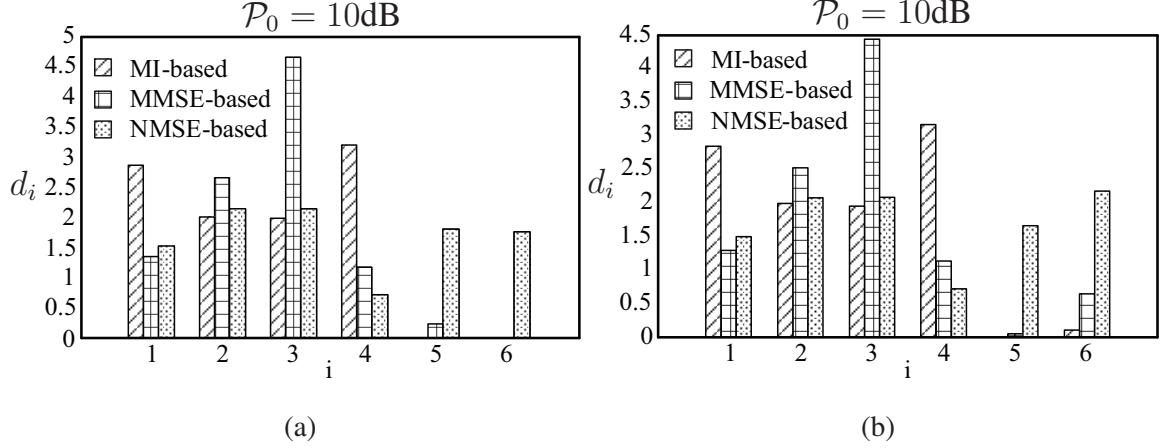


Figure 2.12: Altered power allocation solutions: (a) $\lambda_e = 0.2$; and (b) $\lambda_e = 0.32$.

each criterion, three curves are plotted, namely the blue solid curve for the original NMSE performance, the red dash-dot curve for the altered NMSE performance in the presence of weak error mode $\lambda_e = 0.032$, and the green dashed curve for a stronger error mode $\lambda_e = 0.32$. For the weak error strength $\lambda_e = 0.032$ satisfying the average strength ratio $\sum_{i \in \mathcal{S}_{\text{NMSE}}} \sqrt{\frac{\lambda_e}{\sigma_{\eta_e}^2}} / \frac{\lambda_i}{\sigma_{\eta_i}^2} = 0.9558 < \|\mathcal{S}_{\text{MI}}\|$ (see (2.57) and (2.59)), a larger NMSE variation of the NMSE-based system than that of the MI-based system can be clearly observed from the red dash-dot curves in Figs. 2.13 and 2.14. On the other hand, we have $\sum_{i \in \mathcal{S}_{\text{MMSE}}} \sqrt{\sigma_{\eta_i}^2 / \sigma_{\eta_e}^2} = 4.5839$ close to $\|\mathcal{S}_{\text{MI}}\|$ (see (2.58)), which explains why the MI- and MMSE-based designs have the similar red dash-dot curves shown in Figs. 2.14 and 2.15. Additionally, with a larger error target mode $\lambda_e = 0.32$, the green dashed curves confirm that all three criteria do not exhibit significant NMSE performance deterioration, as predicted by our theoretical analysis. Notice also that the increasing total power does not help reduce the NMSE performance variation. It is the error mode strength itself that does matter.

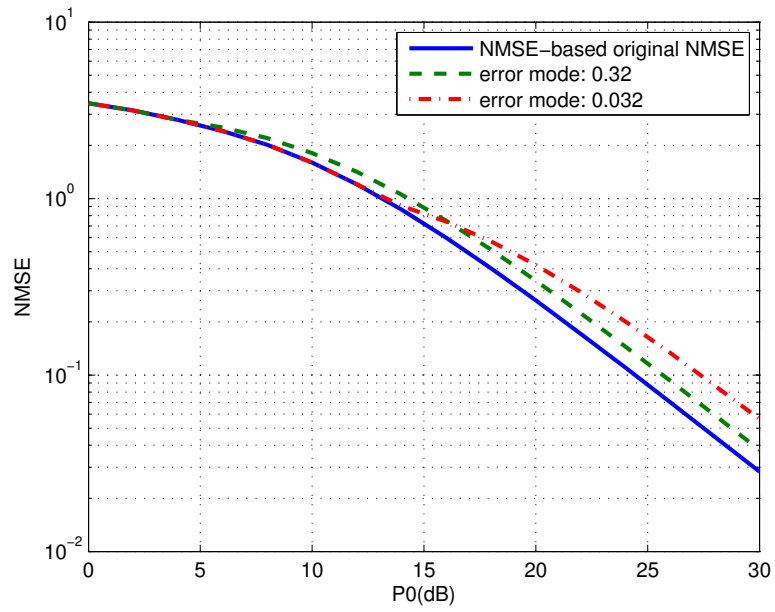


Figure 2.13: The NMSE-based NMSE performance variation.

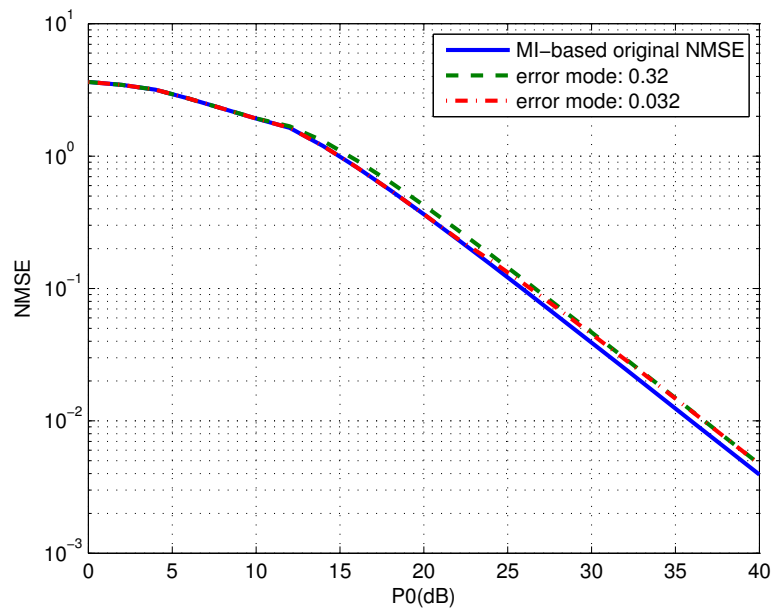


Figure 2.14: The MI-based NMSE performance variation.

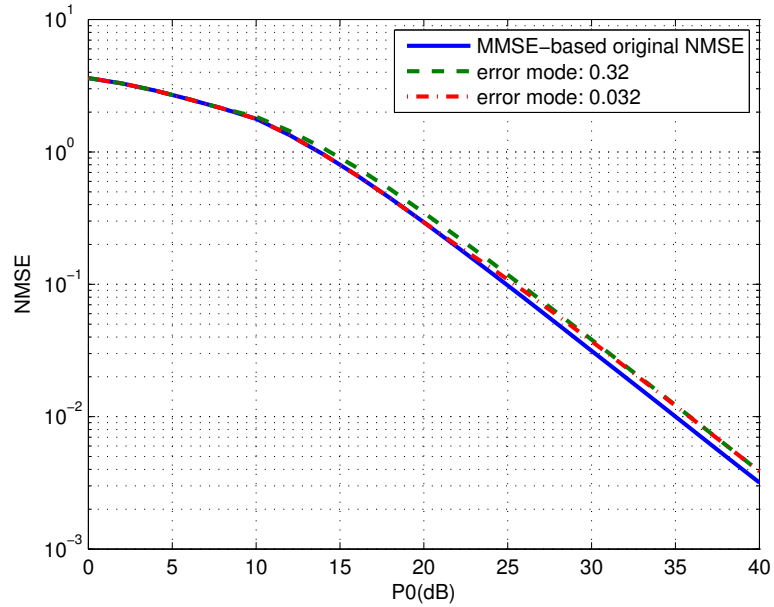


Figure 2.15: The MMSE-based NMSE performance variation.

2.7 Conclusions

In this chapter, we studied the optimum waveform design problem for target parameter estimation. Different from existing works, we considered a mixed MIMO radar setup for which the waveform optimization problem is meaningful, took into account the colored noise, incorporated the NMSE as a design criterion in addition to the MI and MMSE, and derived joint robust designs for both the transmitter (waveforms) and the receiver (estimator) under various uncertainty models. The analytical and numerical results suggest that: i) the equivalence between the MI and MMSE criteria does not hold when the noise is colored; and ii) compared to MMSE criterion, the NMSE criterion seems to share more similarities with the MI. In particular, they lead to identical LFS in the robust designs under various uncertainty models, while the MMSE criterion always suggests otherwise.

Additionally, we analyzed the sensitivity of the optimum designs based all three

criteria, at both the transmitter side (in terms of the waveform optimization solution) and the receiver side (in terms of the estimation NMSE performance). We derived the explicit formulae for the strength thresholds of the single error mode and made the performance variation comparison among the three criteria. The analysis shows that: i) all three criteria do not show significant performance deterioration; ii) the NMSE-based design is more sensitive to the overestimation error than the MI-based design around the error mode strength threshold; and iii) in the special white noise case, the MI- and MMSE-based optimum designs result in identical sensitivity level and both are less sensitive than the NMSE-based design.

Appendix 2-I: Proof of Proposition 2.4

For MI-based robust designs, (2.32) is non-negative if $\frac{\lambda_i}{\sigma_{\eta_i}^2} \geq \frac{\lambda_i^R}{\sigma_{\eta_i}^{2R}}, \forall i$. This suggests that the LFS should consist of $\lambda_i^R = \lambda_i^L$ and $\sigma_{\eta_i}^{2R} = \sigma_{\eta_i}^{2U}, \forall i$; For MMSE-based robust designs, (2.38) is non-positive as long as $\lambda_i \leq \lambda_i^R$ and $\sigma_{\eta_i}^2 \leq \sigma_{\eta_i}^{2R}, \forall i$. Hence the LFS contains $\lambda_i^R = \lambda_i^U$ and $\sigma_{\eta_i}^{2R} = \sigma_{\eta_i}^{2U}, \forall i$. For NMSE-based robust designs, (2.56) will be non-positive if $\frac{\sigma_{\eta_i}^2}{\lambda_i} \leq \frac{\sigma_{\eta_i}^{2R}}{\lambda_i^R}, \forall i$. That is, the LFS is $\lambda_i^R = \lambda_i^L$ and $\sigma_{\eta_i}^{2R} = \sigma_{\eta_i}^{2U}, \forall i$.

Appendix 2-II: Proof of Proposition 2.5

To prove Proposition 2.5, we will validate that the given LFSs in (2.45) for the MI and NMSE criteria or in (2.46) for the MMSE criterion satisfy the inequality conditions in (2.31).

We first define the following sets of the mode index i for convenience, as marked

in Fig. 2.2(a):

$$\begin{cases} \theta_0 \doteq \left\{ i \in \{1, \dots, MK\} : \frac{\sigma_{\eta_i}^{2L}}{\lambda_i} \leq k_n \leq \frac{\sigma_{\eta_i}^{2U}}{\lambda_i} \right\} \\ \theta_+ \doteq \left\{ i \in \{1, \dots, MK\} : \frac{\sigma_{\eta_i}^{2L}}{\lambda_i} > k_n \right\} \\ \theta_- \doteq \left\{ i \in \{1, \dots, MK\} : \frac{\sigma_{\eta_i}^{2U}}{\lambda_i} < k_n \right\} \end{cases} \quad (2.60)$$

where θ_0 , θ_+ and θ_- form a partition of the whole set of index i . Particularly, on the θ_+ set $\sigma_{\eta_i}^{2R} = \sigma_{\eta_i}^{2L}$, and therefore $\frac{\sigma_{\eta_i}^2}{\lambda_i} \geq \frac{\sigma_{\eta_i}^{2R}}{\lambda_i}$; on the θ_- set $\sigma_{\eta_i}^{2R} = \sigma_{\eta_i}^{2U}$ and therefore $\frac{\sigma_{\eta_i}^2}{\lambda_i} \leq \frac{\sigma_{\eta_i}^{2R}}{\lambda_i}$; and the set θ_0 can be further divided into two subsets $\theta_0^+ = \left\{ i \in \theta_0 : \frac{\sigma_{\eta_i}^2}{\lambda_i} \geq \frac{\sigma_{\eta_i}^{2R}}{\lambda_i} \right\}$ and $\theta_0^- = \left\{ i \in \theta_0 : \frac{\sigma_{\eta_i}^2}{\lambda_i} < \frac{\sigma_{\eta_i}^{2R}}{\lambda_i} \right\}$.

NMSE-based: We substitute (2.40) into (2.56) and let $\lambda_i^R = \lambda_i$ (due to the known target PSD assumption):

$$\begin{aligned} & \text{NMSE}(\mathbf{\Lambda}, \mathbf{\Sigma}_\eta; \mathbf{\Phi}^R, \mathbf{D}^R) - \text{NMSE}(\mathbf{\Lambda}, \mathbf{\Sigma}_\eta^R; \mathbf{\Phi}^R, \mathbf{D}^R) \\ &= \sum_{i=1}^{MK} \frac{\left(\frac{\lambda_i}{\sigma_{\eta_i}^{2R}}\right)^2 \left[\gamma_{\text{NMSE}}^R \sqrt{\frac{\sigma_{\eta_i}^{2R}}{\lambda_i} - \frac{\sigma_{\eta_i}^{2R}}{\lambda_i}} \right]^+}{\left(\frac{\lambda_i}{\sigma_{\eta_i}^{2R}} \left[\gamma_{\text{NMSE}}^R \sqrt{\frac{\sigma_{\eta_i}^{2R}}{\lambda_i} - \frac{\sigma_{\eta_i}^{2R}}{\lambda_i}} \right]^+ + 1 \right)^2} \left(\frac{\sigma_{\eta_i}^2}{\lambda_i} - \frac{\sigma_{\eta_i}^{2R}}{\lambda_i} \right). \end{aligned} \quad (2.61)$$

Next, we will evaluate (2.61) in three different cases.

Case 1: $d_i^R > 0, \forall i$. This means that we can remove the “+” sign in (2.61) and simplify it to:

$$\begin{aligned} & \text{NMSE}(\mathbf{\Lambda}, \mathbf{\Sigma}_\eta; \mathbf{\Phi}^R, \mathbf{D}^R) - \text{NMSE}(\mathbf{\Lambda}, \mathbf{\Sigma}_\eta^R; \mathbf{\Phi}^R, \mathbf{D}^R) \\ &= \sum_{i=1}^{MK} \frac{\gamma_{\text{NMSE}}^R \sqrt{\frac{\lambda_i}{\sigma_{\eta_i}^{2R}} - 1}}{(\gamma_{\text{NMSE}}^R)^2} \left(\frac{\sigma_{\eta_i}^2}{\lambda_i} - \frac{\sigma_{\eta_i}^{2R}}{\lambda_i} \right) \end{aligned} \quad (2.62)$$

Define $\Delta = \frac{\gamma_{\text{NMSE}}^R \sqrt{\frac{\lambda_i}{\sigma_{\eta_i}^{2R}} - 1}}{(\gamma_{\text{NMSE}}^R)^2}$. As observed in Fig. 2.2(a), for all $i \in \theta_0$, $\frac{\sigma_{\eta_i}^{2R}}{\lambda_i} = k_n$, and thus $\Delta = \frac{\gamma_{\text{NMSE}}^R \sqrt{\frac{1}{k_n} - 1}}{(\gamma_{\text{NMSE}}^R)^2} \doteq c$ remains a constant. Hence the summation in (2.62) over

set θ_0 is:

$$\sum_{i \in \theta_0} \frac{\gamma_{\text{NMSE}}^R \sqrt{\frac{\lambda_i}{\sigma_{\eta_i}^{2R}} - 1}}{(\gamma_{\text{NMSE}}^R)^2} \left(\frac{\sigma_{\eta_i}^2}{\lambda_i} - \frac{\sigma_{\eta_i}^{2R}}{\lambda_i} \right) = c \sum_{i \in \theta_0} \left(\frac{\sigma_{\eta_i}^2}{\lambda_i} - \frac{\sigma_{\eta_i}^{2R}}{\lambda_i} \right). \quad (2.63)$$

For all $i \in \theta_+$, $\frac{\sigma_{\eta_i}^2}{\lambda_i} - \frac{\sigma_{\eta_i}^{2R}}{\lambda_i} \geq 0$, $\frac{\sigma_{\eta_i}^{2R}}{\lambda_i} > k_n$, and thus $\Delta < c$. So the summation in (2.62) over set θ_+ satisfies

$$\sum_{i \in \theta_+} \frac{\gamma_{\text{NMSE}}^R \sqrt{\frac{\lambda_i}{\sigma_{\eta_i}^{2R}} - 1}}{(\gamma_{\text{NMSE}}^R)^2} \left(\frac{\sigma_{\eta_i}^2}{\lambda_i} - \frac{\sigma_{\eta_i}^{2R}}{\lambda_i} \right) \leq c \sum_{i \in \theta_+} \left(\frac{\sigma_{\eta_i}^2}{\lambda_i} - \frac{\sigma_{\eta_i}^{2R}}{\lambda_i} \right). \quad (2.64)$$

For all $i \in \theta_-$, $\frac{\sigma_{\eta_i}^2}{\lambda_i} - \frac{\sigma_{\eta_i}^{2R}}{\lambda_i} \leq 0$, $\frac{\sigma_{\eta_i}^{2R}}{\lambda_i} < k_n$, and hence $\Delta > c$. We can obtain the summation over set θ_- as:

$$\sum_{i \in \theta_-} \frac{\gamma_{\text{NMSE}}^R \sqrt{\frac{\lambda_i}{\sigma_{\eta_i}^{2R}} - 1}}{(\gamma_{\text{NMSE}}^R)^2} \left(\frac{\sigma_{\eta_i}^2}{\lambda_i} - \frac{\sigma_{\eta_i}^{2R}}{\lambda_i} \right) \leq c \sum_{i \in \theta_-} \left(\frac{\sigma_{\eta_i}^2}{\lambda_i} - \frac{\sigma_{\eta_i}^{2R}}{\lambda_i} \right). \quad (2.65)$$

Adding up (2.63), (2.64) and (2.65) will give us the right hand side of (2.62) as the following:

$$\sum_{i=1}^{MK} \frac{\gamma_{\text{NMSE}}^R \sqrt{\frac{\lambda_i}{\sigma_{\eta_i}^{2R}} - 1}}{(\gamma_{\text{NMSE}}^R)^2} \left(\frac{\sigma_{\eta_i}^2}{\lambda_i} - \frac{\sigma_{\eta_i}^{2R}}{\lambda_i} \right) \leq c \sum_{i=1}^{MK} \left(\frac{\sigma_{\eta_i}^2}{\lambda_i} - \frac{\sigma_{\eta_i}^{2R}}{\lambda_i} \right) = 0$$

where the last equality holds due to the average power ratio constraint. In other words, (2.62) becomes:

$$\text{NMSE}(\mathbf{\Lambda}, \mathbf{\Sigma}_\eta; \mathbf{\Phi}^R, \mathbf{D}^R) - \text{NMSE}(\mathbf{\Lambda}, \mathbf{\Sigma}_\eta^R; \mathbf{\Phi}^R, \mathbf{D}^R) \leq 0. \quad (2.66)$$

Case 2: Some $d_i^R = 0$ on part of the θ_+ set where the weakest modes reside. This happens when the weakest modes are discarded due to the total power constraint. Proof for this case is the same as Case 1 for $i \in \theta_0$ and $i \in \theta_-$. The only difference

occurs for those $i \in \theta_+$, where (2.64) become

$$\begin{aligned} & \sum_{i \in \{\theta_+ \& d_i^R > 0\}} \frac{\gamma_{\text{NMSE}}^R \sqrt{\frac{\lambda_i}{\sigma_{\eta_i}^{2R}} - 1}}{(\gamma_{\text{NMSE}}^R)^2} \left(\frac{\sigma_{\eta_i}^2}{\lambda_i} - \frac{\sigma_{\eta_i}^{2R}}{\lambda_i} \right) \\ & \leq c \sum_{i \in \{\theta_+ \& d_i^R > 0\}} \left(\frac{\sigma_{\eta_i}^2}{\lambda_i} - \frac{\sigma_{\eta_i}^{2R}}{\lambda_i} \right) \leq c \sum_{i \in \theta_+} \left(\frac{\sigma_{\eta_i}^2}{\lambda_i} - \frac{\sigma_{\eta_i}^{2R}}{\lambda_i} \right). \end{aligned} \quad (2.67)$$

This case can be easily extended to $d_i^R = 0$ on the whole θ_+ set and part of the θ_0^+ subset.

Case 3: The total power is very limited so that $d_i^R = 0$, for all $i \in \theta_+ \cup \theta_0^+$ and for some $i \in \theta_0^-$ or even $i \in \theta_-$. In this case, (2.61) becomes:

$$\begin{aligned} & \text{NMSE}(\mathbf{\Lambda}, \mathbf{\Sigma}_\eta; \mathbf{\Phi}^R, \mathbf{D}^R) - \text{NMSE}(\mathbf{\Lambda}, \mathbf{\Sigma}_\eta^R; \mathbf{\Phi}^R, \mathbf{D}^R) \\ & = \sum_{i \in \{(\theta_0^- \cup \theta_-) \& d_i^R > 0\}} \frac{\left(\frac{\lambda_i}{\sigma_{\eta_i}^{2R}} \right)^2 d_i^R}{\left(\frac{\lambda_i}{\sigma_{\eta_i}^{2R}} d_i^R + 1 \right)^2} \left(\frac{\sigma_{\eta_i}^2}{\lambda_i} - \frac{\sigma_{\eta_i}^{2R}}{\lambda_i} \right) \leq 0. \end{aligned} \quad (2.68)$$

Summarizing all three cases, we have verified that the LFS for NMSE criterion in (2.45) satisfies the inequality condition in (2.31).

MI-based: Substitute (2.33) into (2.32), let $\lambda_i^R = \lambda_i$ due to the known target PSD

assumption, and exchange the order of the difference. Then (2.32) becomes:

$$\begin{aligned}
& \text{MI}(\Lambda, \Sigma_\eta^R; \mathbf{D}^R) - \text{MI}(\Lambda, \Sigma_\eta; \mathbf{D}^R) \\
&= \sum_{i=1}^{MK} \log \frac{\frac{\lambda_i}{\sigma_{\eta_i}^{2R}} d_i^R + 1}{\frac{\lambda_i}{\sigma_{\eta_i}^2} d_i^R + 1} = \frac{1}{\ln 2} \sum_{i=1}^{MK} \log_e \frac{\frac{\sigma_{\eta_i}^2}{\lambda_i} d_i^R + \frac{\sigma_{\eta_i}^2}{\lambda_i} \frac{\sigma_{\eta_i}^{2R}}{\lambda_i}}{\frac{\sigma_{\eta_i}^{2R}}{\lambda_i} d_i^R + \frac{\sigma_{\eta_i}^2}{\lambda_i} \frac{\sigma_{\eta_i}^{2R}}{\lambda_i}} \\
&\leq \frac{1}{\ln 2} \sum_{i=1}^{MK} \left(\frac{\frac{\sigma_{\eta_i}^2}{\lambda_i} d_i^R + \frac{\sigma_{\eta_i}^2}{\lambda_i} \frac{\sigma_{\eta_i}^{2R}}{\lambda_i}}{\frac{\sigma_{\eta_i}^{2R}}{\lambda_i} d_i^R + \frac{\sigma_{\eta_i}^2}{\lambda_i} \frac{\sigma_{\eta_i}^{2R}}{\lambda_i}} - 1 \right) \\
&= \frac{1}{\ln 2} \sum_{i=1}^{MK} \frac{\left(\frac{\sigma_{\eta_i}^2}{\lambda_i} - \frac{\sigma_{\eta_i}^{2R}}{\lambda_i} \right) \left[\gamma_{\text{MI}}^R \frac{\lambda_i}{\sigma_{\eta_i}^{2R}} - 1 \right]^+}{\left[\gamma_{\text{MI}}^R - \frac{\sigma_{\eta_i}^{2R}}{\lambda_i} \right]^+ + \frac{\sigma_{\eta_i}^2}{\lambda_i}}. \tag{2.69}
\end{aligned}$$

Similar to the NMSE-based proof, on the set partition θ_0 , θ_+ and θ_- , we need to evaluate (2.69) for LFS in three different cases.

Case 1: $d_i^R > 0, \forall i$. This means that we can remove the “+” sign in (2.69):

$$\begin{aligned}
& \text{MI}(\Lambda, \Sigma_\eta^R; \mathbf{D}^R) - \text{MI}(\Lambda, \Sigma_\eta; \mathbf{D}^R) \\
&= \frac{1}{\ln 2} \sum_{i=1}^{MK} \frac{\left(\frac{\sigma_{\eta_i}^2}{\lambda_i} - \frac{\sigma_{\eta_i}^{2R}}{\lambda_i} \right) \left(\gamma_{\text{MI}}^R \frac{\lambda_i}{\sigma_{\eta_i}^{2R}} - 1 \right)}{\gamma_{\text{MI}}^R + \left(\frac{\sigma_{\eta_i}^2}{\lambda_i} - \frac{\sigma_{\eta_i}^{2R}}{\lambda_i} \right)}. \tag{2.70}
\end{aligned}$$

Define $\Delta = \frac{\gamma_{\text{MI}}^R \frac{\lambda_i}{\sigma_{\eta_i}^{2R}} - 1}{\gamma_{\text{MI}}^R}$. As observed in Fig. 2.2(a), for all $i \in \theta_0$, $\frac{\sigma_{\eta_i}^{2R}}{\lambda_i} = k_n$, and thus $\Delta = \frac{\gamma_{\text{MI}}^R \frac{1}{k_n} - 1}{\gamma_{\text{MI}}^R} \doteq c$ remains a constant. Hence the summation in (2.70) over set θ_0 is

$$\begin{aligned}
& \frac{1}{\ln 2} \sum_{i \in \theta_0} \frac{\left(\frac{\sigma_{\eta_i}^2}{\lambda_i} - \frac{\sigma_{\eta_i}^{2R}}{\lambda_i} \right) \left(\gamma_{\text{MI}}^R \frac{\lambda_i}{\sigma_{\eta_i}^{2R}} - 1 \right)}{\gamma_{\text{MI}}^R + \left(\frac{\sigma_{\eta_i}^2}{\lambda_i} - \frac{\sigma_{\eta_i}^{2R}}{\lambda_i} \right)} \\
&\leq \frac{1}{\ln 2} \sum_{i \in \theta_0} \frac{\left(\frac{\sigma_{\eta_i}^2}{\lambda_i} - \frac{\sigma_{\eta_i}^{2R}}{\lambda_i} \right) \left(\gamma_{\text{MI}}^R \frac{\lambda_i}{\sigma_{\eta_i}^{2R}} - 1 \right)}{\gamma_{\text{MI}}^R} \\
&= \frac{c}{\ln 2} \sum_{i \in \theta_0} \left(\frac{\sigma_{\eta_i}^2}{\lambda_i} - \frac{\sigma_{\eta_i}^{2R}}{\lambda_i} \right). \tag{2.71}
\end{aligned}$$

For all $i \in \theta_+$, $\frac{\sigma_{\eta_i}^2}{\lambda_i} - \frac{\sigma_{\eta_i}^{2R}}{\lambda_i} \geq 0$, $\frac{\sigma_{\eta_i}^{2R}}{\lambda_i} > k_n$, and thus $\Delta < c$. So the summation in (2.62) over set θ_+ satisfies

$$\begin{aligned}
& \frac{1}{\ln 2} \sum_{i \in \theta_+} \frac{\left(\frac{\sigma_{\eta_i}^2}{\lambda_i} - \frac{\sigma_{\eta_i}^{2R}}{\lambda_i}\right) \left(\gamma_{\text{MI}}^R \frac{\lambda_i}{\sigma_{\eta_i}^{2R}} - 1\right)}{\gamma_{\text{MI}}^R + \left(\frac{\sigma_{\eta_i}^2}{\lambda_i} - \frac{\sigma_{\eta_i}^{2R}}{\lambda_i}\right)} \\
& \leq \frac{1}{\ln 2} \sum_{i \in \theta_+} \frac{\left(\frac{\sigma_{\eta_i}^2}{\lambda_i} - \frac{\sigma_{\eta_i}^{2R}}{\lambda_i}\right) \left(\gamma_{\text{MI}}^R \frac{\lambda_i}{\sigma_{\eta_i}^{2R}} - 1\right)}{\gamma_{\text{MI}}^R} \\
& \leq \frac{c}{\ln 2} \sum_{i \in \theta_+} \left(\frac{\sigma_{\eta_i}^2}{\lambda_i} - \frac{\sigma_{\eta_i}^{2R}}{\lambda_i}\right). \tag{2.72}
\end{aligned}$$

For all $i \in \theta_-$, $\frac{\sigma_{\eta_i}^2}{\lambda_i} - \frac{\sigma_{\eta_i}^{2R}}{\lambda_i} \leq 0$, $\frac{\sigma_{\eta_i}^{2R}}{\lambda_i} < k_n$, and hence $\Delta > c$. We can obtain the summation over set θ_- as:

$$\begin{aligned}
& \frac{1}{\ln 2} \sum_{i \in \theta_-} \frac{\left(\frac{\sigma_{\eta_i}^2}{\lambda_i} - \frac{\sigma_{\eta_i}^{2R}}{\lambda_i}\right) \left(\gamma_{\text{MI}}^R \frac{\lambda_i}{\sigma_{\eta_i}^{2R}} - 1\right)}{\gamma_{\text{MI}}^R + \left(\frac{\sigma_{\eta_i}^2}{\lambda_i} - \frac{\sigma_{\eta_i}^{2R}}{\lambda_i}\right)} \\
& \leq \frac{1}{\ln 2} \sum_{i \in \theta_-} \frac{\left(\frac{\sigma_{\eta_i}^2}{\lambda_i} - \frac{\sigma_{\eta_i}^{2R}}{\lambda_i}\right) \left(\gamma_{\text{MI}}^R \frac{\lambda_i}{\sigma_{\eta_i}^{2R}} - 1\right)}{\gamma_{\text{MI}}^R} \\
& \leq \frac{c}{\ln 2} \sum_{i \in \theta_-} \left(\frac{\sigma_{\eta_i}^2}{\lambda_i} - \frac{\sigma_{\eta_i}^{2R}}{\lambda_i}\right). \tag{2.73}
\end{aligned}$$

Adding up (2.71), (2.72) and (2.73) will give us the right hand side of (2.70) as the following:

$$\frac{1}{\ln 2} \sum_{i=1}^{MK} \frac{\left(\frac{\sigma_{\eta_i}^2}{\lambda_i} - \frac{\sigma_{\eta_i}^{2R}}{\lambda_i}\right) \left(\gamma_{\text{MI}}^R \frac{\lambda_i}{\sigma_{\eta_i}^{2R}} - 1\right)}{\gamma_{\text{MI}}^R + \left(\frac{\sigma_{\eta_i}^2}{\lambda_i} - \frac{\sigma_{\eta_i}^{2R}}{\lambda_i}\right)} \leq \frac{c}{\ln 2} \sum_{i=1}^{MK} \left(\frac{\sigma_{\eta_i}^2}{\lambda_i} - \frac{\sigma_{\eta_i}^{2R}}{\lambda_i}\right) = 0,$$

where the last equality holds due to the average power ratio constraint. In other

words, (2.70) becomes:

$$\text{MI}(\mathbf{\Lambda}, \mathbf{\Sigma}_\eta^R; \mathbf{D}^R) - \text{MI}(\mathbf{\Lambda}, \mathbf{\Sigma}_\eta; \mathbf{D}^R) \leq 0. \quad (2.74)$$

Due to the space limit, here we only give the simple but tedious proof for Case 1 to illustrate the similarity and difference from the NMSE-based proof. Case 2 and Case 3 can be readily derived by analogy, which all result in the inequality condition $\text{MI}(\mathbf{\Lambda}, \mathbf{\Sigma}_\eta^R; \mathbf{D}^R) - \text{MI}(\mathbf{\Lambda}, \mathbf{\Sigma}_\eta; \mathbf{D}^R) \leq 0$.

MMSE-based: A new partition should be defined for the mode index i based on the MMSE criterion, as marked in Fig. 2.2(b):

$$\begin{cases} \vartheta_0 \doteq \left\{ i \in \{1, \dots, MK\} : \frac{\sigma_{\eta_i}^{2L}}{\lambda_i^2} \leq k_m \leq \frac{\sigma_{\eta_i}^{2U}}{\lambda_i^2} \right\} \\ \vartheta_+ \doteq \left\{ i \in \{1, \dots, MK\} : \frac{\sigma_{\eta_i}^{2L}}{\lambda_i^2} > k_m \right\} \\ \vartheta_- \doteq \left\{ i \in \{1, \dots, MK\} : \frac{\sigma_{\eta_i}^{2U}}{\lambda_i^2} < k_m \right\} \end{cases}. \quad (2.75)$$

Similar to the NMSE- and MI- based cases, this new partition has the following property: $\forall i \in \vartheta_+$, $\sigma_{\eta_i}^{2R} = \sigma_{\eta_i}^{2L}$, and therefore $\frac{\sigma_{\eta_i}^2}{\lambda_i^2} \geq \frac{\sigma_{\eta_i}^{2R}}{\lambda_i^2}$; $\forall i \in \vartheta_-$, $\sigma_{\eta_i}^{2R} = \sigma_{\eta_i}^{2U}$ and therefore $\frac{\sigma_{\eta_i}^2}{\lambda_i^2} \leq \frac{\sigma_{\eta_i}^{2R}}{\lambda_i^2}$; and the set ϑ_0 can be further divided into two subsets $\vartheta_0^+ = \left\{ i \in \vartheta_0 : \frac{\sigma_{\eta_i}^2}{\lambda_i^2} \geq \frac{\sigma_{\eta_i}^{2R}}{\lambda_i^2} \right\}$ and $\vartheta_0^- = \left\{ i \in \vartheta_0 : \frac{\sigma_{\eta_i}^2}{\lambda_i^2} < \frac{\sigma_{\eta_i}^{2R}}{\lambda_i^2} \right\}$.

Substituting (2.34) into (2.38) and letting $\lambda_i^R = \lambda_i$, we will obtain:

$$\begin{aligned}
& \text{MMSE}(\mathbf{\Lambda}, \mathbf{\Sigma}_\eta; \mathbf{\Phi}^R, \mathbf{D}^R) - \text{MMSE}(\mathbf{\Lambda}, \mathbf{\Sigma}_\eta^R; \mathbf{\Phi}^R, \mathbf{D}^R) \\
&= \sum_{i=1}^{MK} \frac{\left(\frac{\lambda_i}{\sigma_{\eta_i}^{2R}}\right)^2 \lambda_i \left[\gamma_{\text{MMSE}}^R \sqrt{\frac{\sigma_{\eta_i}^{2R}}{\lambda_i^2} - \frac{\sigma_{\eta_i}^{2R}}{\lambda_i}}\right]^+}{\left(\frac{\lambda_i}{\sigma_{\eta_i}^{2R}} \left[\gamma_{\text{MMSE}}^R \sqrt{\sigma_{\eta_i}^{2R} - \frac{\sigma_{\eta_i}^{2R}}{\lambda_i}}\right]^+ + 1\right)^2} (\sigma_{\eta_i}^2 - \sigma_{\eta_i}^{2R}) \\
&= \sum_{i=1}^{MK} \frac{\left(\frac{\lambda_i}{\sigma_{\eta_i}^{2R}}\right)^2 \lambda_i^2 \left[\gamma_{\text{MMSE}}^R \sqrt{\frac{\sigma_{\eta_i}^{2R}}{\lambda_i^2} - \frac{\sigma_{\eta_i}^{2R}}{\lambda_i}}\right]^+}{\left(\frac{\lambda_i}{\sigma_{\eta_i}^{2R}} \left[\gamma_{\text{MMSE}}^R \sqrt{\sigma_{\eta_i}^{2R} - \frac{\sigma_{\eta_i}^{2R}}{\lambda_i}}\right]^+ + 1\right)^2} \left(\frac{\sigma_{\eta_i}^2}{\lambda_i} - \frac{\sigma_{\eta_i}^{2R}}{\lambda_i}\right). \tag{2.76}
\end{aligned}$$

On analogy of the NMSE proof, for MMSE-based LFS to be (2.46), the proof amounts to bounding (2.76) on the three sets ϑ_0 , ϑ_+ and ϑ_- . The procedure is similar to the one used for the NMSE proof and will be omitted here.

CHAPTER 3

ML TOA ESTIMATION OF IR UWB SIGNALS FOR TARGET LOCALIZATION

Rapid and accurate timing synchronization is the first and foremost task in ultra-wideband (UWB) systems. The data-aided timing with dirty templates (TDT) algorithm introduced in [64] is a promising method with low complexity and relaxed operation conditions in the presence of unknown time hopping and multipath channel. Its optimality, however, remains unexplored. In this chapter, we develop the practical maximum-likelihood (ML) timing algorithm and obtain its optimum training sequence. We show that the optimum training sequence of the ML timing estimator coincides with that of the TDT algorithm. In addition, we prove that, using this training sequence, the ML algorithm can be simplified, and that the simplified ML (SML) is equivalent to TDT.

3.1 Motivation

Location awareness is rapidly becoming an essential feature of many commercial, public service, and military wireless networks. Information collected or communicated by a wireless node is often meaningful only in conjunction with knowledge of the node's location [60]. Location-aware wireless networks have broad applications covering from 911 emergency services [8] to asset tracking [24], from health monitoring [7] to intelligent transportation.

For a large scale sensor network, it is impossible to include a global position-

ing system (GPS) receiver on each device, as it is cost and energy prohibitive, not sufficiently robust to jamming for military applications, and limited to outdoor applications. Instead, we consider the localization problem in which some small number of sensors, referred to as base stations/anchors/beacons/reference nodes, can obtain their coordinates through GPS and the rest unknown-location nodes, referred to as mobiles/agents/targets, must determine their own coordinates.

The localization process typically consists of two phases: measurement phase and location update phase. During the first phase, targets obtain signal measurements based on direct communication with neighboring anchors and/or targets. In the second phase, the targets can infer their locations based on the signal measurements and the location information of the neighboring nodes. For distanced-based localization schemes, if a target node can obtain at least three measurements from its neighbors, its location can be estimated through trilateration.

The most popular distance measurement methods are based on Received Signal Strength (RSS) and Time-Of-Arrival (TOA) metrics [51]. RSS based techniques measure the power of the signal at the receiver. Based on the known transmit power, the effective propagation loss can be calculated. Theoretical and empirical models are used to translate this loss into a distance estimate. On the other hand, TOA based methods can translate the propagation time directly into distance, given the signal propagation speed. RSS and TOA give the range information that is used by the trilateration technique. For the time based localization, in the absence of the common time base, Time-Difference-Of-Arrival (TDOA) is used instead of TOA and leads to the hyperbolic localization.

The underlying transmission technology is a critical factor in the estimate accuracy for various distance measurement methods. Ultrawide bandwidth (UWB) signals exhibit prominent features, enabling the UWB systems inherently well suited for

localization. UWB can access Giga Hertz (GHz) level bandwidth by either transmitting nanosecond-wide pulses or the aggregation of subband signals each with bandwidth over 500MHz. These correspond to two UWB transmission approaches, namely impulse radio (IR) and multi-band orthogonal frequency division multiplexing (MB-OFDM). The desired capabilities of UWB resulted from utilization of ultrawide bandwidth include fine delay resolution, simple implementation for multiple-access communications, and obstacle penetration capabilities [60].

RSS is not very suitable for UWB localization, because the RSS approach does not benefit from the huge bandwidth of UWB [26]. Therefore, time based localization is the most widely adopted solution for UWB systems such as the IEEE 802.15.4a low rate WPAN [1].

Traditionally, the targets are only allowed to communicate with the anchors. In the second location update phase, once the target obtain sufficient distance measurements, i.e., three for two-dimensional and four for three-dimensional setup, from the anchors within transmission range, its location can be estimated. An emerging localization mode allows communications between the unknown-location target nodes, which is known as cooperative localization. In general, cooperative localization can dramatically increase localization performance in terms of both accuracy and coverage [60, 51, 47].

In this chapter, we focus on the first distance measurement phase based on TOA estimation using UWB signals. UWB technology exhibits prominent features in many wireless communications, networking and localization applications. Since the ultra-short pulse waveform is transmitted at very low power in UWB systems [63, 58], accurate and rapid timing estimation becomes one of the most critical challenges.

Without invoking impractical assumptions as in several UWB timing research (see e.g., [22, 29, 38]) such as known multipath propagation, timing with dirty tem-

plates (TDT) algorithms developed in [64] are feasible for realistic UWB settings. The most attractive merits of TDT include its low complexity and applicability in narrowband and wideband systems with a single user or multiple ones as long as the intersymbol interference (ISI) is absent or avoided. In [64], both the non-data-aided and data-aided modes are investigated by searching the maximum cross correlation of successive symbol-long received segments. The training sequence used in [64] for data-aided TDT has a repeated pattern $\{+1, +1, -1, -1\}$, with which the data-aided TDT can achieve very rapid acquisition by using as few as four training symbols. More recently, its digital counterparts are investigated in [61], which shows that the digital TDT algorithms remain effective even with very-low-resolution digital UWB receivers. Despite all these appealing advantages, the optimality issue of TDT has never been thoroughly explored.

In this chapter, we address this issue via the establishment of a data-aided maximum likelihood (ML) timing algorithm. Based on the ML criterion, the estimation of all multipath gains and delays was pursued in [43] and the estimation performance was analyzed in [13]. However, [43] is based on an unrealistic multipath channel model which assumes no inter-path overlapping. The real channel with a large number of dense taps would make this method impossible to implement. Unlike [43], we focus on the estimation of a single parameter, namely, the delay of the first arriving path, without invoking any unrealistic channel model assumption. We will show that although our ML estimator does not explicitly involve the channel information, it is able to collect multipath energy without channel estimation.

Considering the ML acquisition performance in terms of the probability of detection, we obtain the *unique* optimum training pattern in the sense of acquisition speed and consistency. By using this optimum training sequence, the ML algorithm can be simplified. Interestingly, we will show that the simplified ML (SML) and TDT

estimators share the identical optimum training sequence and estimation operations. Furthermore, it can be proved that the criterion and performance of the TDT algorithm are essentially the same as those of the SML algorithm. These lead to the conclusion that the data-aided TDT algorithm is ML optimum.

Fine timing with high accuracy is not only desired in communications [54], but also critical to localization with UWB technology [27, 28, 16]. While the data-aided SML and TDT estimators can theoretically achieve any resolution level, from the consideration of practical environment, they may suffer from the ambiguity induced by the weak tail of the multipath channel and the extent of the noise-only region between consecutive symbols. To circumvent the ambiguity, we complement the SML and TDT algorithms with one more step by searching the peak of the first-order difference of the objective functions, which facilitates the SML and TDT comparison at the chip-level fine timing.

The rest of the chapter is organized as follows. Section 3.2 outlines the signal model for impulse radio UWB systems. In Section 3.3, we will develop the ML timing algorithm and its acquisition performance in terms of probability of detection. In Section 3.4, the optimum training sequence pattern is derived and the SML algorithm is obtained. We prove the optimality of the data-aided TDT algorithm in Section 3.5 and discuss the implementation issue in Section 3.6. Simulation results and concluding remarks are provided in Section 3.7 and 3.8, respectively.

3.2 Impulse-Radio (IR) UWB Signal Model

In impulse-radio UWB systems, every information symbol is transmitted over a duration of T_s consisting of N_f frames. During each frame of T_f seconds, a data-modulated ultra-short pulse $p(t)$ with duration $T_p \ll T_f$ is transmitted. With binary

pulse amplitude modulation (PAM), the training symbols are drawn from the binary alphabet $\{\pm 1\}$. Then the transmitted waveform for a single user is modeled as [64, 59]:

$$v(t) = \sqrt{\mathcal{E}} \sum_{n=0}^{+\infty} s_n p_T(t - nT_s) \quad (3.1)$$

where \mathcal{E} is the energy per pulse and $p_T(t)$ represents the *symbol-long transmitted* waveform composed of N_f pulses:

$$p_T(t) = \sum_{j=0}^{N_f-1} p(t - jT_f - c_j T_c). \quad (3.2)$$

The pulse during the j th frame is shifted by the time-hopping code c_j , which takes integer values in the range of $[0, N_c - 1]$. The chip duration is $T_c = T_f/N_c$.

After propagating through a multipath channel with L_c taps, the received waveform can be written as:

$$r(t) = \sum_{l=0}^{L_c-1} \alpha_l v(t - \tau_l) + \eta(t) \quad (3.3)$$

where α_l and τ_l denote the attenuation and delay of the l th channel tap, and $\eta(t)$ is the zero-mean additive white Gaussian noise (AWGN) with power spectral density (PSD) $N_0/2$. In (3.3), the channel is assumed to be either deterministic or quasi-static over one transmission burst. We decouple the propagation delay τ_0 from the dispersive effects of the multipath channel by defining a new set of relative delays with respect to τ_0 , namely $\tau_{l|0} \doteq \tau_l - \tau_0, \forall l$. Without loss of generality (WLOG), $\tau_0 \in [0, T_s)$ is assumed throughout this chapter. Then the *symbol-long received* waveform capturing

the multipath channel effects is given by:

$$p_R(t) = \sum_{l=0}^{L_c-1} \alpha_l p_T(t - \tau_{l0}) \quad (3.4)$$

and the received waveform can be rewritten as:

$$r(t) = \sqrt{\mathcal{E}} \sum_{n=0}^{+\infty} s_n p_R(t - nT_s - \tau_0) + \eta(t) . \quad (3.5)$$

To develop the ML timing algorithm and compare it with the TDT ones, we assume that ISI is absent, but inter-frame interference may be present, as in [64]. This condition can be easily satisfied by constraining the last frame of each symbol such that the nonzero support of $p_R(t)$ does not extend beyond the range $[0, T_s)$. Note that this setup can also accommodate high-rate transmissions since the inter-frame interference is allowed.

For convenient manipulation, we divide the received signal into K consecutive symbol-long segments and shift them so that they all lie in the range $t \in [0, T_s)$. Then each shifted segment can be expressed as:

$$r_k(t) \doteq r(t + kT_s) \text{rect}(t), \quad k = 1, 2, \dots, K \quad (3.6)$$

where $\text{rect}(t) = 1, t \in [0, T_s)$, is the *window* function. Substituting (3.5) into (3.6) and defining $\eta_k(t) \doteq \eta(t + kT_s) \text{rect}(t)$, we have the received segments:

$$r_k(t) = \sqrt{\mathcal{E}} \sum_{n=0}^{+\infty} s_n p_R(t + kT_s - nT_s - \tau_0) \text{rect}(t) + \eta_k(t), \quad \forall k . \quad (3.7)$$

Since $p_R(t)$ and $\text{rect}(t)$ are confined within a finite support $[0, T_s)$, both $0 \leq t + kT_s - nT_s - \tau_0 < T_s$ and $0 \leq t < T_s$ should be satisfied. Then it can be easily induced that

for a certain segment k only $n = k - 1$ and $n = k$ can contribute nonzero summands to $r_k(t)$, and (3.7) can be explicitly expressed as $\forall k$:

$$r_k(t) = \sqrt{\mathcal{E}} (s_{k-1}p_R(t + T_s - \tau_0) + s_k p_R(t - \tau_0)) \text{rect}(t) + \eta_k(t). \quad (3.8)$$

Stack the total K received segments into a vector, and define $\mathbf{r}(t) \doteq [r_1(t), \dots, r_K(t)]^T$, $\mathbf{s}_1 \doteq [s_0, \dots, s_{K-1}]^T$, $\mathbf{s}_2 \doteq [s_1, \dots, s_K]^T$ and $\boldsymbol{\eta}(t) \doteq [\eta_1(t), \dots, \eta_K(t)]^T$. Then the signal model can be rewritten in the following compact vector form:

$$\mathbf{r}(t) = \sqrt{\mathcal{E}} \mathbf{s}_1 p_R^{(a)}(t; \tau_0) + \sqrt{\mathcal{E}} \mathbf{s}_2 p_R^{(b)}(t; \tau_0) + \boldsymbol{\eta}(t) \quad (3.9)$$

where $p_R^{(a)}(t; \tau_0) \doteq p_R(t + T_s - \tau_0) \text{rect}(t)$ and $p_R^{(b)}(t; \tau_0) \doteq p_R(t - \tau_0) \text{rect}(t)$ consist of the circularly shifted version of the symbol-long received waveform $p_R(t)$. It is noteworthy that $p_R^{(a)}(t; \tau_0)$ and $p_R^{(b)}(t; \tau_0)$ are not overlapping in time; that is, for any time instance during $[0, T_s)$, only one of the two can be nonzero. Specifically, the former is strictly zero for $t \in [\tau_0, T_s)$; and the latter for $t \in [0, \tau_0)$.

3.3 The ML Timing Algorithm

In this section, we will first develop the ML algorithm to estimate τ_0 for arbitrary known transmitted symbol sequences, and then evaluate the timing acquisition performance of the algorithm.

Under the signal model in (3.9), the deterministic but unknown parameters are: i) the overall received symbol-long waveform $p_R(t)$ (or equivalently, its circularly shifted version $p_R^{(a)}(t; \tau_0)$ and $p_R^{(b)}(t; \tau_0)$) which carries the dispersive multipath channel information; and ii) the propagation delay τ_0 . Given $p_R(t)$ and τ_0 , the log-likelihood

function for (3.9) bears the form [33]:

$$\begin{aligned}
\ln \Lambda(\mathbf{r}(t); p_R(t), \tau_0) &\propto \int_0^{T_s} -\|\mathbf{r}(t) - \sqrt{\mathcal{E}}\mathbf{s}_1 p_R^{(a)}(t; \tau_0) - \sqrt{\mathcal{E}}\mathbf{s}_2 p_R^{(b)}(t; \tau_0)\|^2 dt \\
&\propto \int_0^{T_s} 2\sqrt{\mathcal{E}}\mathbf{r}^T(t) \left(\mathbf{s}_1 p_R^{(a)}(t; \tau_0) + \mathbf{s}_2 p_R^{(b)}(t; \tau_0) \right) \\
&\quad - \mathcal{E} \|\mathbf{s}_1 p_R^{(a)}(t; \tau_0) + \mathbf{s}_2 p_R^{(b)}(t; \tau_0)\|^2 dt. \tag{3.10}
\end{aligned}$$

Our task is to obtain the ML estimates for $p_R(t)$ and τ_0 by maximizing (3.10). We use the notation \tilde{x} to indicate a conjecture of unknown parameter x . The ML estimation will be accomplished in two stages: based on a fixed conjecture $\tilde{\tau}_0$, we first obtain $\hat{p}_R(t; \tilde{\tau}_0)$ as a function of $\tilde{\tau}_0$; then we replace $p_R(t)$ with $\hat{p}_R(t; \tilde{\tau}_0)$ in (3.10) to find the ML estimate of $\hat{\tau}_0$.

At the first stage, the integral can be removed without affecting the optimality, since the ML estimate of $p_R(t)$ is to be obtained in an instantaneous manner; that is, keeping a guess $\tilde{\tau}_0$ unchanged, the ML estimate $\hat{p}_R(t; \tilde{\tau}_0)$ will be obtained by maximizing the integrand in (3.10). As emphasized before, with any given trial value $\tilde{\tau}_0$, $p_R^{(a)}(t; \tilde{\tau}_0)$ and $p_R^{(b)}(t; \tilde{\tau}_0)$ are non-overlapping in time. Accordingly, we can divide $\mathbf{r}(t)$ into two disjoint parts in time: $\mathbf{r}(t)\text{rect}(t + T_s - \tilde{\tau}_0)$ for $t \in [0, \tilde{\tau}_0)$ and $\mathbf{r}(t)\text{rect}(t - \tilde{\tau}_0)$ for $t \in [\tilde{\tau}_0, T_s)$. The circularly shifted waveforms $p_R^{(a)}(t; \tilde{\tau}_0)$ and $p_R^{(b)}(t; \tilde{\tau}_0)$ can thus be estimated separately. Specifically, the objective function for $p_R^{(a)}(t; \tilde{\tau}_0)$ is [c.f. (3.10)]:

$$J_a(t; \tilde{\tau}_0) = 2\sqrt{\mathcal{E}}\mathbf{r}^T(t)\mathbf{s}_1 p_R^{(a)}(t; \tilde{\tau}_0) - \mathcal{E} \|\mathbf{s}_1 p_R^{(a)}(t; \tilde{\tau}_0)\|^2, \quad t \in [0, \tilde{\tau}_0).$$

Taking the derivative of $J_a(t; \tilde{\tau}_0)$ with respect to the instantaneous $p_R^{(a)}(t; \tilde{\tau}_0)$, and setting it to zero, we have the ML estimate of $p_R^{(a)}(t; \tilde{\tau}_0)$:

$$\hat{p}_R^{(a)}(t; \tilde{\tau}_0) = \frac{1}{K\sqrt{\mathcal{E}}} \sum_{k=1}^K s_{k-1} r_k(t) \text{rect}(t + T_s - \tilde{\tau}_0), \quad t \in [0, \tilde{\tau}_0). \tag{3.11}$$

Likewise, the ML estimate of $p_R^{(b)}(t; \tilde{\tau}_0)$ can be obtained by maximizing the following objective function [c.f. (3.10)]:

$$J_b(t; \tilde{\tau}_0) = 2\sqrt{\mathcal{E}}\mathbf{r}^T(t)\mathbf{s}_2 p_R^{(b)}(t; \tilde{\tau}_0) - \mathcal{E} \|\mathbf{s}_2 p_R^{(b)}(t; \tilde{\tau}_0)\|^2, \quad t \in [\tilde{\tau}_0, T_s)$$

and the resultant estimate is:

$$\hat{p}_R^{(b)}(t; \tilde{\tau}_0) = \frac{1}{K\sqrt{\mathcal{E}}} \sum_{k=1}^K s_k r_k(t) \text{rect}(t - \tilde{\tau}_0), \quad t \in [\tilde{\tau}_0, T_s). \quad (3.12)$$

At the second stage, we plug (3.11) and (3.12) back into (3.10), and discard the norm square term whose integral is not affected by the delay candidate $\tilde{\tau}_0$. It turns out that the new ML objective function for $\tilde{\tau}_0$ becomes:

$$\begin{aligned} J^{\text{ML}}(\tilde{\tau}_0) &= \frac{1}{K^2} \int_0^{T_s} \left(\mathbf{r}^T(t) \mathbf{s}_1 \sum_{k=1}^K s_{k-1} r_k(t) \text{rect}(t + T_s - \tilde{\tau}_0) \right. \\ &\quad \left. + \mathbf{r}^T(t) \mathbf{s}_2 \sum_{k=1}^K s_k r_k(t) \text{rect}(t - \tilde{\tau}_0) \right) dt \\ &= \frac{1}{K^2} \sum_{m=1}^K \sum_{k=1}^K \int_0^{T_s} (r_m(t) r_k(t) s_{m-1} s_{k-1} \text{rect}(t + T_s - \tilde{\tau}_0) \\ &\quad + r_m(t) r_k(t) s_m s_k \text{rect}(t - \tilde{\tau}_0)) dt \end{aligned} \quad (3.13)$$

and the ML estimation of τ_0 reduces to a maximization problem:

$$\hat{\tau}_0 = \arg \max_{\tilde{\tau}_0} J^{\text{ML}}(\tilde{\tau}_0). \quad (3.14)$$

Proposition 3.1 (ML Timing Estimation): *The ML timing estimator can be implemented in four steps:*

- *Step 1: Take K received segments $r_k(t), k = 1, 2, \dots, K$, as in (3.8);*

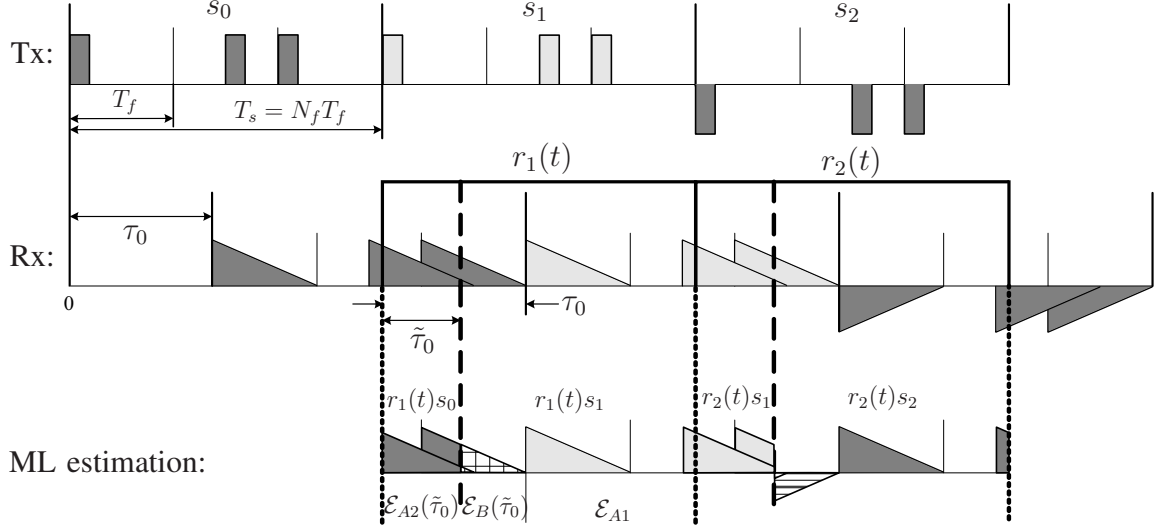


Figure 3.1: Illustration of the ML timing algorithm, $T_s = 3T_f$, $K = 2$.

- *Step 2: For each candidate $\tilde{\tau}_0$ calculate the K^2 cross (and auto) correlations among all pairs of the segments as in (3.13);*
- *Step 3: Average the K^2 correlations as suggested by (3.13);*
- *Step 4: Choose the $\tilde{\tau}_0$ which maximizes $J^{ML}(\tilde{\tau}_0)$ as the ML estimate $\hat{\tau}_0$ according to (3.14).*

From Proposition 3.1 one should be aware that the computational complexity of the ML timing estimator is very high. For each $\tilde{\tau}_0$ evaluation, one need to calculate K^2 correlations and K^2 summations. The high complexity is expected to be reduced for practical implementation.

The ML timing estimation is illustrated in Fig. 3.1, where $T_s = 3T_f$ and $K = 2$. While the thick solid boxes bound the received segments $r_k(t)$, the dashed lines indicate two windows within a received segment based on the shift candidate $\tilde{\tau}_0$: $\text{rect}(t + T_s - \tilde{\tau}_0)$ and $\text{rect}(t - \tilde{\tau}_0)$. When searching across $\tilde{\tau}_0$, the segments themselves do not change, but the window functions $\text{rect}(t + T_s - \tilde{\tau}_0)$ and $\text{rect}(t - \tilde{\tau}_0)$ shift with

$\tilde{\tau}_0$; that is, the solid boxes in the figure do not move, but the dashed windows shift.

In order to evaluate the performance of the ML estimator, we need to find the statistical properties of the objective function. Re-express $J^{\text{ML}}(\tilde{\tau}_0)$ as the sum of its noise-free part $J_0^{\text{ML}}(\tilde{\tau}_0)$ and noise term $\xi^{\text{ML}}(\tilde{\tau}_0)$:

$$J^{\text{ML}}(\tilde{\tau}_0) = J_0^{\text{ML}}(\tilde{\tau}_0) + \xi^{\text{ML}}(\tilde{\tau}_0) . \quad (3.15)$$

Let us first consider the noise-free part:

$$\begin{aligned} J_0^{\text{ML}}(\tilde{\tau}_0) &= \frac{1}{K^2} \sum_{m,k=1}^K \int_0^{T_s} (\rho_m(t)\rho_k(t)s_{m-1}s_{k-1}\text{rect}(t + T_s - \tilde{\tau}_0) \\ &\quad + \rho_m(t)\rho_k(t)s_m s_k \text{rect}(t - \tilde{\tau}_0)) dt \end{aligned} \quad (3.16)$$

where $\rho_k(t)$ denotes the signal part of $r_k(t)$. Assuming that the trial propagation delay $\tilde{\tau}_0 < \tau_0$ WLOG, we further define $\mathcal{E}_{A1} \doteq \sqrt{\mathcal{E}} \int_0^{T_s - \tau_0} p_R^2(t) dt$, $\mathcal{E}_{A2}(\tilde{\tau}_0) \doteq \sqrt{\mathcal{E}} \int_{T_s - \tau_0}^{T_s - \tau_0 + \tilde{\tau}_0} p_R^2(t) dt$, and $\mathcal{E}_B(\tilde{\tau}_0) \doteq \sqrt{\mathcal{E}} \int_{T_s - \tau_0 + \tilde{\tau}_0}^{T_s} p_R^2(t) dt$. Then (3.16) becomes

$$\begin{aligned} J_0^{\text{ML}}(\tilde{\tau}_0) &= \frac{1}{K^2} \sum_{m,k=1}^K (s_m^2 s_k^2 \mathcal{E}_{A1} + s_{m-1}^2 s_{k-1}^2 \mathcal{E}_{A2}(\tilde{\tau}_0) + s_{m-1} s_m s_{k-1} s_k \mathcal{E}_B(\tilde{\tau}_0)) \\ &= \frac{1}{K^2} \sum_{m,k=1}^K (\mathcal{E}_A(\tilde{\tau}_0) + s_{m-1} s_m s_{k-1} s_k \mathcal{E}_B(\tilde{\tau}_0)) \end{aligned} \quad (3.17)$$

where $\mathcal{E}_A(\tilde{\tau}_0) \doteq \mathcal{E}_{A1} + \mathcal{E}_{A2}(\tilde{\tau}_0)$. Notice that $\mathcal{E}_A(\tilde{\tau}_0) + \mathcal{E}_B(\tilde{\tau}_0) = \mathcal{E} \int_0^{T_s} p_R^2(t) dt = \mathcal{E}_R$ is the unknown but constant energy of a received segment independent of the trial value $\tilde{\tau}_0$. The noise-free part of the objective function can thus be simplified as

$$J_0^{\text{ML}}(\tilde{\tau}_0) = \mathcal{E}_R - \frac{\Delta_K}{K^2} \mathcal{E}_B(\tilde{\tau}_0) \quad (3.18)$$

where $\Delta_K \doteq \sum_{m,k=1}^K (1 - s_{m-1} s_m s_{k-1} s_k)$ is a positive (as long as not all $s_{m-1} s_m s_{k-1} s_k =$

1, $\forall m, k$, which can be easily avoided.) parameter determined by the transmitted pilot sequence. By definition, the condition of correct timing $\tilde{\tau}_0 = \tau_0$ ensures that $\mathcal{E}_B(\tilde{\tau}_0)$ vanishes and $J_0^{\text{ML}}(\tilde{\tau}_0)$ achieves its unique maximum \mathcal{E}_R . Indeed, in Fig. 3.1, the correlation between the two segments at the ML stage is essentially $\mathcal{E}_{A1} + \mathcal{E}_{A2}(\tilde{\tau}_0) - \mathcal{E}_B(\tilde{\tau}_0)$, which clearly achieves its maximum when $\mathcal{E}_B(\tilde{\tau}_0) = 0$ iff $\tilde{\tau}_0 = \tau_0$. It is necessary to point out that since Δ_K is a sum of K^2 constants, its value is on the order of K^2 , or can be explicitly written as αK^2 , where α is a constant. As K increases, $J_0^{\text{ML}}(\tilde{\tau}_0) = \mathcal{E}_R - \alpha \mathcal{E}_B(\tilde{\tau}_0)$ will *not* converge to a constant \mathcal{E}_R ; that is, the effectiveness of $J_0^{\text{ML}}(\tilde{\tau}_0)$ does not deteriorate at large K , as implied by (3.18).

We now go to the noise term $\xi^{\text{ML}}(\tilde{\tau}_0)$ in (3.15). As shown in Appendix 3-I, $\xi^{\text{ML}}(\tilde{\tau}_0)$ is Gaussian distributed with mean and variance:

$$\begin{aligned} \text{E}\{\xi^{\text{ML}}(\tilde{\tau}_0)\} &= \frac{N_0 T_s}{2K}, \\ \text{var}\{\xi^{\text{ML}}(\tilde{\tau}_0)\} &= \frac{2N_0 J_0^{\text{ML}}(\tilde{\tau}_0)}{K} + \frac{N_0^2 B T_s}{K^2}. \end{aligned} \quad (3.19)$$

Then, one can obtain the mean and variance of the overall Gaussian distributed ML objective function:

$$\begin{aligned} \text{E}\{J^{\text{ML}}(\tilde{\tau}_0)\} &= J_0^{\text{ML}}(\tilde{\tau}_0) + \text{E}\{\xi^{\text{ML}}(\tilde{\tau}_0)\} = J_0^{\text{ML}}(\tilde{\tau}_0) + \frac{N_0 T_s}{2K}, \\ \text{var}\{J^{\text{ML}}(\tilde{\tau}_0)\} &= \text{var}\{\xi^{\text{ML}}(\tilde{\tau}_0)\} = \frac{2N_0 J_0^{\text{ML}}(\tilde{\tau}_0)}{K} + \frac{N_0^2 B T_s}{K^2}. \end{aligned} \quad (3.20)$$

As one can see from (3.20), $J^{\text{ML}}(\tilde{\tau}_0)$ asymptotically converges to $J_0^{\text{ML}}(\tilde{\tau}_0)$ as $K \rightarrow \infty$, suggesting the optimality of the ML estimator.

We adopt the probability of detection lower bound \underline{P}_d as in [64] to evaluate the coarse timing (acquisition) performance of the ML algorithm. Instead of estimating the true τ_0 , coarse timing aims at finding n_0 such that $|n_0 T_i - \tau_0| < T_i$, where T_i is the

searching step size in the ML algorithm. Correspondingly, the maximization problem in (3.14) becomes:

$$\hat{n}_0 = \arg \max_{\tilde{n}_0} J^{\text{ML}}(\tilde{n}_0 T_i), \quad (3.21)$$

and the probability of detection is given by

$$P_d^{\text{ML}} = \Pr\{\hat{n}_0 = n_0\} = \Pr\{\max_{\tilde{n}_0} J^{\text{ML}}(\tilde{n}_0 T_i) = J^{\text{ML}}(n_0 T_i)\}. \quad (3.22)$$

Since $J^{\text{ML}}(n_0 T_i)$ is Gaussian distributed, according to [64], the lower bound of (3.22) is

$$\underline{P}_d^{\text{ML}} = \prod_{\tilde{n}_0 \neq n_0} F \left(\frac{\text{E}\{J^{\text{ML}}(n_0 T_i)\} - \text{E}\{J^{\text{ML}}(\tilde{n}_0 T_i)\}}{\sqrt{\text{var}\{J^{\text{ML}}(n_0 T_i)\} + \text{var}\{J^{\text{ML}}(\tilde{n}_0 T_i)\}}} \right), \quad (3.23)$$

where $F(\cdot)$ is the cumulative distribution function (cdf) of Gaussian distribution with zero mean and unit variance.

Substituting the mean and variance of the objective function given in (3.20), we can obtain the probability of detection lower bound:

$$\underline{P}_d^{\text{ML}} = \prod_{\tilde{n}_0 \neq n_0} F \left(\frac{\Delta_K (\mathcal{E}_B(\tilde{n}_0 T_i) - \mathcal{E}_B(n_0 T_i))}{\sqrt{4N_0 \mathcal{E}_R K^3 - 2N_0 \Delta_K (\mathcal{E}_B(\tilde{n}_0 T_i) - \mathcal{E}_B(n_0 T_i)) K + 2N_0^2 B T_s K^2}} \right) \quad (3.24)$$

Remarks: i) As K increases the variance of the objective function decreases and the probability of detection lower bound increases. This suggests that the timing performance would benefit from more correlation averaging; and ii) As Δ_K increases the variance of the objective function is reduced and the probability of detection lower bound increases. Intuitively, (3.18) provides another evidence that the objective function becomes sharper along with the increase of Δ_K , making n_0 easier to be

detected. Since Δ_K is determined by the transmitted symbol sequence, one can imagine that the acquisition performance would be markedly improved by optimizing the training sequence such that Δ_K is maximized.

3.4 Training Sequence Design and The SML Algorithm

3.4.1 The Optimum Training Sequence Pattern

Keeping in mind our goal of maximizing $\Delta_K = \sum_{m,k=1}^K (1 - s_{m-1}s_m s_{k-1}s_k)$, we find that the value of Δ_K is determined by the signs of the consecutive symbols. Define $c_k \doteq s_{k-1}s_k \in \{\pm 1\}, k = 1, \dots, K$, as the product of two consecutive symbols, which must belong to one and only one of the two groups: one is denoted by $\Gamma_+ \doteq \{c_k, \forall k : c_k = 1\}$ with cardinality K_+ ; the other is $\Gamma_- \doteq \{c_k, \forall k : c_k = -1\}$ with cardinality K_- . Evidently, $K_+ + K_- = K$.

Lemma 3.1 *For a specific K , $\max\{\Delta_K\} = K^2$ is achieved when $K_+ = K_- = K/2$; that is, half of the $\{c_k\}_k$ elements belong to Γ_+ and the other half belong to Γ_- .*

Proof. Substituted with c_m and c_k , $\Delta_K = \sum_{m,k=1}^K (1 - c_m c_k)$. Only those (m, k) pairs which satisfy the condition $c_m c_k = -1$ can contribute positive values to Δ_K . Evidently, $c_m c_k = -1$ holds only when c_m and c_k come from different groups Γ_+ or Γ_- . In other words, Δ_K can be simplified to $\Delta_K = \sum_{\{c_m \in \Gamma_+, c_k \in \Gamma_-\}} (1 - c_m c_k) + \sum_{\{c_m \in \Gamma_-, c_k \in \Gamma_+\}} (1 - c_m c_k) = 4K_+ K_-$. Together with the sum constraint $K_+ + K_- = K$, the Δ_K maximization problem is essentially equivalent to

$$\max 4K_+(K - K_+), \text{ for } 0 \leq K_+ \leq K. \quad (3.25)$$

It can be easily verified that the quadratic function of K_+ achieves its unique max-

imum K^2 when $K_+ = K/2$ and correspondingly $K_- = K/2$. This completes the proof. ■

Notice that we only considered even K WLOG, since odd K has the same maximization result with its even neighbor $K-1$. Indeed, for odd K , $\max\{\Delta_K\} = (K-1)^2$ when $K_+ = \lfloor K/2 \rfloor$ and $K_- = \lfloor K/2 \rfloor + 1$, or $K_+ = \lfloor K/2 \rfloor + 1$ and $K_- = \lfloor K/2 \rfloor$.

Lemma 3.1 gives the condition that maximizes Δ_K for a particular K . However, the optimum training sequence should also be consistent; that is, applicable to arbitrary K . To this end, we first notice that the ML timing estimator requires $K \geq 2$, since when $K = 1$, $J_0^{\text{ML}}(\tilde{\tau}_0) = \mathcal{E}_R$ [c.f. (3.17)] is simply a constant and gives no information about τ_0 . Following Lemma 3.1, the consistency property can be ensured $\forall K \geq 2$ by: i) partitioning the $\{c_k\}_k$ sequence into doublets $\{c_{2n-1} c_{2n}\}$, $n = 1, 2, \dots, K/2$; and ii) designing the training sequence such that each $\{c_{2n-1} c_{2n}\}$ doublet contains a “+1” and a “-1”, i.e., each doublet should be either $\{+1, -1\}$ or $\{-1, +1\}$. With this condition, the $\{c_k\}_k$ sequence always has $K_+ = K_-$ regardless of K . Note that, the special $K = 2$ case which ensures rapid acquisition using as few as 2 segments (3 symbols) is a natural corollary of the consistency property.

In addition, to guarantee that the “+1”, “-1” pairing condition holds for any doublet starting from odd- and even-indexed symbols, all the doublets should be the same. In other words, they are either all $\{+1, -1\}$ or all $\{-1, +1\}$. As a result, this gives rise to a *unique* training sequence $\{s_k\}_k$ consisting of the repeated pattern $\{+1, +1, -1, -1\}$ (or its circularly shifted versions). We summarize the analysis in the following result:

Proposition 3.2 (Optimum Training Sequence): *The unique optimum training sequence for the ML estimator has the structure*

$$s_k = (-1)^{\lfloor k/2 \rfloor} \quad (3.26)$$

which ensures rapid acquisition using as few as 3 symbols and is applicable to arbitrary $K (\geq 2)$.

Interestingly, this optimum training sequence for the ML estimator is identical to that for the TDT estimator [64]. We will discuss more about the relationship between the ML and TDT estimators in Section 3.5.

3.4.2 Simplified ML (SML) Algorithm

For simplicity, denote the integrals in the objective function for $\tilde{\tau}_0$ (3.13) as $j_{m,k}$. Considering the partition of the training sequence by groups Γ_+ and Γ_- , (3.13) can be rewritten as

$$J^{\text{ML}}(\tilde{\tau}_0) = \frac{1}{K^2} \left\{ \sum_{\{(m,k):c_m,c_k \in \Gamma_+\}} j_{m,k} + \sum_{\{(m,k):c_m,c_k \in \Gamma_-\}} j_{m,k} \right. \\ \left. + \sum_{\{(m,k):c_m \in \Gamma_+,c_k \in \Gamma_-\}} j_{m,k} + \sum_{\{(m,k):c_m \in \Gamma_-,c_k \in \Gamma_+\}} j_{m,k} \right\}. \quad (3.27)$$

Consider the first two summations. Since c_m and c_n are chosen from the same group (namely Γ_+ in the first summation and Γ_- in the second summation), the noise-free parts of the summands are exclusively $\mathcal{E}_A(\tilde{\tau}_0) + \mathcal{E}_B(\tilde{\tau}_0) = \mathcal{E}_R$ [c.f.(3.17)]. Furthermore, it is not difficult to verify that the noise terms in the first two summations do not change with the shift candidate $\tilde{\tau}_0$. Therefore, the first two summations are nothing

but constants, which provide no information on τ_0 . If one knows which (c_m, c_k) pairs give rise to these summands, one can avoid calculating their corresponding cross correlations.

The optimum training sequence given by (3.26) precisely allows one to achieve this. The repeated pattern $\{+1, +1, -1, -1\}$ indicates that the received K symbol-long segments can be divided into two groups by simply checking their indices. Specifically, if the symbol-long received segment with odd index $r_{2k-1}(t)$ carries two successive symbols satisfying $c_{2k-1} = s_{2k-2}s_{2k-1} \in \Gamma_+$ (or Γ_-), then the symbol-long received segment with even index r_{2k} must carry two successive symbols satisfying $c_{2k} = s_{2k-1}s_{2k} \in \Gamma_-$ (or Γ_+). Retaining only the cross correlations between the two groups, and assuming an even K WLOG, we can obtain the simplified ML (SML) objective function as

$$\begin{aligned}
J^{\text{SML}}(\tilde{\tau}_0) &= \frac{2}{K^2} \sum_{m,k=1}^{K/2} j_{m,k}^{\text{SML}}, \\
j_{m,k}^{\text{SML}} &= \int_0^{T_s} r_{2m-1}(t)r_{2k}(t)(-1)^{\lfloor \frac{2m-2}{2} \rfloor} (-1)^{\lfloor \frac{2k-1}{2} \rfloor} \text{rect}(t + T_s - \tilde{\tau}_0) \\
&\quad + r_{2m-1}(t)r_{2k}(t)(-1)^{\lfloor \frac{2m-1}{2} \rfloor} (-1)^{\lfloor \frac{2k}{2} \rfloor} \text{rect}(t - \tilde{\tau}_0) dt. \tag{3.28}
\end{aligned}$$

Note that the last two summation terms in (3.27) are exactly the same, which explains the reason why coefficient 2 shows up as a scaling factor in (3.28).

We can rewrite $J^{\text{SML}}(\tilde{\tau}_0)$ by putting the double summations into the integral and simplify it to:

$$\begin{aligned}
J^{\text{SML}}(\tilde{\tau}_0) &= \frac{1}{2} \int_0^{T_s} \left(\frac{2}{K} \sum_{m=1}^{K/2} (-1)^m r_{2m-1}(t) \right) \left(\frac{2}{K} \sum_{k=1}^{K/2} (-1)^k r_{2k}(t) \right) \\
&\quad \cdot (\text{rect}(t + T_s - \tilde{\tau}_0) - \text{rect}(t - \tilde{\tau}_0)) dt. \tag{3.29}
\end{aligned}$$

The above integrand includes the product of three terms. The first is the average of the odd indexed received segments which satisfies the condition for the group Γ_+ ; the second is the average of those even indexed received segments falling into the group Γ_- ; and the last term is the window function accounting for the guess shift $\tilde{\tau}_0$. Rather than the operations of K^2 correlations and then averaging for the ML estimator, the operation order would be different for the SML estimator.

Proposition 3.3 (SML Timing Estimation): *By employing the optimum training sequence given in Proposition 3.2, the SML estimator can be implemented with much lower complexity than the ML estimator:*

- *Step 1: Take K received segments $r_k(t), \forall k$, as in (3.8);*
- *Step 2: Average the odd and even indexed segments respectively as suggested by (3.29);*
- *Step 3: For each candidate $\tilde{\tau}_0$, form the window functions $\text{rect}(t + T_s - \tilde{\tau}_0)$ and $-\text{rect}(t - \tilde{\tau}_0)$, and calculate $J^{SML}(\tilde{\tau}_0)$ as (3.29);*
- *Step 4: Choose the $\tilde{\tau}_0$ which maximizes $J^{SML}(\tilde{\tau}_0)$ as the SML estimate $\hat{\tau}_0$; that is, $\hat{\tau}_0 = \arg \max_{\tilde{\tau}_0} J^{SML}(\tilde{\tau}_0)$.*

It is important to note that the complexity of the SML timing estimator is significantly reduced; that is, one only needs to evaluate K summations and 1 correlation for each $\tilde{\tau}_0$ candidate. Moreover, in a digital implementation, it is not necessary to compute the correlation for every new $\tilde{\tau}_0$ value. Note that most of the correlation is identical from the current $\tilde{\tau}_0$ value to the next. Therefore, additional computing saving can be obtained by only updating the difference instead of calculating every correlation anew.

Like the ML estimator, we are also interested in the acquisition performance of the SML estimator. Inherited from (3.17) with $s_{2m-2}s_{2m-1}s_{2k-1}s_{2k} = -1, \forall m, k$, the noise-free part of the SML objective function in (3.28) can be expressed as:

$$J_0^{\text{SML}}(\tilde{\tau}_0) = \frac{\mathcal{E}_A(\tilde{\tau}_0) - \mathcal{E}_B(\tilde{\tau}_0)}{2} = \frac{\mathcal{E}_R - 2\mathcal{E}_B(\tilde{\tau}_0)}{2}. \quad (3.30)$$

The noise term $\xi^{\text{SML}}(\tilde{\tau}_0)$ is Gaussian distributed with zero mean and variance (the proof is similar to that for the ML, thus omitted here):

$$\text{var}\{\xi^{\text{SML}}(\tilde{\tau}_0)\} = \frac{N_0\mathcal{E}_R}{2K} + \frac{N_0^2BT_s}{2K^2}. \quad (3.31)$$

After calculating the mean and variance for $J^{\text{SML}}(\tilde{\tau}_0)$:

$$\begin{aligned} \text{E}\{J^{\text{SML}}(\tilde{\tau}_0)\} &= \frac{\mathcal{E}_A(\tilde{\tau}_0) - \mathcal{E}_B(\tilde{\tau}_0)}{2}, \\ \text{var}\{J^{\text{SML}}(\tilde{\tau}_0)\} &= \frac{N_0\mathcal{E}_R}{2K} + \frac{N_0^2BT_s}{2K^2}, \end{aligned} \quad (3.32)$$

we obtain the probability of detection lower bound for the SML algorithm as:

$$P_d^{\text{SML}} = \prod_{\tilde{n}_0 \neq n_0} F\left(\frac{K(\mathcal{E}_B(\tilde{n}_0T_i) - \mathcal{E}_B(n_0T_i))}{\sqrt{KN_0\mathcal{E}_R + N_0^2BT_s}}\right). \quad (3.33)$$

3.5 The Optimality of Data-Aided TDT in the ML Sense

As mentioned in Section 3.4.1, **the SML and TDT estimators share the identical optimum training sequence.** In this section, we will investigate the relationship between the two estimators.

For comparison convenience, we briefly review the TDT estimator under our nota-

tion system. In principle, TDT algorithm estimates τ_0 by finding the maximum of the average cross correlation of successive symbol-long segments. Specifically, under our signal model developed in Section 3.2, we obtain the k th symbol-long *shifted* received segment $y_k(t; \tilde{\tau}_0) \doteq r(t + kT_s + \tilde{\tau}_0)\text{rect}(t)$, $\forall k$, which can be expressed as

$$y_k(t; \tilde{\tau}_0) = \sqrt{\mathcal{E}} (s_{k-1}p_R(t + T_s - \tau_0 + \tilde{\tau}_0) + s_k p_R(t - \tau_0 + \tilde{\tau}_0)) \text{rect}(t) + \eta_k(t; \tilde{\tau}_0), \quad \forall k \quad (3.34)$$

where $\eta_k(t; \tilde{\tau}_0) \doteq \eta(t + kT_s + \tilde{\tau}_0)\text{rect}(t)$. Then the TDT objective function employing the optimum training sequence is formed as [64, *Proposition 4*]

$$J^{\text{TDT}}(\tilde{\tau}_0) = \frac{1}{2} \int_0^{T_s} \bar{y}_o(t; \tilde{\tau}_0) \bar{y}_e(t; \tilde{\tau}_0) dt, \quad (3.35)$$

where $\bar{y}_o \doteq \frac{2}{K} \sum_{k=1}^{K/2} (-1)^{k-1} y_{2k-1}(t; \tilde{\tau}_0)$ is the average of the odd indexed shifted received segments, and $\bar{y}_e \doteq \frac{2}{K} \sum_{k=1}^{K/2} (-1)^k y_{2k}(t; \tilde{\tau}_0)$ is the average of the even indexed shifted received segments. The cross correlation is scaled by 1/2 for comparison with the SML algorithm while maintaining TDT's original criterion.

Proposition 3.4 (TDT Timing Estimation [64, Proposition 4]): *There are four steps to implement the TDT algorithm:*

- *Step 1: Take K shifted received segment $y_k(t; \tilde{\tau}_0)$, $\forall k$, for each candidate $\tilde{\tau}_0$ as in (3.34);*
- *Step 2: Average the odd and even indexed segments respectively as in (3.35);*
- *Step 3: Calculate the correlation between the two averaged segments as in (3.35);*
- *Step 4: Choose the $\tilde{\tau}_0$ which maximizes $J^{\text{TDT}}(\tilde{\tau}_0)$ as the TDT estimate $\hat{\tau}_0$; that is, $\hat{\tau}_0 = \arg \max_{\tilde{\tau}_0} J^{\text{TDT}}(\tilde{\tau}_0)$.*

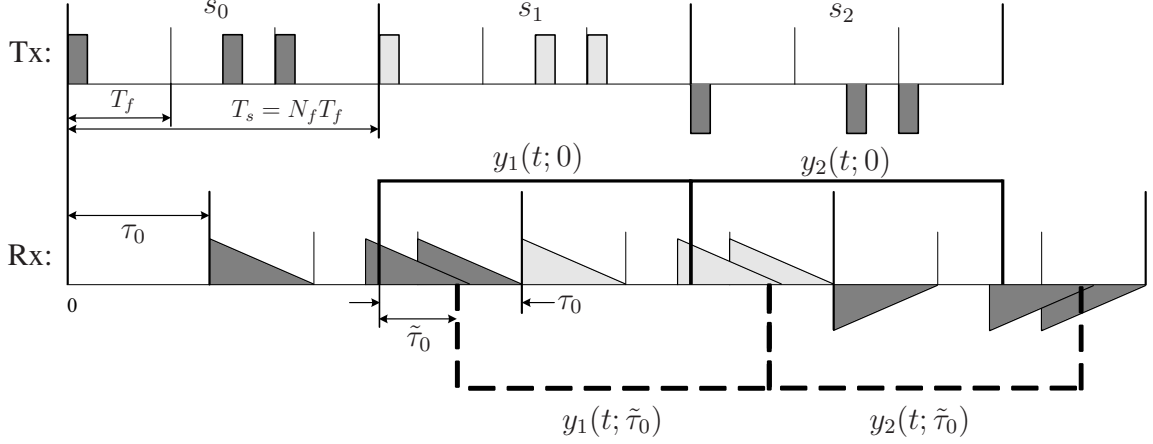


Figure 3.2: Illustration of the TDT timing algorithm, $T_s = 3T_f$, $K = 2$.

The TDT algorithm is illustrated in Fig. 3.2. At first glance, it appears that SML and TDT are two different schemes. In the SML algorithm, the received symbol-long segments do not change. What is changing is the time shift candidate $\tilde{\tau}_0$ in the window functions (see Fig. 3.1). In the data-aided TDT algorithm, on the other hand, the received symbol-long segments are shifted with the trial value $\tilde{\tau}_0$ (see Fig. 3.2). In the meantime, however, one can also find that **the SML and TDT estimators are implemented in the same operation order, namely, averaging and then correlation, at low computational complexity.**

In order to gain more insights about the TDT estimator, we treat $J^{\text{TDT}}(\tilde{\tau}_0)$ as the summation of the noise-free part $J_0^{\text{TDT}}(\tilde{\tau}_0)$ and the noise term $\xi^{\text{TDT}}(\tilde{\tau}_0)$. $J_0^{\text{TDT}}(\tilde{\tau}_0)$ can be explicitly expressed as

$$\begin{aligned}
 J_0^{\text{TDT}}(\tilde{\tau}_0) &= \frac{1}{2} \int_0^{T_s} p_R^2(t + T_s - \tau_0 + \tilde{\tau}_0) dt - \frac{1}{2} \int_0^{T_s} p_R^2(t - \tau_0 + \tilde{\tau}_0) dt \\
 &= \frac{1}{2} (\mathcal{E}_A(\tilde{\tau}_0) - \mathcal{E}_B(\tilde{\tau}_0))
 \end{aligned} \tag{3.36}$$

and $\xi^{\text{TDT}}(\tilde{\tau}_0)$ is zero-mean Gaussian distributed with variance

$$\text{var}\{\xi^{\text{TDT}}(\tilde{\tau}_0)\} = \frac{N_0\mathcal{E}_R}{2K} + \frac{N_0^2BT_s}{2K^2}. \quad (3.37)$$

Compared with SML, the TDT objective function provides the same noise-free part (i.e., (3.36) for TDT and (3.30) for SML) and the same noise statistics (i.e., (3.37) for TDT and (3.31) for SML), which demonstrates that **the objective function (and therefore the estimation criterion) of the TDT is essentially equivalent to that of the SML** in (3.29) except for the explicit noise elements. One can therefore calculate the expression of the probability of detection bound for the data-aided TDT algorithm, and the result will with no doubt show that **the TDT's probability of detection performance is the same as that of the SML algorithm.**

Now we are ready to make a conclusion of the relationship of the data-aided SML and TDT estimators. Although they use different approaches, the SML and TDT estimators are equivalent in the sense that they share the same optimum training sequence, operation order (computational complexity), estimation criterion and the same performance. Their equivalence will be further illustrated by simulations in Section 3.7.

3.6 Implementation Consideration

Theoretically, the SML and TDT algorithms can always detect n_0 such that $|n_0T_i - \tau_0| < T_i$ on any resolution level T_i as long as the complexity of the receiver is allowed. One expects that $\mathcal{E}_B(\tilde{n}_0T_i)$ in the objective function [c.f.(3.30)] can provide noticeable change along with the shift candidate \tilde{n}_0 , especially when \tilde{n}_0 is shifted in the neighborhood of n_0 . In practical implementation, however, the significant atten-

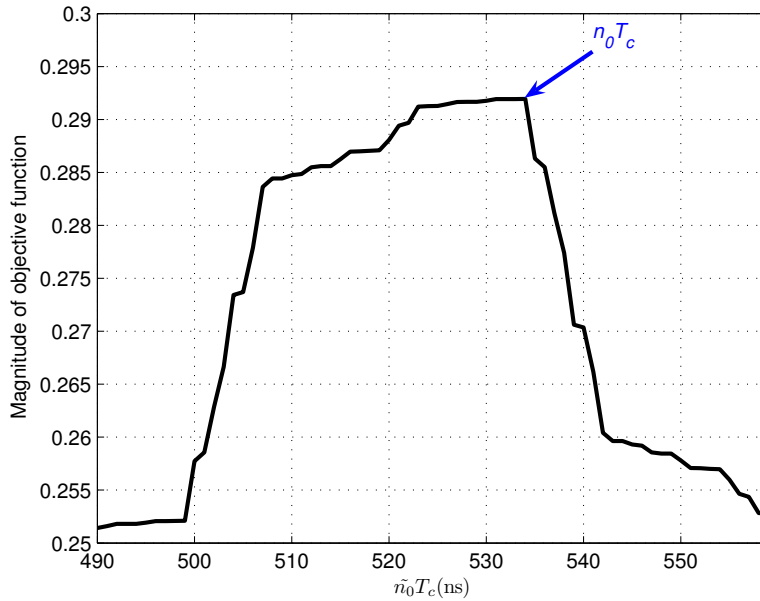


Figure 3.3: The noise-free part of the SML (TDT) objective function, $K = 8$ and $n_0 = 534$.

uation at the tail of a multipath channel and the extent of noise-only region between consecutive symbols can make things more complicated. The unique peak ($\tilde{n}_0 = n_0$) of the objective function tends to be comparable with its left neighbors (namely $\tilde{n}_0 < n_0$) even when the noise is absent as illustrated in Fig. 3.3, which plots the noise-free part of the SML objective function around the peak. Therefore, the correct timing of $\tilde{n}_0 = n_0$ with fine (e.g., chip-level) resolution is not easily distinguishable as the peak. On the other hand, we notice that the value of the objective function decreases dramatically for $\tilde{n}_0 > n_0$, as a result of the first few strong taps of the channel. Thanks to the different behavior of the regions $\tilde{n}_0 < n_0$ and $\tilde{n}_0 > n_0$, one can resort to the first-order difference of the objective function in aid of finding n_0 at the chip level.

Suppose the frame-level acquisition has already been achieved. After obtaining the values of $J(\tilde{n}_0 T_c)$ in the right frame where n_0 is located, take the difference

$\Delta J(\tilde{n}_0 T_c) = J(\tilde{n}_0 T_c) - J(\tilde{n}_0 T_c - w T_c)$, where $w \in [1, N_c]$ and $w T_c$ denotes the step size. Then the candidate \tilde{n}_0 which maximizes $\Delta J(\tilde{n}_0 T_c)$ will be regarded as the estimate of n_0 .

The performance of this approach clearly depends on the step size $w T_c$ and SNR, and the optimum $w T_c$ will vary according to the statistical characteristics of the channel. Additionally, the SML and TDT algorithms, together with the complementary differential operation, essentially turns out to be an energy detection method using a sliding window with length $w T_c$ and sliding step size T_c . The difference is that, in our schemes, the noise is averaged out in the first place of the SML and TDT correlations, which gives better performance than directly employing the energy detection method.

3.7 Simulations

In the simulations, we will compare their frame-level acquisition performance of ML and TDT estimators, followed by the chip-level fine timing performance.

We use the channel model IEEE 802.15.3a CM1 [23] to generate the multipath channel. The UWB pulse is the second derivative of the Gaussian function with unit energy and duration $T_p \approx 1$ ns. The frame duration is $T_f = 35$ ns, and each symbol contains $N_f = 32$ frames. A random time hopping code c_j is uniformly distributed over $[0, N_c - 1]$, with $N_c = 35$ and $T_c = 1$ ns. To avoid ISI, the time hopping code for the last frame of each symbol is set to $c_{N_f-1} = 0$. Since [61] has already illustrated that the digital TDT algorithms remain effective and their performance is only slightly altered by the resolution of ADC, we will use the digital counterparts with sampling duration 1 ns and assume ADC has infinite resolution to exclude the error from quantization.

Test 1 illustrates the optimality of the training sequence given in (3.26) for the

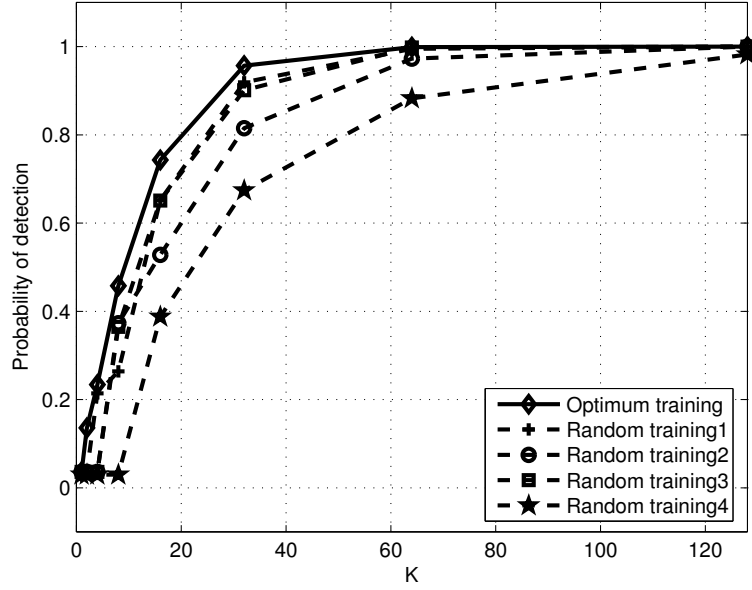


Figure 3.4: P_d for various sequences, $\mathcal{E}/N_0 = 1dB$.

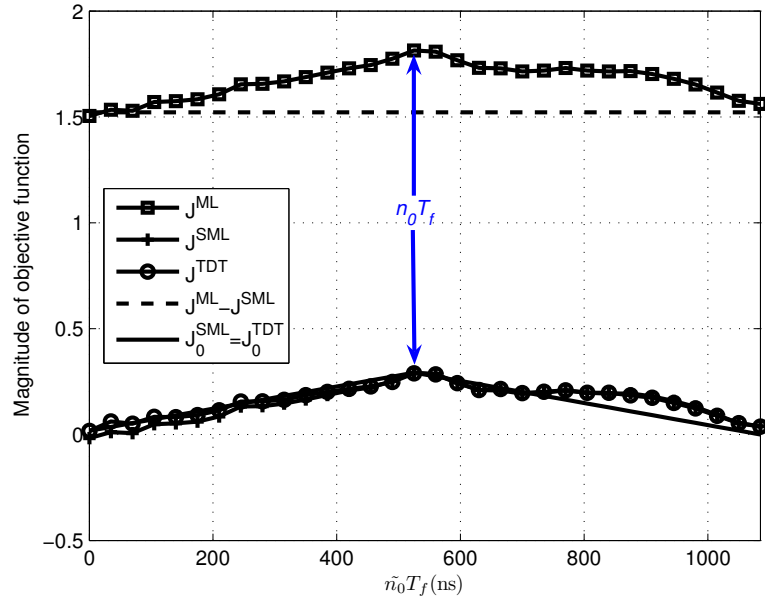


Figure 3.5: Objective function magnitude for the ML, SML and TDT algorithms, $\mathcal{E}/N_0 = 5dB$, $K = 8$ and $n_0 = 15$.

ML estimator. Fig. 3.4 compares our optimum training pattern with four randomly chosen sequences. We can observe that for $K = 2$ only our optimum training sequence works. With $K > 2$, although the other four can also work, the optimum training sequence provides the best performance consistently for any K . Notice that even though some random training sequences could accidentally comply with Lemma 3.1 for a certain K , it only performs as well as our optimum training sequence with that specific K . We will employ the optimum training sequence in the following simulations.

Test 2 plots the objective functions of the ML, SML and TDT algorithms in one realization at the frame level in Fig. 3.5. For comparison, the corresponding noise-free part of the SML (and TDT) algorithm is also provided. Fig. 3.5 shows that the objective functions of the ML and SML algorithms have identical shape. The difference between them remains the same for all candidates \tilde{n}_0 . Furthermore, the shapes of the objective functions of SML and TDT are very close except for the effect of the noise part.

Test 3 compares the acquisition performance of the SML and TDT algorithms to demonstrate the optimality of the data-aided TDT algorithm in the ML sense. Their probabilities of detection, together with the analytical lower bounds (3.33) are plotted in Fig. 3.6. Their normalized mean square errors (MSE), which are normalized with respect to T_s^2 , are also compared in Fig. 3.7. Firstly, it is observed that the probability of detection (and its lower bound) increases and the normalized MSE decreases as K increases for each algorithm, which suggests that the performance of both algorithms can be improved by choosing a larger K . Secondly, when K is small, TDT performs slightly worse than the SML algorithm; with increasing K , TDT can achieve the same performance as SML. This phenomena is reasonable. For the SML algorithm, the received segments do not change with the time shift candidate \tilde{n}_0 , which means

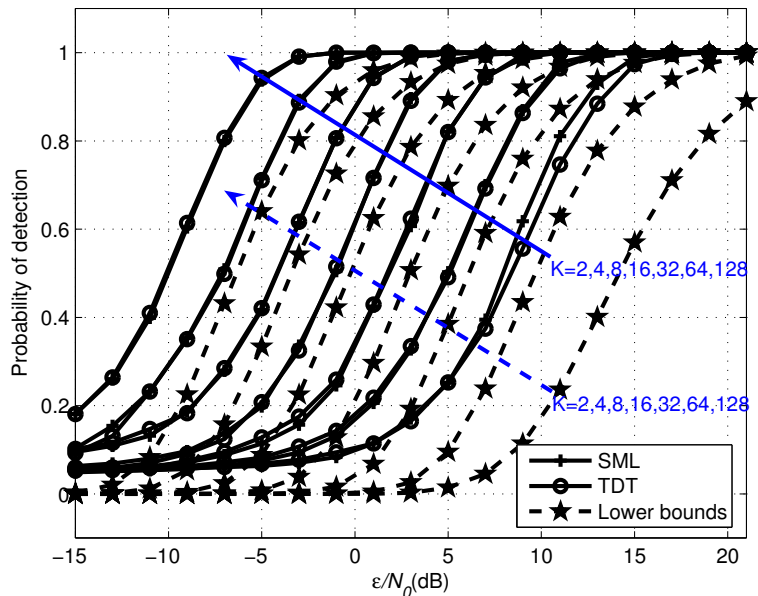


Figure 3.6: P_d and the lower bounds for the SML and TDT algorithms, coarse timing.

that the noise components contained in the segment correlations do not change with \tilde{n}_0 . For the TDT algorithm, however, the received segments are shifted based on \tilde{n}_0 , and the noise components in the correlation operation are changed accordingly, which is not in favor of peak searching for the objective function. When K increases, the noise will be better averaged out, and the different effects from the noise part can be further reduced. Thus the TDT and SML algorithms would achieve the same performance with a large K .

Test 4 further investigates the effect of timing acquisition to BER performance in Fig. 3.8 while isolating the error from channel estimation. Same as the synchronization performance, BER decreases monotonically as K increases for both the SML and TDT algorithms. Again, SML outperforms TDT when K is small, and the superiority disappears as K increases.

Test 5 is designed for chip-level fine timing comparison. The frame-level acquisition is assumed to be achieved beforehand. As illustrated in Fig. 3.9, the performance

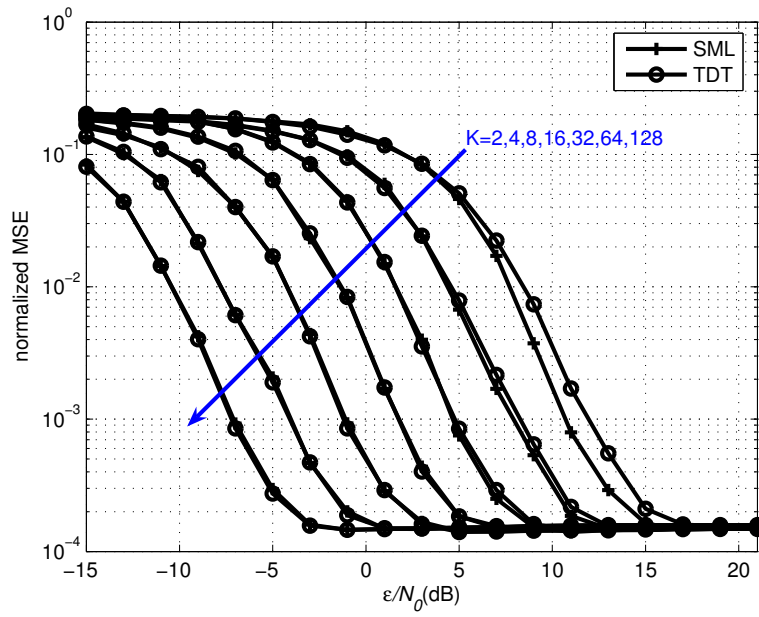


Figure 3.7: Normalized MSE for the SML and TDT algorithms, coarse timing.

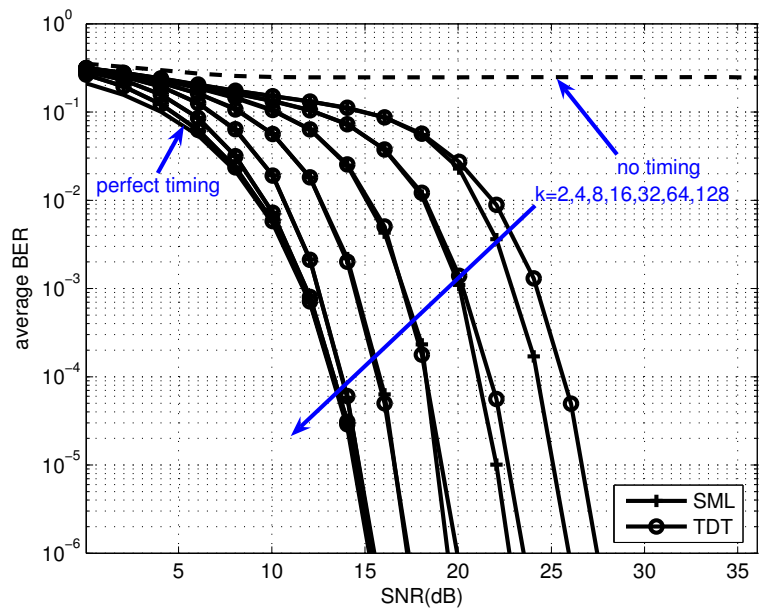


Figure 3.8: Average BER for the SML and TDT algorithms, coarse timing.

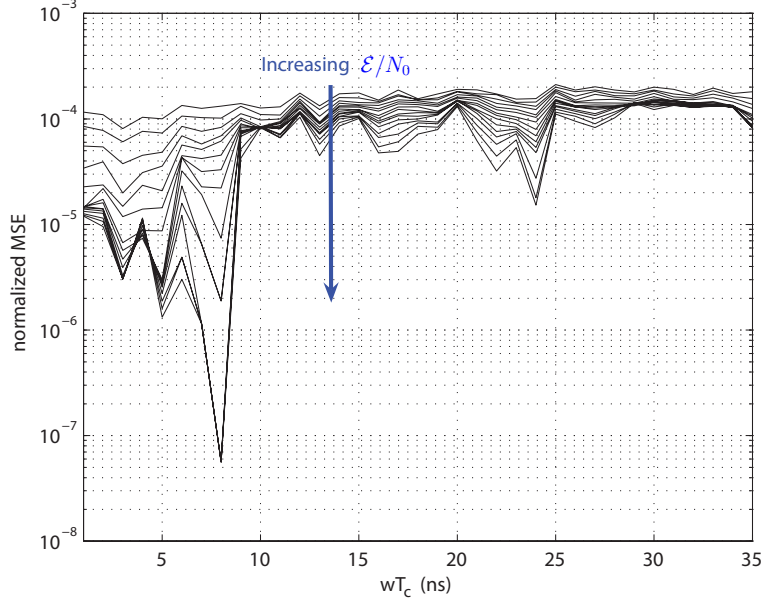


Figure 3.9: Normalized MSE versus differential step wT_c under various \mathcal{E}/N_0 .

of the difference operation depends on the step size wT_c . Accordingly, we choose the optimum value for CM1 in our simulation as: $wT_c = 3\text{ns}$ at low SNR and $wT_c = 8\text{ns}$ at high SNR. The normalized MSE for the SML and TDT algorithms with various K are plotted in Fig. 3.10. Similar to the performance shown in frame-level acquisition, the SML estimator enjoys a slightly better performance than TDT when K is small, while their difference disappears with increasing K . Notice that all curves also reach an error floor since the timing with chip-level resolution is performed.

3.8 Conclusions

In this chapter, we developed the practical data-aided ML timing algorithm, and designed an optimum training sequence for the ML algorithm. This training sequence turned out to be identical to the one used in TDT. Based on this optimum sequence, the original ML algorithm can be simplified without affecting its optimality. We proved that the resultant SML algorithm is equivalent to the TDT timing algorithm,

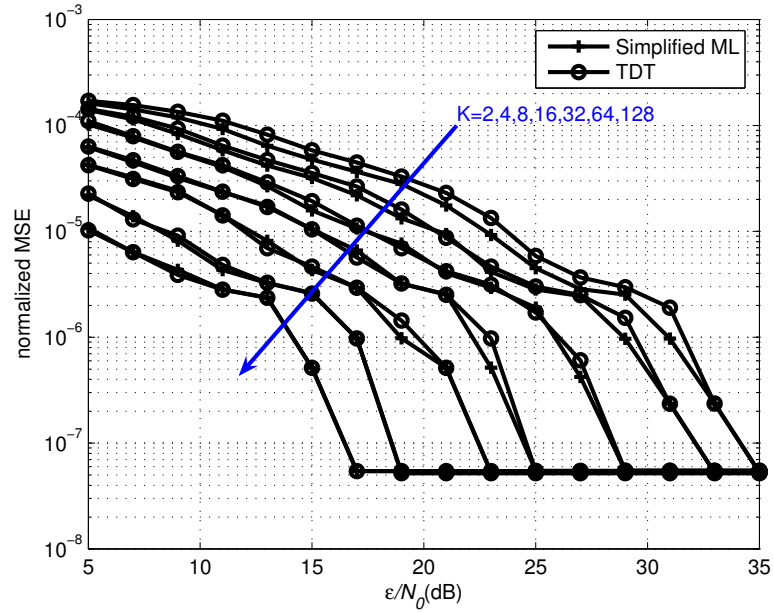


Figure 3.10: Normalized MSE for the SML and TDT algorithms, fine timing.

demonstrating the optimality of the data-aided TDT in the ML sense. Extensive simulations have been performed to corroborate our theoretical analysis.

Appendix 3-I: Proof of Equation (3.19)

It turns out that the noise term $\xi^{\text{ML}}(\tilde{\tau}_0)$ is the superposition of the following three terms:

$$\xi^{(1)}(\tilde{\tau}_0) = \frac{1}{K^2} \sum_{m,k=1}^K \zeta_{m,k}^{(1)}(\tilde{\tau}_0),$$

$$\xi^{(2)}(\tilde{\tau}_0) = \frac{1}{K^2} \sum_{m,k=1}^K \zeta_{m,k}^{(2)}(\tilde{\tau}_0), \quad (3.38)$$

$$\xi^{(3)}(\tilde{\tau}_0) = \frac{1}{K^2} \sum_{m,k=1}^K \zeta_{m,k}^{(3)}(\tilde{\tau}_0),$$

with the corresponding noise elements that constitute the above equations:

$$\begin{aligned} \zeta_{m,k}^{(1)}(\tilde{\tau}_0) &\doteq \int_0^{T_s} (\eta_m(t)\rho_k(t)s_{m-1}s_{k-1}\text{rect}(t+T_s-\tilde{\tau}_0) \\ &\quad + \eta_m(t)\rho_k(t)s_ms_k\text{rect}(t-\tilde{\tau}_0)) dt, \\ \zeta_{m,k}^{(2)}(\tilde{\tau}_0) &\doteq \int_0^{T_s} (\rho_m(t)\eta_k(t)s_{m-1}s_{k-1}\text{rect}(t+T_s-\tilde{\tau}_0) \\ &\quad + \rho_m(t)\eta_k(t)s_ms_k\text{rect}(t-\tilde{\tau}_0)) dt, \\ \zeta_{m,k}^{(3)}(\tilde{\tau}_0) &\doteq \int_0^{T_s} (\eta_m(t)\eta_k(t)s_{m-1}s_{k-1}\text{rect}(t+T_s-\tilde{\tau}_0) \\ &\quad + \eta_m(t)\eta_k(t)s_ms_k\text{rect}(t-\tilde{\tau}_0)) dt. \end{aligned} \tag{3.39}$$

In order to calculate the mean and variance of $\xi^{\text{ML}}(\tilde{\tau}_0)$, we will first derive the statistical properties of the noise elements in (3.39) respectively. Note that essentially $\xi^{(1)}(\tilde{\tau}_0) = \xi^{(2)}(\tilde{\tau}_0)$ so that we only consider $\xi^{(1)}(\tilde{\tau}_0)$ and $\xi^{(3)}(\tilde{\tau}_0)$.

The receiver frontend can be modeled as an ideal bandpass filter with double-sided bandwidth B ($B \gg 1/T_s$) and center frequency f_0 , thus we have $\{\eta_m(t)\}_m$ being bandpass-filtered AWGN with zero mean and double-sided PSD $N_0/2$. The autocorrelation function for $\eta_m(t)$, $\forall m$, is [[62], eq. (2)]:

$$\text{E}\{\eta_m(t_1)\eta_m(t_2)\} = N_0B\text{sinc}(B(t_2-t_1))\cos(2\pi f_0(t_2-t_1))$$

where $\text{sinc}(t) \doteq \sin(\pi t)/(\pi t)$. Since the bandwidth of the receiver frontend satisfies $B \gg 1/T_s$, the noises in different symbol-long received segments (i.e. $\eta_m(t)$ and $\eta_n(t)$, $\forall m \neq n$) are assumed to be uncorrelated. As a consequence, $\zeta_{m,k}^{(1)}(\tilde{\tau}_0)$ is Gaussian distributed and $\zeta_{m,k}^{(3)}(\tilde{\tau}_0)$ can be approximated as Gaussian distributed due to the

central limit theorem. In the following, we will derive the means and correlations of the noise elements to describe their distribution.

Clearly, $\zeta_{m,k}^{(1)}(\tilde{\tau}_0)$ has zero mean. The mean of $\zeta_{m,k}^{(3)}(\tilde{\tau}_0)$ can be calculated as [62, eqs. (37)-(38)]:

$$\mathbb{E}\{\zeta_{m,k}^{(3)}(\tilde{\tau}_0)\} = \delta_{m,k} \int_0^{T_s} \mathbb{E}\{\eta_m(t)\eta_k(t)\}dt = \left(\frac{N_0 T_s}{2}\right) \delta_{m,k}. \quad (3.40)$$

Next, let us exploit the correlation functions of $\zeta_{m,k}^{(1)}(\tilde{\tau}_0)$ and $\zeta_{m,k}^{(3)}(\tilde{\tau}_0)$. The correlation function of $\zeta_{m,k}^{(1)}(\tilde{\tau}_0)$, $\forall m, k$, is defined as:

$$\begin{aligned} & \mathbb{E}\{\zeta_{m,k}^{(1)}(\tilde{\tau}_0), \zeta_{n,l}^{(1)}(\tilde{\tau}_0)\} \\ &= \int_0^{T_s} \int_0^{T_s} \mathbb{E}\{(\eta_m(t_1)\rho_k(t_1)s_{m-1}s_{k-1}\text{rect}(t_1 + T_s - \tilde{\tau}_0) + \eta_m(t_1)\rho_k(t_1)s_m s_k \text{rect}(t_1 - \tilde{\tau}_0)) \\ & \quad \cdot (\eta_n(t_2)\rho_l(t_2)s_{n-1}s_{l-1}\text{rect}(t_2 + T_s - \tilde{\tau}_0) + \eta_n(t_2)\rho_l(t_2)s_n s_l \text{rect}(t_2 - \tilde{\tau}_0))\} dt_1 dt_2 \\ &= \delta_{m,n} \frac{N_0}{2} \int_0^{T_s} (\rho_k(t)\rho_l(t)s_{k-1}s_{l-1}\text{rect}(t + T_s - \tilde{\tau}_0) + \rho_k(t)\rho_l(t)s_k s_l \text{rect}(t - \tilde{\tau}_0)) dt \\ &= \frac{N_0}{2} (\mathcal{E}_A(\tilde{\tau}_0) + s_{m-1}s_m s_{k-1}s_k \mathcal{E}_B(\tilde{\tau}_0)) \delta_{m,n} \end{aligned} \quad (3.41)$$

where the second equality refers to [62, eqs. (37)-(38)].

For the double-noise term $\zeta_{m,k}^{(3)}(\tilde{\tau}_0)$, $\forall m, k$, with correlation

$$\begin{aligned} & \mathbb{E}\{\zeta_{m,k}^{(3)}(\tilde{\tau}_0), \zeta_{n,l}^{(3)}(\tilde{\tau}_0)\} \\ &= \int_0^{T_s} \int_0^{T_s} \mathbb{E}\{(\eta_m(t_1)\eta_k(t_1)s_{m-1}s_{k-1}\text{rect}(t_1 + T_s - \tilde{\tau}_0) \\ & \quad + \eta_m(t_1)\eta_k(t_1)s_m s_k \text{rect}(t_1 - \tilde{\tau}_0)) \\ & \quad \cdot (\eta_n(t_2)\eta_l(t_2)s_{n-1}s_{l-1}\text{rect}(t_2 + T_s - \tilde{\tau}_0) \\ & \quad + \eta_n(t_2)\eta_l(t_2)s_n s_l \text{rect}(t_2 - \tilde{\tau}_0))\} dt_1 dt_2 \end{aligned} \quad (3.42)$$

taking into account the correlation relationships among $\eta_k(t)$, $\forall k$, we further group

the subscripts m, n, k, l in (3.42) into three sets: $\Theta_1 \doteq \{\{m, n, k, l\} : \delta_{m,n,k,l} = 1\}$, $\Theta_2 \doteq \{\{m, n, k, l\} : (\delta_{m,n}\delta_{k,l} + \delta_{m,l}\delta_{k,n})(1 - \delta_{m,k}) = 1\}$, and $\Theta_3 \doteq \{\{m, n, k, l\} : \delta_{m,k}\delta_{n,l}(1 - \delta_{m,n}) = 1\}$. Therefore, $\mathbb{E}\{\zeta_{m,k}^{(3)}(\tilde{\tau}_0), \zeta_{n,l}^{(3)}(\tilde{\tau}_0)\}$ can be calculated in three cases correspondingly:

$$\mathbb{E}\{\zeta_{m,k}^{(3)}(\tilde{\tau}_0), \zeta_{n,l}^{(3)}(\tilde{\tau}_0)\} = \begin{cases} \int_0^{T_s} \int_0^{T_s} \mathbb{E}\{\eta_m^2(t_1)\eta_m^2(t_2)\} dt_1 dt_2, & \Theta_1 \\ \int_0^{T_s} \int_0^{T_s} \mathbb{E}\{\eta_m(t_1)\eta_k(t_1)\eta_m(t_2)\eta_k(t_2)\} dt_1 dt_2, & \Theta_2 \\ \int_0^{T_s} \int_0^{T_s} \mathbb{E}\{\eta_m^2(t_1)\eta_n^2(t_2)\} dt_1 dt_2, & \Theta_3. \end{cases} \quad (3.43)$$

For set Θ_1 , the expectation in the integral can be decomposed as [3]:

$$\begin{aligned} & \mathbb{E}\{\eta_m^2(t_1)\eta_m^2(t_2)\} \\ = & \mathbb{E}\{\eta_m^2(t_1)\}\mathbb{E}\{\eta_m^2(t_2)\} + \mathbb{E}\{\eta_m(t_1)\eta_m(t_2)\}\mathbb{E}\{\eta_m(t_1)\eta_m(t_2)\} \\ & + \mathbb{E}\{\eta_m(t_1)\eta_m(t_2)\}\mathbb{E}\{\eta_m(t_1)\eta_m(t_2)\} - 2\mathbb{E}\{\eta_m(t_1)\}\mathbb{E}\{\eta_m(t_1)\}\mathbb{E}\{\eta_m(t_2)\}\mathbb{E}\{\eta_m(t_2)\} \\ = & \mathbb{E}\{\eta_m^2(t_1)\}\mathbb{E}\{\eta_m^2(t_2)\} + 2\mathbb{E}\{\eta_m(t_1)\eta_m(t_2)\}\mathbb{E}\{\eta_m(t_1)\eta_m(t_2)\}. \end{aligned}$$

Accordingly, the correlation for set Θ_1 in (3.43) becomes:

$$\begin{aligned} & \int_0^{T_s} \int_0^{T_s} \mathbb{E}\{\eta_m^2(t_1)\eta_m^2(t_2)\} dt_1 dt_2 \\ = & \int_0^{T_s} \mathbb{E}\{\eta_m^2(t_1)\} dt_1 \int_0^{T_s} \mathbb{E}\{\eta_m^2(t_2)\} dt_2 + 2 \int_0^{T_s} \int_0^{T_s} \mathbb{E}\{\eta_m(t_1)\eta_m(t_2)\} dt_1 dt_2 \\ = & \left(\frac{N_0 T_s}{2}\right)^2 + 2N_0^2 \int_0^{T_s} \int_0^{T_s} (B \text{sinc}(B(t_2 - t_1)) \cos(2\pi f_0(t_2 - t_1)))^2 dt_1 dt_2 \\ = & \left(\frac{N_0 T_s}{2}\right)^2 + N_0^2 B T_s \end{aligned}$$

where the integral of the first summand is calculated using [62, eqs. (37)-(38)], and the second one using [62, eqs. (42)-(43)].

For set Θ_2 , noticing that the noise in different received segments are independent, we obtain:

$$\begin{aligned} & \int_0^{T_s} \int_0^{T_s} \mathbb{E} \{ \eta_m(t_1) \eta_k(t_1) \eta_m(t_2) \eta_k(t_2) \} dt_1 dt_2 \\ &= \int_0^{T_s} \int_0^{T_s} \mathbb{E} \{ \eta_m(t_1) \eta_m(t_2) \} \mathbb{E} \{ \eta_k(t_1) \eta_k(t_2) \} dt_1 dt_2 = N_0^2 B T_s / 2 \end{aligned}$$

and for set Θ_3 , the following holds:

$$\int_0^{T_s} \int_0^{T_s} \mathbb{E} \{ \eta_m^2(t_1) \eta_n^2(t_2) \} dt_1 dt_2 = \int_0^{T_s} \mathbb{E} \{ \eta_m^2(t_1) \} dt_1 \cdot \int_0^{T_s} \mathbb{E} \{ \eta_n^2(t_2) \} dt_2 = (N_0 T_s / 2)^2 .$$

As a result, the correlation function for $\zeta_{m,k}^{(3)}(\tilde{\tau}_0)$ can be obtained:

$$\begin{aligned} & \mathbb{E} \{ \zeta_{m,k}^{(3)}(\tilde{\tau}_0), \zeta_{n,l}^{(3)}(\tilde{\tau}_0) \} \\ &= \left(\left(\frac{N_0 T_s}{2} \right)^2 + N_0^2 B T_s \right) \delta_{m,n,k,l} + \frac{N_0^2}{2} B T_s (\delta_{m,n} \delta_{k,l} + \delta_{m,l} \delta_{k,n}) (1 - \delta_{m,k}) \\ & \quad + \left(\frac{N_0 T_s}{2} \right)^2 (\delta_{m,k} \delta_{n,l} (1 - \delta_{m,n})) \\ &= \frac{N_0^2}{2} B T_s (\delta_{m,n} \delta_{k,l} + \delta_{m,l} \delta_{k,n}) + \left(\frac{N_0 T_s}{2} \right)^2 \delta_{m,k} \delta_{n,l} . \end{aligned}$$

At last, we define the correlation between $\zeta_{m,k}^{(1)}(\tilde{\tau}_0)$ and $\zeta_{m,k}^{(3)}(\tilde{\tau}_0)$ as

$$\begin{aligned} & \mathbb{E} \{ \zeta_{m,k}^{(1)}(\tilde{\tau}_0), \zeta_{n,l}^{(3)}(\tilde{\tau}_0) \} \\ &= \int_0^{T_s} \int_0^{T_s} \mathbb{E} \{ (\eta_m(t_1) \rho_k(t_1) s_{m-1} s_{k-1} \text{rect}(t_1 + T_s - \tilde{\tau}_0) + \eta_m(t_1) \rho_k(t_1) s_m s_k \text{rect}(t_1 - \tilde{\tau}_0)) \\ & \quad \cdot (\eta_n(t_2) \eta_l(t_2) s_{n-1} s_{l-1} \text{rect}(t_2 + T_s - \tilde{\tau}_0) + \eta_n(t_2) \eta_l(t_2) s_n s_l \text{rect}(t_2 - \tilde{\tau}_0)) \} dt_1 dt_2 \\ &= \delta_{m,n} \delta_{m,l} \int_0^{T_s} \int_0^{T_s} (\mathbb{E} \{ \eta_m(t_1) \eta_m^2(t_2) \} \rho_k(t_1) s_{m-1} s_{k-1} \text{rect}(t_1 + T_s - \tilde{\tau}_0) \\ & \quad + \mathbb{E} \{ \eta_m(t_1) \eta_m^2(t_2) \} \rho_k(t_1) s_m s_k \text{rect}(t_1 - \tilde{\tau}_0)) dt_1 dt_2 \\ &= 0 \end{aligned}$$

where the last equality comes from the fact that $E\{\eta_m(t_1)\eta_m^2(t_2)\} = 0$ [3]. Therefore, $\zeta_{m,k}^{(1)}(\tilde{\tau}_0)$ and $\zeta_{m,k}^{(3)}(\tilde{\tau}_0)$ are mutually uncorrelated.

Since the noise terms of (3.38) are the superpositions of $\zeta_{m,k}^{(1)}(\tilde{\tau}_0)$ and $\zeta_{m,k}^{(3)}(\tilde{\tau}_0)$, they are also Gaussian distributed with means

$$\begin{aligned} E\{\xi^{(1)}(\tilde{\tau}_0)\} &= 0, \\ E\{\xi^{(3)}(\tilde{\tau}_0)\} &= \frac{E\{\zeta_{m,k}^{(3)}(\tilde{\tau}_0)\}}{K} = \frac{N_0 T_s}{2K}. \end{aligned}$$

Their variances can be computed by adding $E\{\zeta_{m,k}^{(1)}(\tilde{\tau}_0), \zeta_{n,l}^{(1)}(\tilde{\tau}_0)\}$ and $E\{\zeta_{m,k}^{(3)}(\tilde{\tau}_0), \zeta_{n,l}^{(3)}(\tilde{\tau}_0)\}$ with appropriate weights respectively:

$$\begin{aligned} \text{var}\{\xi^{(1)}(\tilde{\tau}_0)\} &= \frac{N_0 J_0^{\text{ML}}(\tilde{\tau}_0)}{2K}, \\ \text{var}\{\xi^{(3)}(\tilde{\tau}_0)\} &= \frac{N_0^2 B T_s}{K^2}. \end{aligned}$$

Combining the uncorrelated noise term together, we can obtain the mean and variance of the overall Gaussian noise $\xi^{\text{ML}}(\tilde{\tau}_0)$:

$$\begin{aligned} E\{\xi^{\text{ML}}(\tilde{\tau}_0)\} &= E\{\xi^{(3)}(\tilde{\tau}_0)\} = \frac{N_0 T_s}{2K}, \\ \text{var}\{\xi^{\text{ML}}(\tilde{\tau}_0)\} &= 4 \times \text{var}\{\xi^{(1)}(\tilde{\tau}_0)\} + \text{var}\{\xi^{(3)}(\tilde{\tau}_0)\} = \frac{2N_0 J_0^{\text{ML}}(\tilde{\tau}_0)}{K} + \frac{N_0^2 B T_s}{K^2}. \end{aligned}$$

CHAPTER 4

THE ℓ_1 -REGULARIZED LEAST SQUARES FORMULATION FOR COOPERATIVE TARGET LOCALIZATION AND MALICIOUS ANCHOR IDENTIFICATION

Secure target localization in the presence of malicious anchors is a critical issue in wireless sensor networks (WSNs), where compromised anchors attempt to mislead the target to a false position by broadcasting incorrect self location information. In this chapter, we explicitly incorporate anchors' misplacements into the distance measurement model and explore the pairwise sparse nature of the misplacements. We formulate the secure target localization problem as an ℓ_1 -regularized least squares (LS) problem, whose objective is to simultaneously locate the targets as well as identify the compromised anchors. We establish the pairwise sparsity threshold which defines the upper bound for the number of identifiable malicious anchors, and propose a simple projected gradient search algorithm to solve this novel ℓ_1 -regularized LS problem in WSNs. Particularly, we consider two localization situations, namely, a single target noncooperative scenario and two-target cooperative scenario. It is demonstrated that with target cooperation, the capability of target location estimation is enhanced in terms of estimation accuracy, and the capability of malicious anchor identification is also improved in the sense of misplacement estimation. Simulations are provided to corroborate the results.

4.1 Motivation

A localization process is accomplished in two phases, i.e., the distance measurement phase and the location update phase. While the first phase, by the means of TOA estimation for IR UWB signals, is the topic of the preceding chapter, we will move on to the second phase in this chapter.

Secure target localization in the presence of malicious anchors is a fundamental and intriguing problem in wireless sensor networks (WSNs) [45]. When targets are deployed in hostile environments, attackers may disturb the localization process and make the location estimation unreliable. Unreliable target locations lead to severe consequences, e.g., wrong military decisions on the battlefield or mistakenly granting access rights to people [67]. Localization attacks can be launched in either the network layer or the physical layer. This chapter focuses on the physical layer attack which can be classified into simple attacks and complicated attacks [67]. In a simple attack, an attacker may fake the distance measurement between the target and a compromised anchor by reporting fake self location or manipulating the transmission power [68]. A complicated attack involves multiple compromised anchors which can either independently broadcast fake information or collaborate to mislead the target to the same false location [67]. The former is referred to as an uncoordinated attack and the latter is often termed as a collusion attack. A collusion attack is usually much more powerful than an uncoordinated one.

The presence of malicious anchors induces discrepancy, or inconsistency, between the measured distance obtained from the first phase and the calculated distance from second phase target location estimate. Based on this, malicious anchors can be filtered out such that the remaining anchors yield more consistent estimate [40, 41, 35]. Reference [35] starts from a randomly picked subset of size 3 and make an LS es-

timation of the target location. It then accumulates the number of the remaining anchors which have the consistent distance measurements with this estimate. If the consistency number is beyond a certain predetermined threshold, then the estimate is regarded as correct and the algorithm stops; otherwise, it randomly picks another subset to repeat the consistency check procedure until a correct estimate can be obtained. The problem with this method is that, without knowledge of the number of malicious anchors, it is hard to choose the consistency threshold. Reference [41] adopts a suboptimal searching method. Unlike [35], it starts from the entire available anchor set and deletes one malicious anchor which induces the largest inconsistency at each stage, until all malicious anchors are removed. Reference [40] tries to identify the outliers by minimizing the median of the squared distance measurement errors. These methods are straightforward and easy to implement. However, they do not directly tackle the false location information. The optimal estimation can only be achieved by enumerating all possible attack scenarios.

To address this problem, we explicitly incorporate anchors' misplacements, i.e., location errors, into the distance measurement model to locate the target and identify malicious anchors simultaneously. By exploring the pairwise sparse nature inherent in the misplacements, we are able to formulate secure target localization as an ℓ_1 -regularized LS problem. Under this problem formulation, we establish the pairwise sparsity threshold, which defines the largest possible number of identifiable malicious anchors. We then propose a simple projected gradient search algorithm to solve the ℓ_1 -regularized LS problem in WSNs.

Particularly, we consider two scenarios for the secure localization problem, namely, a single target noncooperative localization and two-target cooperative localization. While single target localization is a typical scenario in the field of secure localization as in [45, 68, 41, 37, 40, 41], to the authors' knowledge, we are the first to incorporate

target cooperation into this area. With the proposed ℓ_1 -regularized LS formulation, we recognize the misplacement estimation limitation in the single target case; that is, solving the ℓ_1 -regularized LS problem can only identify the malicious anchors but fails to yield correct misplacement estimates. It is demonstrated that the misplacement estimation can be enhanced by incorporating target cooperation. Certainly, due to cooperation, target location estimation accuracy can be improved as well.

The organization of this chapter is as follows. We first provide preliminary knowledge on sparse reconstruction in Section 4.2, and describe the secure localization problem in the presence of malicious anchors in Section 4.3. In Section 4.4, we propose the novel ℓ_1 -regularized LS formulation, derive the upper bound for the number of identifiable malicious anchors, and discuss the misplacement estimation capability for both single target and cooperative targets scenarios. A simple projected gradient search algorithm is developed in Section 4.5 to solve the ℓ_1 -regularized LS problem. Simulation results are provided in Section 4.6, followed by conclusions in Section 4.7.

4.2 Sparse Reconstruction Preliminaries

Many problems in signal processing and statistics involve finding sparse solutions to underdetermined, or ill-conditioned, linear equations in the absence of noise

$$\mathbf{y} = \mathbf{A}\mathbf{x}$$

where $\mathbf{x} \in \mathbf{R}^N$ is the unknown vector, $\mathbf{y} \in \mathbf{R}^M$ is the observation vector, and $\mathbf{A} \in \mathbf{R}^{M \times N}$ is a fat matrix with $M < N$. The sparsest solution is given by [9]

$$\min_{\mathbf{x}} \|\mathbf{x}\|_0 \quad \text{subject to} \quad \mathbf{A}\mathbf{x} = \mathbf{y} \quad (4.1)$$

where $\|\mathbf{u}\|_0$ denotes the ℓ_0 norm of \mathbf{u} which is the number of nonzero components. Solving this problem requires exhaustive searches over all subsets of columns of \mathbf{A} looking for the smallest subset representing the signal. This is clearly combinatorial in nature and has exponential complexity [9].

An alternative method is to use the ℓ_1 norm suggested by Basis Pursuit [12]:

$$\min_{\mathbf{x}} \|\mathbf{x}\|_1 \quad \text{subject to} \quad \mathbf{A}\mathbf{x} = \mathbf{y} \quad (4.2)$$

where $\|\mathbf{u}\|_1 = \sum_i |u_i|$ denotes the ℓ_1 norm of \mathbf{u} . It is well known that the ℓ_1 norm is convex and the problem in (4.2) can be recast as a linear program [12].

The tractable ℓ_1 norm problem in (4.2) always has a solution. However, this solution is not necessarily unique. It is also not necessarily equivalent to the ℓ_0 norm minimization solution of (4.1). Among a handful of works which discussed uniqueness of the sparsest solution and equivalence between (4.1) and (4.2), [18] derived inspiring results without invoking limited assumptions on the data matrix \mathbf{A} , such as concatenation of two orthobases. Instead, it studied the threshold for sparsity reconstruction given a general non-orthogonal data matrix \mathbf{A} .

[18] defines the Spark of a matrix as the size of the smallest linearly dependent subset, and shows that whenever the unknown vector \mathbf{x} has less than $\text{Spark}(\mathbf{A})/2$ nonzeros, the sparsest reconstruction can be uniquely determined. Additionally, $\mu_{1/2}(\mathbf{G})$ of a symmetric matrix \mathbf{G} with normalized diagonal elements is defined as the smallest number m such that some collection of m off-diagonal magnitudes arising in a single row or column of \mathbf{G} sums at least to $\frac{1}{2}$. [18] proves that when the unknown vector \mathbf{x} has less than $\mu_{1/2}(\mathbf{A}^T \mathbf{A})$ nonzeros, the solutions to (4.1) and (4.2) are equivalent. Since $\frac{1}{2}\text{Spark}(\mathbf{A}) > \mu_{1/2}(\mathbf{A}^T \mathbf{A})$, the latter is a more strict condition.

With the uniqueness and equivalence condition satisfied, one easily knows that a

highly sparse solution, if it exists, to the ℓ_0 norm problem in (4.1) is identical to the solution of the ℓ_1 norm problem in (4.2). Also, if the ℓ_1 solution is sparse beyond a certain specific threshold, then the solution is known (without checking) to be solution of the ℓ_0 problem.

For realistic noisy data, the measurement has the form

$$\mathbf{y} = \mathbf{A}\mathbf{x} + \mathbf{n}$$

where $\mathbf{n} \in \mathbf{R}^M$ is the Gaussian noise. Instead of an exact sparse reconstruction from \mathbf{y} , an ℓ_1 -regularized LS problem [12] is preferable here:

$$\min_{\mathbf{x}} \frac{1}{2} \|\mathbf{y} - \mathbf{A}\mathbf{x}\|_2^2 + \lambda \|\mathbf{x}\|_1 \quad (4.3)$$

where $\|\mathbf{u}\|_2 = (\sum_i u_i^2)^{1/2}$ denotes the ℓ_2 norm of \mathbf{u} , and λ is the nonnegative regularization parameter. The use of ℓ_1 regularization yields decomposition of \mathbf{y} to signal plus residue, and λ is an important parameter for signal and residue tradeoff: as $\lambda \rightarrow 0$, the solution behaves exactly like BP applied to \mathbf{y} ; as $\lambda \rightarrow \infty$, the residue dominates. Recently, the idea of ℓ_1 regularization has been receiving a lot of interest. BP denoising, the least absolute shrinkage and selection operator (Lasso), and compressed sensing are well-known examples of this approach.

The objective function of the ℓ_1 -regularized linear LS problem in (4.3) is convex but not differentiable. Therefore, there is no analytic formula for the optimal solution. In the literature, several optimization algorithms and codes have been proposed to solve this problem. For a detailed review of these algorithms, the readers are referred to [34, 19] and references therein. For example, generic methods for nondifferentiable convex problem such as subgradient methods [5] can be used. The ℓ_1 regularized

problem in (4.3) can be transformed to a convex quadratic problem with linear inequality constraints, which can be solved by various interior-point methods [34]. A gradient projection algorithm in [19] is shown to be able to handle large problems efficiently.

4.3 Distance Measurement Model and Misplacement Sparsity

The compromised anchors may cheat by reporting fake self locations or distance measurements. In this chapter, we focus on the former case, which has been much less studied.

The structure of a sensor network in the presence of cheating anchors is illustrated in Fig. 4.1. On the two-dimensional (2-D) plane, suppose that we have N_t targets, each with unknown location $\mathbf{t}_j = [t_{j_x}, t_{j_y}]^T, j = 1, \dots, N_t$, and N_s anchors, each with true location $\bar{\mathbf{s}}_i = [\bar{s}_{i_x}, \bar{s}_{i_y}]^T, i = 1, \dots, N_s$. The sub-subscripts x and y stand for the 2-D Cartesian coordinates. In the presence of malicious attack, some of the anchors may broadcast incorrect self locations. Denote the claimed anchor locations as $\mathbf{s}_i = [s_{i_x}, s_{i_y}]^T, i = 1, \dots, N_s$, and the misplacements, i.e., the differences between the true and claimed locations, as $\Delta\mathbf{s}_i = [\Delta s_{i_x}, \Delta s_{i_y}]^T \doteq \bar{\mathbf{s}}_i - \mathbf{s}_i, i = 1, \dots, N_s$. Of course, for honest anchors, $\mathbf{s}_i = \bar{\mathbf{s}}_i$ and $\Delta\mathbf{s}_i = 0$. Generally, the targets have no idea about which anchors are honest and which are malicious. Without malicious anchor identification, the targets can be misled to false locations.

In this chapter, we consider two cases, namely the $N_t = 1$ single target case and the $N_t = 2$ cooperative targets case. While single target localization is the common scenario in the existing secure localization work, secure localization capability can be further improved by allowing target cooperation.

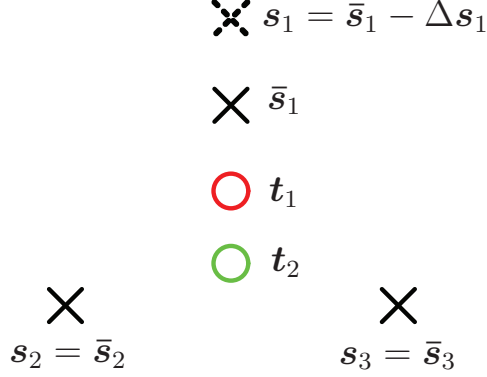


Figure 4.1: Illustration of a wireless sensor network in the presence of malicious anchors.

4.3.1 The $N_t = 1$ Single Target Case

We first consider the single target case with $N_t = 1$ following the literature [40, 41, 68, 45]. Although the system can have multiple targets, $N_t = 1$ means that these targets only communicate with anchors and do not communicate with each other. Additionally, the central unit processes the location information for each target separately. This corresponds to a noncooperative scenario.

Let $d_{j,i}$ denote the distance measurement from the i th anchor to the j th target, which can be obtained by RSS or TOA based ranging. Without loss of generality, we consider localization of the first target in the single target scenario. Then the distance measurement model accounting for anchor misplacements can be written as

$$d_{1,i} = \|\mathbf{s}_i + \Delta \mathbf{s}_i - \mathbf{t}_1\|_2 + n_{1,i}, \quad \forall i = 1, \dots, N_s \quad (4.4)$$

where the $n_{1,i}$ s are i.i.d. zero-mean Gaussian distributed measurement noise with variance σ^2 . Note that we incorporate the misplacement $\Delta \mathbf{s}_i$ into (4.4) to explicitly explore the influence of misplacement on the target location estimation.

Based on the distance measurement model (4.4), the traditional LS approach looks

for the best estimates via minimizing the sum of squared errors

$$\sum_{i=1}^{N_s} (d_{1,i} - \|\mathbf{s}_i + \Delta\mathbf{s}_i - \mathbf{t}_1\|_2)^2 \quad (4.5)$$

over all possible \mathbf{t}_1 and $\Delta\mathbf{s}_i$ s. This is obviously an underdetermined problem as there are $(2N_s + 2)$ unknowns but only N_s observations. As a result, it is hard to obtain the desired solution from traditional LS, unless we have more restrictions on the unknowns.

In secure localization, in order to successfully combat the attack of malicious anchors, we must have sufficient honest ones. This means that out of the total N_s misplacements, only a few $\Delta\mathbf{s}_i$ s corresponding to the malicious anchors can take nonzero values. In other words, the stacked misplacement vector

$$\Delta\mathbf{s} = [\Delta\mathbf{s}_1^T, \dots, \Delta\mathbf{s}_{N_s}^T]^T$$

is a sparse vector. Besides, since a 2-D location is represented by a pair of x - and y -coordinates, the nonzero values of $\Delta\mathbf{s}$ must appear in pairs corresponding to the associated malicious anchors.

Definition 4.1 (Pairwise Sparse): *A vector $\mathbf{u} \in \mathbf{R}^{2N}$ is said to be pairwise sparse, if it has only a few pairs of nonzero components $\{u_{2i-1}, u_{2i}\}$, for some $i \in [1, N]$, and zero components elsewhere.*

The underdetermined LS problem has a unique solution only if the number of nonzero pairs in the pairwise sparse $\Delta\mathbf{s}$ is below a threshold, which will be established in the next section.

4.3.2 The $N_t = 2$ Cooperative Targets Case

In this chapter, two-target cooperative localization means that the central unit processes the location information from both targets together and the targets can communicate with each other to obtain an additional target-target distance measurement. The signal model for two cooperative targets can be adapted from the single target case of (4.4) with slight modification. In addition to anchor-target distances $d_{j,i}$ s, target cooperation provides target-target distance measurement, denoted by d_c . Therefore, the overall distance measurement model can be written as

$$d_{j,i} = \|\mathbf{s}_i + \Delta\mathbf{s}_i - \mathbf{t}_j\|_2 + n_{j,i}, \quad \forall j = 1, 2, \quad i = 1, \dots, N_s \quad (4.6)$$

and

$$d_c = \|\mathbf{t}_1 - \mathbf{t}_2\|_2 + n_c \quad (4.7)$$

where the subscript c denotes the “cooperative” measurement. The objective for the traditional LS location estimation is to minimize the sum of squared errors accounting for both anchor-target measurements in (4.6) and target-target measurement in (4.7):

$$\sum_{j=1}^2 \sum_{i=1}^{N_s} (d_{j,i} - \|\mathbf{s}_i + \Delta\mathbf{s}_i - \mathbf{t}_j\|_2)^2 + (d_c - \|\mathbf{t}_1 - \mathbf{t}_2\|_2)^2. \quad (4.8)$$

This is, again, an underdetermined LS problem with $(2N_s + 4)$ unknowns and $(2N_s + 1)$ observations. It can be uniquely solved only if the number of nonzero pairs in the pairwise sparse $\Delta\mathbf{s}$ does not exceed the upper bound established next. Note that, compared with the single target case, target cooperation enables twice as many observations but adds only two more unknowns. Therefore, we have reasons to expect

improved secure localization capability with target cooperation.

4.4 The Novel ℓ_1 -Regularized LS Formulation

Given the pairwise sparse nature of the misplacement vector $\Delta \mathbf{s}$, our goal is to simultaneously estimate the target location and identify the nonzero pairs in $\Delta \mathbf{s}$. The ℓ_1 norm minimization technique is well known to solve underdetermined or ill-conditioned linear sparse problems. Inspired by this idea, we start from the ℓ_1 norm minimization problem formulation in the single target case, assuming that the distance measurement is noise-free and only affected by the misplacement

$$\begin{aligned} \min_{\Delta \mathbf{s}, \mathbf{t}_1} \quad & \|\Delta \mathbf{s}\|_1 \\ \text{s. t.} \quad & d_{1,i} = \|\mathbf{s}_i + \Delta \mathbf{s}_i - \mathbf{t}_1\|_2, \quad \forall i = 1, \dots, N_s. \end{aligned} \quad (4.9)$$

Compared to the linear problem in (4.2), the above problem is more difficult due to its nonlinear and nonconvex form. In addition, instead of the simple component-wise sparsity, our misplacement vector possesses a pairwise sparse property. Furthermore, unlike (4.2), our problem does not require the entire unknown vector $\mathbf{x} = [\Delta \mathbf{s}^T, \mathbf{t}_1^T]^T$ to be sparse. While the misplacement $\Delta \mathbf{s}$ is pairwise sparse, the target location \mathbf{t}_1 is generally not. Despite these differences and difficulties, we will establish the rationale for (4.9) from two aspects. The first one is the pairwise sparsity upper bound below which the desired misplacement estimate is the sparsest solution together with correct target location estimate. The other is the equivalence condition which makes sure that the desired misplacement estimate and the target location estimate can be obtained via solving the ℓ_1 norm minimization problem in (4.9).

4.4.1 Pairwise Sparsity Upper Bound

An underdetermined problem can have infinitely many solutions satisfying the observations. Among all the possible solutions, if we are looking for the sparsest one, then a unique solution can be determined. Therefore, to uniquely identify nonzero misplacements and obtain target location estimate in (4.9), we need to develop a condition under which the desired solution is sparsest in terms of misplacement estimate $\widehat{\Delta \mathbf{s}}$ and correct in terms of target location estimate $\hat{\mathbf{t}}_1$.

To this end, we first present three basic assumptions on the network structure and malicious attack scenarios. In these assumptions and the following analysis, consistency between target location and anchor location means that the calculated distance between the two locations satisfies the corresponding noiseless distance measurement.

AS(i): We assume that no three anchors are located on a straight line. This is a common assumption made for wireless sensor networks. It guarantees that the target location can be uniquely determined by any three anchors in the absence of malicious attack. It also implies that the image of the target's true location with respect to straight line connecting any two anchors is distinct.

AS(ii): It is assumed that each malicious anchor's claimed location is not consistent with the target's true location. Otherwise, this anchor is obviously not harmful to target localization and will not be labeled as malicious from the perspective of infrastructure. Therefore, it is safe to assume that the distance $\|\mathbf{s}_i - \mathbf{t}_1\|_2 \neq \|\bar{\mathbf{s}}_i - \mathbf{t}_1\|_2 = d_{1,i}$ and the malicious anchor's claimed location is not on the circle centered at the target with radius of being measurement $d_{1,i}$.

AS(iii): The target's misled location is assumed to be consistent with at most one honest anchor. Target's misled location is defined as the location which is consistent with one or some malicious anchors' claimed locations in an uncoordinated attack, or consistent with all malicious anchors' claimed locations in a collusion attack. Firstly,

the possibility that the misled location is consistent with more than two honest anchors is eliminated by AS(ii), since consistency with more than two honest anchors implies that the misled location is nothing but the target's true location. Secondly, it is not practical for the misled location to be consistent with two honest anchors. This amounts to moving the target to its image position with respect to straight line connecting two honest anchors. Without location information of the target and honest anchors, malicious attack is not able to accomplish this task. However, it is still possible for the target's misled location to coincidentally be consistent with one honest anchor.

With these assumptions, all the possible solutions satisfying observations in (4.9) can be divided into three groups. Suppose that the number of malicious anchors is N_m .

In the first group, the target location estimate is consistent with all honest anchors; that is, the target is correctly located at its true position. According to AS(ii), none of the malicious anchors' claimed locations is consistent with the target's true location. Therefore, we have nonzero misplacement estimates for all malicious anchors and the number of nonzero misplacement estimates is N_m . This is our desired solution which identifies all the malicious anchors and obtains the target's location. The honest anchors may have nonzero misplacement estimates, which will definitely result in more nonzero misplacement estimates than the desired solution.

In the second group, the target location estimate is consistent with some or all malicious anchors' claimed locations. In this group, the target is consistent with at most N_m malicious anchors. According to AS(iii), the misled location is also consistent with at most one honest anchor. Therefore, the total number of nonzero misplacement estimates in this group is no less than $N_s - N_m - 1$. Of course, if the target's misled location turns out to be inconsistent with any honest anchor, the

nonzero misplacement estimates can be $N_s - N_m$.

In the third group, the target location estimate can be arbitrarily anywhere on the field other than positions in the first and second groups. According to AS(i), the target is at most consistent with two honest anchors. As a result, the number of nonzero misplacement estimates is no less than $N_s - 2$.

The desired solution in the first group identifies all the malicious anchors and obtains the target's location. In order to make sure that the desired solution is the sparsest one, we need the following conditions:

$$N_m < N_s - N_m - 1, \text{ and } N_m < N_s - 2$$

which are equivalent to $N_m < (N_s - 1)/2$ for $N_s > 3$. In other words, given the total anchor number $N_s > 3$, the largest number of malicious anchors with which the desired solution is sparsest is

$$N_m = \left\lfloor \frac{N_s - 2}{2} \right\rfloor. \quad (4.10)$$

This is the pairwise sparsity upper bound for the single target case. As long as the number of malicious anchors does not exceed this upper bound, unique identification of the malicious anchors as well as target location estimation can be achieved simultaneously. Note that, for some malicious attack where the target's misled location turns out to be not consistent with any honest anchor, we can have $N_m < N_s/2$ tolerable malicious anchors.

Given the cooperative distance measurement models in (4.6) and (4.7), in the absence of measurement noise, the ℓ_1 norm minimization problem for $N_t = 2$ cooperative

targets case can be formulated as

$$\begin{aligned}
& \min_{\Delta \mathbf{s}, \mathbf{t}_1, \mathbf{t}_2} \|\Delta \mathbf{s}\|_1 & (4.11) \\
& \text{s. t.} & d_{j,i} = \|\mathbf{s}_i + \Delta \mathbf{s}_i - \mathbf{t}_j\|_2, \quad \forall j = 1, 2, \quad i = 1, \dots, N_s \\
& & d_c = \|\mathbf{t}_1 - \mathbf{t}_2\|_2.
\end{aligned}$$

The pairwise sparsity upper bound in (4.10) for the single target case can be directly applied to the two-target cooperative case, except for a slightly relaxed AS(ii). With two cooperative targets, we assume that each malicious anchor's claimed location is not consistent with both targets' true locations simultaneously. This essentially eliminates the possibility that a malicious anchor's claimed location falls at the image of its own true location with respect to the two targets.

The pairwise sparsity upper bound accounting for both the single target case and the two cooperative targets case is summarized in the following.

Proposition 4.1 *In secure target localization in the presence of malicious anchors, suppose that there are N_s anchors and $N_t = 1$ single target or $N_t = 2$ cooperative targets. The largest tolerable number of malicious anchors such that unique identification of malicious anchors and estimation of the target location can be simultaneously achieved is $\lfloor (N_s - 2)/2 \rfloor$.*

4.4.2 Misplacement Estimation Capability

We learned from the preceding subsection that the single target case and two-target cooperative case have the same identification upper bound with slightly different AS(ii). This means that, below the upper bound, both cases can identify the nonzero misplacements associated to the malicious anchors. However, in terms of estimating the x - and y -coordinates within each misplacement estimate, they exhibit

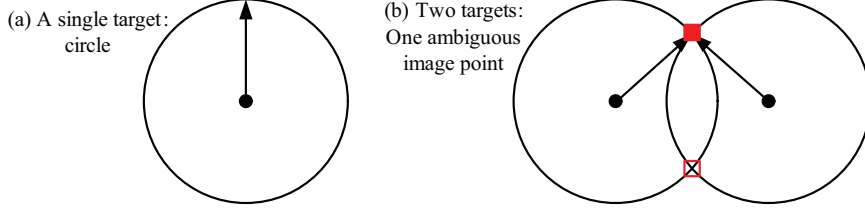


Figure 4.2: Illustration of anchor location estimation ambiguity regions for (a) a single target case and (b) two cooperative targets case.

different capability.

Anchor misplacement estimation can essentially be interpreted as a reverse problem of target localization. In a pure localization problem, unknown target location is inferred from known anchors' locations and distance measurements. On a 2-D plane, one needs at least three anchors to uniquely determine the location of a target. Likewise, in a pure misplacement estimation problem, unknown anchor location is estimated from known targets' locations and distance measurements. One needs at least three targets to uniquely determine the location of an anchor.

With the problem of anchor misplacement estimation, each target provides one observation for each misplacement. Therefore, in both the single target and two targets cases, insufficient observations result in misplacement ambiguity, and eventually anchor location estimation ambiguity. As illuminated in Fig. 4.2, in the single target case, the ambiguity region of the estimated anchor location, defined as $\widehat{\mathbf{s}}_i = \mathbf{s}_i + \widehat{\Delta \mathbf{s}}_i$, includes the entire circle centered at the target with radius equal to the measured distance between the target and the anchor. This inevitably causes misplacement estimation limitation in the single target case.

In the two-target case, however, the ambiguity region is greatly reduced to two points as shown in Fig. 4.2. One is the anchor's true location, and the other is the image of the true location with respect to the straight line connecting both targets. The reduced ambiguity region means enhanced misplacement estimation capability.

By allowing target cooperation, it is more likely that misplacement estimates will be correct. Certainly, the enhanced misplacement estimation capability resulted from target cooperation is not limited to the proposed approach. It can be appropriately generalized to any other secure localization technique to improve that technique's capability.

4.4.3 Equivalence Condition

In order to simultaneously identify the malicious anchors as well as estimate the target locations via solving the ℓ_1 norm minimization problem, we need to address the other issue; whether the desired sparsest solution has the smallest ℓ_1 norm among all possible solutions. This issue is even more complicated due to nonlinearity, non-convexity and the misplacement estimation limitation in the single target case. To simplify the analysis, we only consider the two-target cooperative case here. We will calculate ℓ_1 norms of the misplacement estimates for the alternative solutions satisfying observations in (4.11) and compare those with $\|\widehat{\Delta\mathbf{s}}\|_1$ of the desired sparsest solution $\hat{\mathbf{x}}_c$, where $\mathbf{x}_c \doteq [\Delta\mathbf{s}^T, \mathbf{t}_1^T, \mathbf{t}_2^T]^T$.

The alternative solutions satisfying the observations, other than the expected sparsest $\hat{\mathbf{x}}_c$, are comprised of solutions which preserve the relative structure of the original network but allow the entire network rotation and/or parallel shift. With rotation and parallel shift, all the anchors can have nonzero misplacement values. Note that it is unnecessary to consider rotation and shift over the entire field, but only the local area around the true network position. Suppose that the rotation angle is $\theta \in (-\pi, \pi]$, and the parallel shift is $\mathbf{e} = [e_x, e_y]^T$, for a particular alternative solution. Then, the resultant location for the i th anchor with true location $\bar{\mathbf{s}}_i$ becomes

$\bar{\mathbf{s}}_i^{(a)}$ with x - and y -coordinates:

$$\begin{aligned}\bar{s}_{i_x}^{(a)} &= \bar{s}_{i_x} \cos \theta - \bar{s}_{i_y} \sin \theta - e_x, \\ \bar{s}_{i_y}^{(a)} &= \bar{s}_{i_x} \sin \theta + \bar{s}_{i_y} \cos \theta - e_y\end{aligned}$$

and the alternative misplacement estimate is the difference between the resultant location $\bar{\mathbf{s}}_i^{(a)}$ and the claimed location \mathbf{s}_i with ℓ_1 norm $L_i = \|\bar{\mathbf{s}}_i^{(a)} - \mathbf{s}_i\|_1$. Denote the set of honest anchors as Γ_h with cardinality N_h , and the set of malicious anchors as Γ_m with cardinality N_m . Clearly, $N_h + N_m = N_s$. For the honest anchor whose claimed location is $\mathbf{s}_i = \bar{\mathbf{s}}_i$, we have the ℓ_1 norm of the misplacement estimate as

$$L_i = \|\bar{\mathbf{s}}_i^{(r)} - \mathbf{e}\|_1, \quad i \in \Gamma_h$$

where $\bar{\mathbf{s}}_i^{(r)} \doteq [\bar{s}_{i_x} \cos \theta - \bar{s}_{i_y} \sin \theta, \bar{s}_{i_x} \sin \theta + \bar{s}_{i_y} \cos \theta]^T - \bar{\mathbf{s}}_i$ is the anchor location change resulted from rotation. For the malicious anchor whose claimed location is $\mathbf{s}_i = \bar{\mathbf{s}}_i - \Delta \mathbf{s}_i$, we have

$$L_i = \|\bar{\mathbf{s}}_i^{(r)} - \mathbf{e} + \Delta \mathbf{s}_i\|_1, \quad i \in \Gamma_m .$$

Then the ℓ_1 norm of the overall misplacement estimate for the alternative solution can be calculated as $L = \sum_{i \in \Gamma_h} L_i + \sum_{i \in \Gamma_m} L_i$. Subtract $\|\widehat{\Delta \mathbf{s}}\|_1 = \sum_{i \in \Gamma_m} \|\Delta \mathbf{s}_i\|_1$ from L , and the difference of the ℓ_1 norm between the alternative solution and the sparsest

solution can be written as

$$\begin{aligned}
& L - \|\widehat{\Delta \mathbf{s}}\|_1 \\
&= \sum_{i \in \Gamma_h} \|\bar{\mathbf{s}}_i^{(r)} - \mathbf{e}\|_1 + \sum_{i \in \Gamma_m} \|\bar{\mathbf{s}}_i^{(r)} - \mathbf{e} + \Delta \mathbf{s}_i\|_1 - \sum_{i \in \Gamma_m} \|\Delta \mathbf{s}_i\|_1 \\
&\geq \sum_{i \in \Gamma_h} \|\bar{\mathbf{s}}_i^{(r)} - \mathbf{e}\|_1 + \sum_{i \in \Gamma_m} \max\{\|\bar{\mathbf{s}}_i^{(r)} - \mathbf{e}\|_1 - \|\Delta \mathbf{s}_i\|_1, \|\Delta \mathbf{s}_i\|_1 - \|\bar{\mathbf{s}}_i^{(r)} - \mathbf{e}\|_1\} - \sum_{i \in \Gamma_m} \|\Delta \mathbf{s}_i\|_1 \\
&= \sum_{i \in \Gamma_h} \|\bar{\mathbf{s}}_i^{(r)} - \mathbf{e}\|_1 + \sum_{i \in \Gamma_m^+} (\|\bar{\mathbf{s}}_i^{(r)} - \mathbf{e}\|_1 - \|\Delta \mathbf{s}_i\|_1) + \sum_{i \in \Gamma_m^-} (\|\Delta \mathbf{s}_i\|_1 - \|\bar{\mathbf{s}}_i^{(r)} - \mathbf{e}\|_1) - \sum_{i \in \Gamma_m} \|\Delta \mathbf{s}_i\|_1 \\
&= \sum_{i \in \Gamma_h} \|\bar{\mathbf{s}}_i^{(r)} - \mathbf{e}\|_1 + \sum_{i \in \Gamma_m^+} \|\bar{\mathbf{s}}_i^{(r)} - \mathbf{e}\|_1 - \sum_{i \in \Gamma_m^-} \|\bar{\mathbf{s}}_i^{(r)} - \mathbf{e}\|_1 - 2 \sum_{i \in \Gamma_m^+} \|\Delta \mathbf{s}_i\|_1 \tag{4.12} \\
&\geq \sum_{i \in \Gamma_h} \|\bar{\mathbf{s}}_i^{(r)} - \mathbf{e}\|_1 + \sum_{i \in \Gamma_m} (\|\Delta \mathbf{s}_i\|_1 - \|\bar{\mathbf{s}}_i^{(r)} - \mathbf{e}\|_1) - \sum_{i \in \Gamma_m} \|\Delta \mathbf{s}_i\|_1 \\
&= \sum_{i \in \Gamma_h} \|\bar{\mathbf{s}}_i^{(r)} - \mathbf{e}\|_1 - \sum_{i \in \Gamma_m} \|\bar{\mathbf{s}}_i^{(r)} - \mathbf{e}\|_1 \tag{4.13}
\end{aligned}$$

The difference lower bound in (4.13) is an interesting one. It only depends on the true locations of the anchors. Ideally, suppose that both the honest and malicious anchors are densely and uniformly deployed on the entire field of interest. Then after any rotation and parallel shift location change, the average norm for the honest anchors is identical to the average norm for the malicious anchors. Therefore, if the number of honest anchors is greater than that of malicious anchors, the lower bound is strictly greater than zero, and the sparsest solution indeed has the smallest ℓ_1 norm. (4.13) confirms the fact that, even in the ideal scenario, the number of identifiable malicious anchors cannot be larger than the number of honest anchors. In a practical network, however, there are only a finite number of anchors residing at certain locations. In this case, as indicated by a tighter bound given in (4.12), the ℓ_1 norm difference depends on the anchor locations as well as the malicious anchors' misplacements. To ensure the difference greater than zero, the overall ℓ_1 norm increase from the honest anchors and part of the malicious anchors should be able to compensate the ℓ_1 norm

decrease from the other malicious anchors and the misplacements. Depending on the real network structure and attack scenario, one may need more than $(N_s - 1)/2$ honest anchors to meet the positive difference condition. In other words, Proposition 4.1 provides an upper bound for the number of identifiable malicious anchors, but to guarantee that the equivalence condition holds locally, the upper bound may not be achieved.

Recall that in the two-target cooperative case, two observations for each misplacement result in an additional ambiguous location which is the image of the true anchor location with respect to the straight line connecting both targets. Whenever the malicious anchor is determined to be at the image position, its ℓ_1 norm change should be accounted for accordingly. For those alternative solutions, honest anchors also have their images. But due to the all-zero misplacement initial point, it is less likely to end up with an image estimate for an honest anchor.

To refine the ℓ_1 norm difference addressing possible image location estimates, define the image of the i th malicious anchor's true location with respect to the straight line connecting two targets as $\bar{\mathbf{s}}_i^{(\text{im})}$. Then the ℓ_1 norm of the misplacement estimate for the i th malicious anchor in the sparsest solution is

$$\|\bar{\mathbf{s}}_i^{(\text{im})} - \bar{\mathbf{s}}_i + \Delta \mathbf{s}_i\|_1 \leq \|\Delta \mathbf{s}_i\|_1 + \|\bar{\mathbf{s}}_i - \bar{\mathbf{s}}_i^{(\text{im})}\|_1. \quad (4.14)$$

Also define the image of the i th malicious anchor's location in the alternative solution as $\bar{\mathbf{s}}_i^{(a,\text{im})}$. Then the ℓ_1 norm of the misplacement estimate for the i th malicious anchor

in the alternative solution can be written as

$$\begin{aligned}
\|\bar{\mathbf{s}}_i^{(a,\text{im})} - \bar{\mathbf{s}}_i + \Delta \mathbf{s}_i\|_1 &= \|\bar{\mathbf{s}}_i^{(a,\text{im})} - \bar{\mathbf{s}}_i^{(a)} + \bar{\mathbf{s}}_i^{(a)} - \bar{\mathbf{s}}_i + \Delta \mathbf{s}_i\|_1 \\
&\geq \|\bar{\mathbf{s}}_i^{(a)} - \bar{\mathbf{s}}_i + \Delta \mathbf{s}_i\|_1 - \|\bar{\mathbf{s}}_i^{(a)} - \bar{\mathbf{s}}_i^{(a,\text{im})}\|_1 \\
&= \|\bar{\mathbf{s}}_i^{(r)} - \mathbf{e} + \Delta \mathbf{s}_i\|_1 - \|\bar{\mathbf{s}}_i^{(a)} - \bar{\mathbf{s}}_i^{(a,\text{im})}\|_1. \quad (4.15)
\end{aligned}$$

(4.14) and (4.15) provide the worst case bounds; that is, the image ambiguity may introduce at most the amount of $\|\bar{\mathbf{s}}_i - \bar{\mathbf{s}}_i^{(\text{im})}\|_1$ increase to the sparsest solution, and the amount of $\|\bar{\mathbf{s}}_i^{(a)} - \bar{\mathbf{s}}_i^{(a,\text{im})}\|_1$ decrease to the alternative solution. These changes should be involved in (4.12) and (4.13) to get a refined lower bound. Note that for the sparsest solution and any alternative solution, not all of the malicious anchors end up with image location estimates, and not all ℓ_1 norm changes achieve the worst case bound.

At the end of this section, it is time to incorporate measurement noise. Similar to the BP denoising in (4.3), the measurement noise can be taken into account via minimizing the ℓ_1 -regularized LS objective function for a single target

$$\min_{\mathbf{x}} f = \sum_{i=1}^{N_s} (d_{1,i} - \|\mathbf{s}_i + \Delta \mathbf{s}_i - \mathbf{t}_1\|_2)^2 + \lambda \|\Delta \mathbf{s}\|_1 \quad (4.16)$$

and the ℓ_1 -regularized LS objective function for cooperative targets

$$\min_{\mathbf{x}} f = \sum_{j=1}^2 \sum_{i=1}^{N_s} (d_{j,i} - \|\mathbf{s}_i + \Delta \mathbf{s}_i - \mathbf{t}_j\|_2)^2 + (d_c - \|\mathbf{t}_1 - \mathbf{t}_2\|_2)^2 + \lambda \|\Delta \mathbf{s}\|_1 \quad (4.17)$$

where λ is the regularization parameter whose value is related to the noise level. Note that the ℓ_1 norm regularization is only induced to $\Delta \mathbf{s}$, but not to targets \mathbf{t}_1 and \mathbf{t}_2 . By solving (4.16) and (4.17) respectively, secure target localization and malicious anchor identification can be obtained simultaneously, avoiding the exhaustive consistency

verification in [35, 40, 41].

4.5 The Projected Gradient Search Algorithm

In preceding sections, we explored the pairwise sparsity of the misplacement vector, formulated the target localization and misplacement identification as an ℓ_1 -regularized LS problem, and studied the pairwise sparsity upper bound and equivalence condition. In this section, we discuss the algorithm to solve the general ℓ_1 -regularized LS problems in the presence of misplacements and measurement noise. Here, we use the problem in (4.16) for the single target localization as an example to illustrate the proposed algorithm, which can be readily generalized to the cooperative target localization problem given in (4.17).

In the literature, several algorithms have been proposed to solve the linear ℓ_1 -regularized LS problems, e.g., [34, 19]. Our problem in (4.16) is more difficult, since it is nonlinear and nonconvex. According to [5], it is better to use simple approach in difficult problem because sophisticated methods typically rely on assumptions that are likely to be violated. We adopt the projected gradient search algorithm with constant stepsize to solve our problem in (4.16).

Since the ℓ_1 norm is nondifferentiable, we introduce two nonnegative vectors $\mathbf{u} = [\mathbf{u}_1^T, \dots, \mathbf{u}_{N_s}^T]^T$ and $\mathbf{v} = [\mathbf{v}_1^T, \dots, \mathbf{v}_{N_s}^T]^T$ to split $\Delta \mathbf{s}$ to its positive and negative parts as in [12, 19]. Particularly, let $\mathbf{u}_i = \max(0, \Delta \mathbf{s}_i)$ and $\mathbf{v}_i = \max(0, -\Delta \mathbf{s}_i)$, where $\max(\cdot, \cdot)$ is an element-wise operator. Then we can make the substitution

$$\Delta \mathbf{s} = \mathbf{u} - \mathbf{v}, \quad \mathbf{u} \geq 0, \quad \mathbf{v} \geq 0 \quad (4.18)$$

and rewrite the constrained ℓ_1 -regularized LS problem as

$$\begin{aligned} \min_{\mathbf{z}} f &= \sum_{i=1}^{N_s} (d_{1,i} - \|\mathbf{s}_i + \mathbf{u}_i - \mathbf{v}_i - \mathbf{t}_1\|_2)^2 + \lambda \mathbf{1}_{2N_s}^T \mathbf{u} + \lambda \mathbf{1}_{2N_s}^T \mathbf{v} \\ \text{s. t. } &\mathbf{u} \geq 0, \mathbf{v} \geq 0 \end{aligned}$$

where $\mathbf{z} = [\mathbf{u}^T, \mathbf{v}^T, \mathbf{t}_1^T]^T \in \mathbf{R}^{4N_s+2}$ is the entire unknown vector to estimate and $\mathbf{1}_{2N_s} = [1, \dots, 1]^T$ is the all-one vector of length $2N_s$.

In the simple projected gradient search algorithm with constant stepsize α , we search the unknown vector $\mathbf{z}^{(k)}$ along the negative gradient direction $-\nabla f(\mathbf{z}^{(k)})$ and project the first $4N_s$ components onto the nonnegative orthant. Specifically,

$$\begin{aligned} \mathbf{z}^{(k+1)} &= \mathbf{z}^{(k)} - \alpha \nabla f(\mathbf{z}^{(k)}), \text{ and} \\ \mathbf{z}^{(k+1)}(1 : 4N_s) &= \max(0, \mathbf{z}^{(k+1)}(1 : 4N_s)) . \end{aligned}$$

After the algorithm terminates at the K th iteration, we can obtain the estimates

$$\hat{\mathbf{t}}_1 = \mathbf{t}_1^{(K)}, \widehat{\Delta \mathbf{s}} = \mathbf{u}^{(K)} - \mathbf{v}^{(K)}$$

where $\mathbf{u}^{(K)} = \mathbf{z}^{(K)}(1 : 2N_s)$, $\mathbf{v}^{(K)} = \mathbf{z}^{(K)}(2N_s + 1 : 4N_s)$, and $\mathbf{t}_1^{(K)} = \mathbf{z}^{(K)}(4N_s + 1 : 4N_s + 2)$. Notice that the algorithm is able to simultaneously obtain the target location estimate $\hat{\mathbf{t}}_1$ and the misplacement estimate $\widehat{\Delta \mathbf{s}}$, which suggests that the proposed ℓ_1 -regularized LS approach is computationally efficient.

The complete projected gradient search algorithm with constant stepsize is summarized as follows.

Step 0 (initialization): choose the initial point $\mathbf{z}^{(0)}$, the ℓ_1 regularization parameter λ , the constant stepsize α , and the iteration stopping criterion; set $k = 0$.

Step 1 (projected gradient search): update $\mathbf{z}^{(k+1)}$ as $\mathbf{z}^{(k+1)} = \mathbf{z}^{(k)} - \alpha \nabla f(\mathbf{z}^{(k)})$,

and project $\mathbf{z}^{(k+1)}(1 : 4N_s) = \max(0, \mathbf{z}^{(k+1)}(1 : 4N_s))$ to the nonnegative orthant.

Step 2 (termination check): terminate with the solution $\mathbf{z}^{(k+1)}$ if the stopping criterion is satisfied; otherwise set $k \leftarrow k + 1$ and go to Step 1.

To solve the ℓ_1 -regularized LS problem using the above projected gradient search algorithm, one should carefully choose the parameters, including regularization parameter λ , constant stepsize α and the stopping criterion. These parameters can significantly affect the optimization performance.

Due to the presence of measurement noise, the algorithm may produce spurious nonzero values which are supposed to be zero. The selection of nonnegative λ can trade off the LS error for a higher degree of sparsity; as λ increases, it typically yields a sparser solution [19]. Judicious selection of λ tends to locate the nonzero pairs in \mathbf{z} and sacrifice true value estimates. One can remove those malicious anchors after successful identification and improve the target location estimation using only the honest anchors.

The constant stepsize α should be chosen carefully, as too small stepsizes result in slow convergence, and excessively large stepsizes may cause the iteration to become divergent. There are some other options in choosing the stepsize. For example, one can adaptively change the stepsize $\alpha^{(k)}$ at each iteration to assure that the objective function is descendent.

Selection of the stopping criterion is also crucial. An appropriate stopping criterion renders the solution reasonably close to the optimal point and avoids computational waste. According to [14], a good stopping criterion is $\|\mathbf{z}^{(k+1)} - \mathbf{z}^{(k)}\|_2 < \epsilon$, or its relative version $\|\mathbf{z}^{(k+1)} - \mathbf{z}^{(k)}\|_2 / \|\mathbf{z}^{(k)}\|_2 < \epsilon$.

Like all other nonconvex optimization problems, we need a good starting point near the minimizer. Otherwise the iteration might be trapped in a local minima other than the global minimum. For the target locations, we employ the linearized

LS method [52], assuming that all anchors are honest, to obtain the initial points. For the misplacement, it is reasonable to set the initial point to all zeros.

4.6 Simulations

In the simulations, we consider an $L \times L$ square target field, where $L = 6$ and the unit is 10 meters. The total number of anchors is $N_s = 8$. According to Proposition 4.1, the largest possible number of the identifiable malicious anchors via the ℓ_1 -regularized LS approach is $\lfloor (N_s - 2)/2 \rfloor = 3$. Therefore, we consider two attack cases, namely the two colluding malicious anchors case and the three colluding malicious anchors case. In the simulation figures, true locations of the first target \mathbf{t}_1 and the second target \mathbf{t}_2 are represented by red and green circles, respectively. For the i th anchor, the cross, square and diamond denote its true location $\bar{\mathbf{s}}_i$, claimed location \mathbf{s}_i and estimated location defined as $\widehat{\mathbf{s}}_i = \mathbf{s}_i + \widehat{\Delta}\mathbf{s}_i$, respectively. While black anchors are honest, the colored ones are malicious. Moreover, in the following simulations, we set the constant stepsize to $\alpha = 0.05$, use linearized LS estimates as target initial points, and use an all-zero misplacement initial point. For simplicity, fixed iteration number $K = 1000$ is adopted for low noise levels and $K = 2000$ for high noise levels.

We first test the validity of the proposed ℓ_1 -regularized LS formulation in the absence of measurement noise. Fig. 4.3 depicts the noiseless convergence path for the single target location estimation in the presence of two colluding malicious anchors. Both of the malicious anchors, in pink and blue respectively, cheat their locations by reporting their own y -coordinate four units larger than it actually is. This essentially misleads the target to be four units away in the y -direction from its true location. A small regularization parameter $\lambda = 0.03$ is set empirically in this case, which results in the best performance in terms of target location estimation and malicious anchor identification. First, it can be observed that the target can be located precisely. The

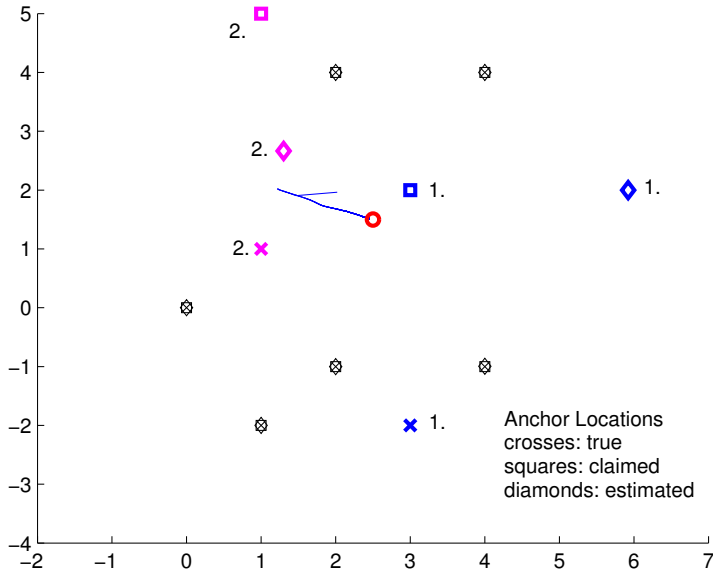


Figure 4.3: Noiseless convergence path for the single target location estimation in the presence of two malicious anchors.

convergence path is not the shortest path from the initial point to the true target location. This is a consequence of the nonconvexity of the objective function. Second, the malicious anchors are successfully identified, which is illustrated by zero misplacement estimates for all the honest anchors and nonzero misplacement estimates for the malicious anchors. Third, as expected, the nonzero misplacement estimates are incorrect, evidenced by the non-overlapped colored diamonds and crosses. These observations conform with our analysis on the malicious anchor identification capability and the misplacement estimation limitation for the single target case in Section 4.4.2.

Considering measurement noise, Table 4.1 summarizes the malicious anchor identification probability for the single target case in the presence of two colluding malicious anchors under various noise levels. The measurement noise is modeled as truncated zero-mean Gaussian noise with variance σ^2 as in [68]. The noise is truncated to

Table 4.1: Identification probability and target location mean absolute error, a single target, two colluding malicious anchors

Noise σ	λ	Identification probability	Mean target location error	Mean target location error (AR-MMSE)
0.3	1.0	98.8%	0.2315	0.2275
0.2	1.0	99.4%	0.1517	0.1519
0.1	0.8	99.9%	0.0757	0.0749
0.05	0.8	100%	0.0380	0.0376

have maximum absolute value of 2σ . For each noise level, we run 1000 realizations to obtain the convincing probability. The regularization parameter λ varies with noise level. Since its optimal value is data dependent, with a given λ , there may appear spurious small nonzero misplacement estimate which is supposed to be zero for some noise realization. We complement the estimation with a thresholding operation and choose the maximum noise 2σ as the threshold of the norm of individual misplacement estimate. It can be seen that, as the noise level increases, the identification probability decreases slightly. However, even when $\sigma = 0.3$ which means roughly $2\sigma/(L/2) = 20\%$ maximum distance measurement error, the probability is still very high. The 20% maximum distance measurement error level is also adopted by [40, 41, 35].

Table 4.1 also provides comparison of the mean absolute error for target location estimation between our ℓ_1 -regularized LS and the attack-resistant MMSE [40]. While they have comparable localization accuracy, our improvement is mainly in efficiency. To find a malicious anchor, the suboptimal attack-resistant MMSE needs to test consistency for every available anchor. In detail, when there are 2 malicious anchors

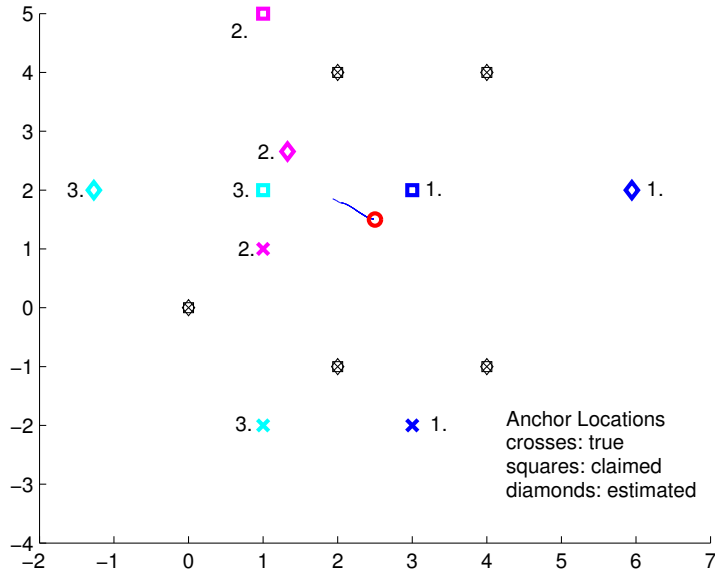


Figure 4.4: Noiseless convergence path for the single target location estimation in the presence of three malicious anchors.

out of 8, it implements the nonlinear MMSE optimization procedure 8 times to find the first inconsistent malicious anchor, and another 7 times to find the second one. This means that the complexity of this method is $\mathcal{O}(N_s^2)$. As the total number of anchors increases, the complexity grows rapidly. In contrast, our ℓ_1 -regularized LS approach is able to find all malicious anchors and locate the target with complexity $\mathcal{O}(N_s)$.

The noiseless convergence path for the single target in the presence of three colluding malicious anchors is illustrated in Fig. 4.4. Similar to the previous case, the target can be located with incorrect misplacement estimates. The corresponding comparisons between the proposed approach and the attack-resistant MMSE are provided in Table 4.2. They still have comparable target location estimation accuracy. Note that, as the number of malicious anchors increases, the attack-resistant MMSE needs a third round of consistency checks and therefore requires more computation,

Table 4.2: Identification probability and target location mean absolute error, a single target, three colluding malicious anchors

Noise σ	λ	Identification probability	Mean target location error	Mean target location error (AR-MMSE)
0.3	1.0	99.2%	0.2375	0.2356
0.2	1.0	100%	0.1534	0.1539
0.1	0.8	100%	0.0790	0.0798
0.05	0.8	100%	0.0404	0.0395

whereas the complexity of the proposed approach remains the same.

The misplacement estimates for the malicious anchors can be enhanced by allowing target cooperation. This is illustrated by the noiseless convergence paths for the two cooperative targets in the presence of two and three malicious anchors in Figs. 4.5 and 4.6, respectively. The regularization parameter $\lambda = 0.01$ is set in both figures. By executing the projected gradient algorithm once, we immediately obtain three outcomes: cooperative target location estimates, malicious anchor identification, and misplacement estimates. In Fig. 4.5, both malicious anchors are correctly located. In Fig. 4.6, the first two malicious anchors are successfully located, while the estimate of the third one turns out to be the image of its true location with respect to the straight line connecting two targets.

Comparisons between the single-target scenario and the two-target cooperative scenario, in terms of malicious anchor identification probability and target location estimation accuracy, are summarized in Tables 4.3 and 4.4. Obviously, in both two and three malicious anchor cases, incorporating target cooperation leads to higher identification probability and improved target location estimation accuracy compared

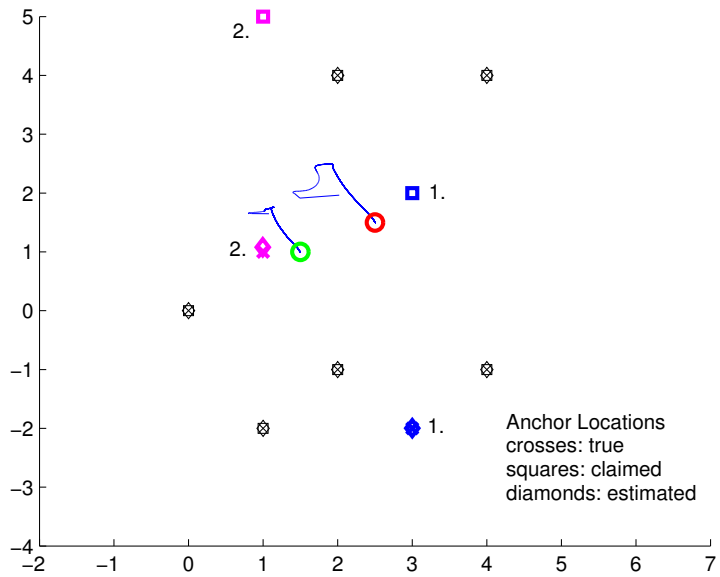


Figure 4.5: Noiseless convergence paths for two cooperative targets location estimation in the presence of two malicious anchors.

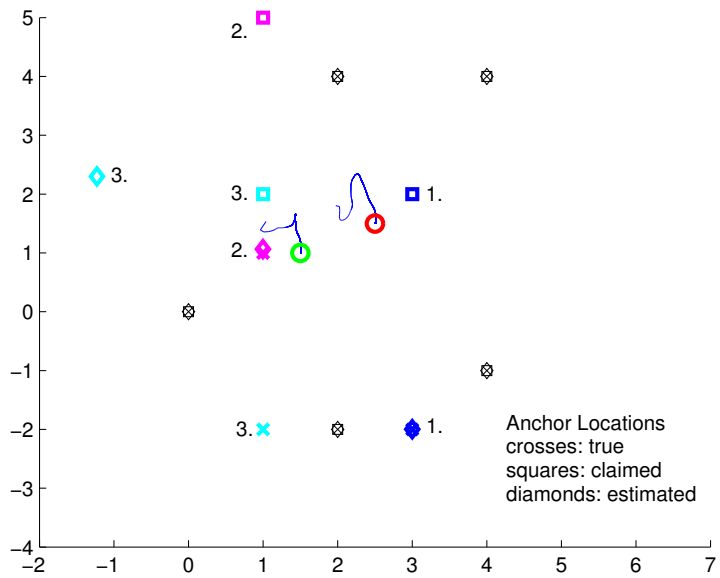


Figure 4.6: Noiseless convergence paths for two cooperative targets location estimation in the presence of three malicious anchors.

Table 4.3: Identification probability and target location mean absolute error, two colluding malicious anchors

Noise σ	λ	Identification probability (single-target)	Identification probability (cooperative)	Mean target location error (single-target)	Mean target location error (cooperative)
0.3	1.0	98.8%	99.8%	0.2315	0.2211/0.2172
0.2	1.0	99.4%	100%	0.1517	0.1476/0.1392
0.1	0.8	99.9%	100%	0.0757	0.0712/0.0685
0.05	0.8	100%	100%	0.0380	0.0359/0.0344

Table 4.4: Identification probability and target location mean absolute error, three colluding malicious anchors

Noise σ	λ	Identification probability (single-target)	Identification probability (cooperative)	Mean target location error (single-target)	Mean target location error (cooperative)
0.3	1.0	99.2%	99.7%	0.2375	0.2290/0.2275
0.2	1.0	100%	100%	0.1534	0.1487/0.1436
0.1	0.8	100%	100%	0.0790	0.0731/0.0729
0.05	0.8	100%	100%	0.0404	0.0363/0.0362

to the single target case. These results illustrate the advantages of target cooperation.

4.7 Conclusions

In this chapter, we explicitly incorporate anchors' misplacements into the distance measurement model and explore the pairwise sparse nature of the misplacements. We formulate the secure target localization issue as an ℓ_1 -regularized LS problem and establish the pairwise sparsity upper bound for the number of identifiable malicious anchors. A simple projected gradient search algorithm is proposed to solve this problem in WSNs. Unlike the existing methods, which rely on enumerative consistency verification, the proposed approach is able to identify malicious anchors and locate the targets simultaneously. Particularly, we consider two localization situations, namely, a single target scenario and two-target cooperative scenario. It is demonstrated that, with target cooperation, the capability of target location estimation is enhanced in terms of estimation accuracy, and the capability of malicious anchor identification is also improved in the sense of misplacement estimation. Simulations are provided to corroborate the results.

CHAPTER 5

CONCLUSIONS AND FUTURE WORKS

5.1 Conclusions

In this dissertation, we have considered two important issues in cooperative sensing, namely, cooperative target estimation and cooperative target localization. By utilizing the concept of “cooperation”, which incorporates communications and information exchange among multiple sensing devices, e.g. radar transceivers in radar systems, sensor nodes in wireless sensor networks, or mobile handsets in cellular systems, the sensing capability can achieve significant improvement compared to the conventional noncooperative mode in many aspects. For example, cooperative target estimation is inspired by the concept of MIMO in communications, where multiple transmit and/or receive antennas can increase the diversity to combat channel fading for enhanced transmission reliability and increase the degrees of freedom for improved data rate. On the other hand, cooperative target localization is able to dramatically increase localization performance in terms of both accuracy and coverage.

From the perspective of cooperative target estimation, we studied the optimum waveform designs to facilitate better target estimation in the presence of colored noise, and the robust joint waveform and estimator designs to address the *a priori* information uncertainties. Different from existing works, we considered a mixed MIMO radar setup for which the waveform optimization problem is meaningful, took into account the colored noise, incorporated the NMSE as a design criterion in addition to the MI

and MMSE, and derived joint robust designs for both the transmitter (waveforms) and the receiver (estimator) under various uncertainty models. The analytical and numerical results suggest that: i) the equivalence between the MI and MMSE criteria does not hold when the noise is colored; and ii) compared to MMSE criterion, the NMSE criterion seems to share more similarities with the MI. In particular, they lead to identical LFS in the robust designs under various uncertainty models, while the MMSE criterion always suggests otherwise. Additionally, we analyzed the sensitivity of the optimum waveform designs to the overestimation errors for all three criteria, at both the transmitter side (in terms of the waveform optimization solution) and the receiver side (in terms of the estimation NMSE performance). We derived the explicit formulae for the strength thresholds of the single error mode and made the performance variation comparison among the three criteria. The analysis shows that: i) all three criteria do not show significant performance deterioration; ii) the NMSE-based design is more sensitive to the overestimation error than the MI-based design around the error mode strength threshold; and iii) in the special white noise case, the MI- and MMSE-based optimum designs result in identical sensitivity level and both are less sensitive than the NMSE-based design.

From the perspective of cooperative target localization, we studied two phases of a localization process, i.e., the distance measurement phase and the location update phase. In the first phase, thanks to UWB signals' many desirable features including high delay resolution and obstacle penetration capabilities, we adopt UWB technology for TOA estimation, and then translate the TOA estimate into distance given light propagation speed. We developed a practical data-aided ML timing algorithm, and designed an optimum training sequence for the ML algorithm. This training sequence turned out to be identical to the one used in TDT. Based on this optimum sequence, the original ML algorithm can be simplified without affecting its optimality. We

proved that the resultant SML algorithm is equivalent to the TDT timing algorithm, demonstrating the optimality of the data-aided TDT in the ML sense. Extensive simulations have been performed to corroborate our theoretical analysis. In the second phase, we considered the challenging issue of target localization in the presence of malicious anchors in WSNs. We explicitly incorporated anchors' misplacements into distance measurement model and explored the pairwise sparse nature of the misplacements. We formulated the secure target localization issue as an ℓ_1 -regularized LS problem and established the sparsity upper bound for the number of identifiable malicious anchors. A simple projected gradient search algorithm was proposed to solve this problem in WSNs. Unlike the existing methods, which rely on enumerative consistency verification, the proposed approach is able to identify malicious anchors and locate the targets simultaneously. Particularly, we considered two localization situations, namely, a single target scenario and two-target cooperative scenario. It is demonstrated that, with target cooperation, the capability of target location estimation is enhanced in terms of estimation accuracy, and the capability of malicious anchor identification is also improved in the sense of misplacement estimation. Simulations are provided to corroborate the results.

5.2 Future Works

In Chapter 4, we proposed the novel ℓ_1 -regularized LS formulation to tackle the secure localization problem in WSNs. The solving algorithm of projected gradient search is relatively simple. We use this simple algorithm, with constant stepsize, empirically chosen regularization parameter and fixed iteration number, to illustrate that the problem formulation is valid and efficient. There is still a huge space to improve by developing new algorithms for this problem, as we can observe clearly

from the simulations that the identification and estimation performance heavily rely on the parameter selection, especially the regularization parameter λ . The method of intelligently choosing parameter values is a critical issue worth of further discussion.

Secondly, in this work we use linearized LS approach, assuming that all anchors are honest, to calculate initial points of targets' locations. Reference anchor selection in linearized LS is important. Inappropriate reference can result in large target location deviation even without malicious anchors. For this reason, we assume that there is at least one authenticated anchor and choose this one as reference. In real environment, however, one may not be able to acquire such information. Therefore, reference selection in the compromised environment is also a necessary and interesting task.

Another possible future extension includes developing algorithms applicable to large-scale network. As any localization method or secure localization method, it is not quite straightforward to extend the algorithm which works well for small-scale network to a larger one, because the network becomes more complicated, but the complexity requirement is still stringent.

LIST OF REFERENCES

- [1] “Part 15.4: Wireless medium access control (MAC) and physical layer (PHY) specifications for low-rate wireless personal area networks (WPANs), amendment 1: Add alternate PHYs,” Approved: Mar. 2007, IEEE-SA Standards Board.
- [2] G. S. Antonio, D. R. Fuhrmann, and F. C. Robey, “MIMO radar ambiguity functions,” *IEEE Journal of Selected Topics in Signal Processing*, vol. 1, no. 1, pp. 167–177, June 2007.
- [3] W. Bar and F. Dittrich, “Useful formula for moment computation of normal random variables with nonzero means,” *IEEE Trans. on Automatic Control*, vol. 16, no. 3, pp. 263–265, June 1971.
- [4] M. R. Bell, “Information theory and radar waveform design,” *IEEE Trans. on Information Theory*, vol. 39, no. 5, pp. 1578–1597, September 1993.
- [5] D. P. Bertsekas, *Nonlinear Programming*. Athena Scientific, Belmont, Massachusetts, 1995.
- [6] D. W. Bliss and K. W. Forsythe, “Multiple-input multiple-output (MIMO) radar and imaging: Degrees of freedom and resolution,” in *Proc. of Asilomar Conf. on Signals, Systems, and Computers*, vol. 1, 2003, pp. 54–59.
- [7] T. Budinger, “Biomonitoring with wireless communications,” *Annual Review on Biomedical Engineering*, vol. 5, no. 1, pp. 383–412, August 2003.
- [8] J. Caffery and G. Stuber, “Radio location in urban CDMA microcells,” in *Proceedings of IEEE International Symposium on Personal, Indoor Mobile Radio Communications*, Toronto, ON, Canada, September 1995, pp. 858–862.
- [9] E. J. Candes and T. Tao, “Decoding by linear programming,” *IEEE Trans. on Information Theory*, vol. 51, no. 12, pp. 4203–4215, December 2005.
- [10] C. Chen and P. P. Vaidyanathan, “MIMO radar space-time adaptive processing using prolate spheroidal wave functions,” *IEEE Trans. on Signal Processing*, vol. 56, no. 2, pp. 623–635, February 2008.
- [11] C. Y. Chen and P. P. Vaidyanathan, “Properties of the MIMO radar ambiguity function,” in *Proc. of Intl. Conf. on Acoustics, Speech, and Signal Processing*, April 2008, pp. 2309–2312.

- [12] S. S. Chen, D. L. Donoho, and M. A. Saunders, “Atomic decomposition by basis pursuit,” *SIAM Review*, vol. 43, no. 1, pp. 129–159, April 2001.
- [13] Y. Chen and N. C. Beaulieu, “CRLBs for NDA ML estimation of UWB channels,” *IEEE Communication Letters*, vol. 9, pp. 709–711, August 2005.
- [14] E. K. P. Chong and S. H. Zak, *An Introduction to Optimization (Second Edition)*. Wiley, 2001.
- [15] H. Cox, R. M. Zeskind, and M. M. Owen, “Robust adaptive beamforming,” *IEEE Trans. on Acoustics, Speech, and Signal Processing*, vol. ASSP-35, no. 10, pp. 1365–1376, October 1987.
- [16] D. Dardari and M. Z. Win, “Threshold-based time-of-arrival estimators in UWB dense multipath channels,” in *Proceedings of International Conference on Ultra-Wideband*, Waltham, MA, September 24-27,.
- [17] H. Deng, “Polyphase code design for orthogonal netted radar systems,” *IEEE Trans. on Signal Processing*, vol. 52, no. 11, pp. 3126–3135, November 2004.
- [18] D. L. Donoho and M. Elad, “Optimally sparse representation in general (nonorthogonal) dictionaries via ℓ^1 minimization,” in *Proc. Natl. Acad. Sci. USA*, March 2003, pp. 2197–2202.
- [19] M. A. T. Figueiredo, R. D. Nowak, and S. J. Wright, “Gradient projection for sparse reconstruction: Application to compressed sensing and other inverse problems,” *IEEE Journal of Selected Topics in Signal Processing*, vol. 1, no. 4, pp. 586–597, December 2007.
- [20] E. Fishler, A. Haimovich, R. Blum, D. Chizhik, L. Cimini, and R. Valenzuela, “MIMO radar: An idea whose time has come,” in *Proc. of the IEEE Radar Conference*, 2004, pp. 71–78.
- [21] E. Fishler, A. Haimovich, R. S. Blum, L. Cimini, D. Chizhik, and R. A. Valenzuela, “Spatial diversity in radar-models and detection performance,” *IEEE Trans. on Signal Processing*, vol. 54, no. 3, pp. 823–838, March 2006.
- [22] R. Fleming, C. Kushner, G. Roberts, and U. Nandiwada, “Rapid acquisition for Ultra-Wideband localizers,” in *Proc. of IEEE Conf. on Ultra-Wideband Systems and Technologies*, Baltimore, MD, May 20-23, 2002, pp. 245–250.
- [23] J. R. Foerster, “The performance of a direct-sequence spread Ultra Wideband system in the presence of multipath, narrowband interference, and multiuser interference,” in *Proc. of IEEE Conf. on Ultra-Wideband Systems and Technologies*, Baltimore, MD, May 20-23, 2002, pp. 87–92.

- [24] R. Fontana, E. Richley, and J. Barney, "Commercialization of an ultra wideband precision asset location system," in *Proceedings of IEEE International Conference on Ultra-Wideband*, November 2003, pp. 369–373.
- [25] D. R. Fuhrmann and G. S. Antonio, "Transmit beamforming for MIMO radar systems using signal cross-correlation," *IEEE Trans. on Aerospace and Electronic Systems*, vol. 44, no. 1, pp. 171–186, January 2008.
- [26] S. Gezici and H. V. Poor, "Position estimation via ultra-wide-band signals," in *Proceedings of IEEE*, vol. 97, no. 2, 2009, pp. 386–403.
- [27] S. Gezici, Z. Tian, G. B. Giannakis, H. Kobayashi, A. F. Molisch, H. V. Poor, and Z. Sahinoglu, "Localization via ultra-wideband radios: a look at positioning aspects for future sensor networks," *IEEE Signal Processing Magazine*, vol. 22, no. 4, pp. 70–84, July 2005.
- [28] I. Guvenc and Z. Sahinoglu, "Threshold-based TOA estimation for impulse radio UWB systems," in *Proceedings of International Conference on Ultra-Wideband*, Zurich, Switzerland, September 5-8,.
- [29] E. A. Homier and R. A. Scholtz, "Rapid acquisition of Ultra-Wideband signals in the dense multipath channel," in *Proc. of IEEE Conf. on Ultra-Wideband Systems and Technologies*, Baltimore, MD, May 20-23, 2002, pp. 105–110.
- [30] E. A. Jorswieck and H. Boche, "Transmission strategies for the MIMO MAC with MMSE receiver: Average MSE optimization and achievable individual MSE region," *IEEE Trans. on Signal Processing*, vol. 51, no. 11, pp. 2872–2881, November 2003.
- [31] S. A. Kassam and T. L. Lim, "Robust wiener filters," *Journal of The Franklin Institute*, vol. 304, no. 4/5, pp. 171–185, October/November 1977.
- [32] S. A. Kassam and H. V. Poor, "Robust techniques for signal processing: a survey," *Proceedings of the IEEE*, vol. 73, no. 3, pp. 433–481, March 1985.
- [33] S. M. Kay, *Fundamentals of Statistical Signal Processing: Estimation Theory*. Prentice-Hall, 1993.
- [34] S. J. Kim, K. Koh, M. Lustig, S. Boyd, and D. Gorinevsky, "An interior-point method for large-scale ℓ_1 -regularized least squares," *IEEE Journal on Selected Topics in Signal Processing*, vol. 1, no. 4, pp. 606–617, December 2007.
- [35] N. Kiyavash and F. Koushanfar, "Anti-collusion position estimation in wireless sensor networks," in *Proceedings of IEEE International Conference on Mobile Adhoc and Sensor Systems, 2007*, 2007, pp. 1–9.

- [36] H. Krim and M. Viberg, “Two decades of array signal processing research,” *IEEE Signal Processing Magazine*, vol. 13, no. 4, pp. 67–94, July 1996.
- [37] L. Lazos and R. Poovendran, “HiRLoc: high-resolution robust localization for wireless sensor networks,” *IEEE Journal on Selected Areas in Communications*, vol. 24, no. 2, pp. 233–246, February 2006.
- [38] J. Y. Lee and R. A. Scholtz, “Ranging in a dense multipath environment using an UWB radio link,” *IEEE Journal on Selected Areas in Communications*, vol. 20, no. 9, pp. 1677–1683, December 2002.
- [39] A. Leshem, O. Naparstek, and A. Nehorai, “Information theoretic adaptive radar waveform design for multiple extended targets,” *IEEE Journal on Selected Topics in Signal Processing*, vol. 1, no. 1, pp. 42–55, June 2007.
- [40] Z. Li, W. Trappe, Y. Zhang, and B. Nath, “Robust statistical methods for securing wireless localization in sensor networks,” in *Proceedings of Fourth International Symposium on Information Processing in Sensor Networks (IPSN’05)*, April 2005, pp. 91–98.
- [41] D. Liu, P. Ning, and W. Du, “Attack-resistant location estimation in sensor networks,” in *Proceedings of Fourth International Symposium on Information Processing in Sensor Networks (IPSN’05)*, April 2005, pp. 99–106.
- [42] Y. Liu, T. F. Wong, and W. W. Hager, “Training signal design for estimation of correlated MIMO channels with colored interference,” vol. 55, no. 4, pp. 1486–1497, April 2007.
- [43] V. Lottici, A. D’Andrea, and U. Mengali, “Channel estimation for Ultra-Wideband communications,” *IEEE Journal on Selected Areas in Communications*, vol. 20, no. 9, pp. 1638–1645, December 2002.
- [44] A. D. Maio and M. Lops, “Design principles of MIMO radar detectors,” *IEEE Trans. on Aerospace and Electronic Systems*, vol. 43, no. 3, pp. 886–898, July 2007.
- [45] A. Misra, G. Xue, and S. Bhardwaj, “Secure and robust localization in a wireless Ad Hoc environment,” *IEEE Trans. on Vehicular Technology*, vol. 58, no. 3, pp. 1480–1489, March 2009.
- [46] L. W. Nolte, S. C. Lee, and S. C. Liu, “On performance of array signal processing,” *IEEE Journal of Oceanic Engineering*, vol. OE-12, no. 1, pp. 148–154, January 1987.
- [47] N. Patwari, J. N. Ash, S. Kyperountas, A. O. Hero III, R. L. Moses, and N. S. Correal, “Locating the nodes: Cooperative localization in wireless sensor networks,” *IEEE Signal Processing Magazine*, vol. 22, no. 4, pp. 54–69, July 2005.

- [48] G. G. Raleigh and J. M. Cioffi, "Spatio-temporal coding for wireless communication," *IEEE Trans. on Communications*, vol. 46, pp. 357–366, 1998.
- [49] H. Sampath and A. Paulraj, "Joint transmit and receive optimization for high data rate wireless communications using multiple antennas," in *Proc. Asilomar Conf. Signals, Systems and Computers*, 1999.
- [50] H. Sampath, P. Stoica, and A. Paulraj, "Generalized linear precoder and decoder design for MIMO channels using the weighted MMSE criterion," *IEEE Trans. on Communications*, vol. 49, no. 12, pp. 2198–2206, December 2001.
- [51] A. Savvides, C. Hans, and M. Srivastava, "Dynamic fine-grained localization in ad-hoc networks of sensors," in *Proceedings of ACM MobiCom*, 2001, pp. 166–179.
- [52] A. H. Sayed, A. Tarighat, and N. Khajehnouri, "Network-based wireless location: challenges faced in developing techniques for accurate wireless location information," *IEEE Signal Processing Magazine*, vol. 22, no. 4, pp. 24–40, July 2005.
- [53] A. Scaglione, S. Barbarossa, and G. B. Giannakis, "Filterbank transceivers optimizing information rate in block transmissions over dispersive channels," *IEEE Trans. on Information Theory*, vol. 45, pp. 1019–1032, April 1999.
- [54] Z. Tian and G. B. Giannakis, "BER sensitivity to mis-timing in ultra-wideband communications, part i: Non-random channels," *IEEE Trans. on Signal Processing*, vol. 53, no. 4, pp. 1550–1560, April 2005.
- [55] H. L. V. Trees, *Detection, Estimation and Modulation Theory*. Wiley, New York, 1983.
- [56] —, *Optimum array processing*. Wiley-Interscience, New York, 2002.
- [57] U. Tureli, D. Kivanc, and H. Liu, "Experimental and analytical studies on a high-resolution OFDM carrier frequency offset estimator," *IEEE Trans. on Vehicular Tech.*, vol. 50, no. 2, pp. 629–643, March 2001.
- [58] M. Z. Win and R. A. Scholtz, "Impulse radio: how it works," *IEEE Communications Letters*, vol. 2, no. 2, pp. 36–38, February 1998.
- [59] —, "Ultra wide bandwidth time-hopping spread-spectrum impulse radio for wireless multiple access communications," *IEEE Trans. on Communications*, vol. 48, no. 4, pp. 679–691, April 2000.
- [60] H. Wymeersch, J. Lien, and M. Z. Win, "Cooperative localization in wireless networks," *Proceedings of the IEEE*, vol. 97, no. 2, pp. 427–450, February 2009.

- [61] H. Xu and L. Yang, "Timing with dirty templates for low-resolution digital UWB receivers," *IEEE Trans. on Wireless Communications*, vol. 7, no. 1, pp. 54–59, January 2008.
- [62] L. Yang and G. B. Giannakis, "Optimal pilot waveform assisted modulation for Ultra-Wideband communications," *IEEE Trans. on Wireless Communications*, vol. 3, no. 4, pp. 1236–1249, July 2004.
- [63] —, "Ultra-wideband communications: An idea whose time has come," *IEEE Signal Processing Magazine*, vol. 21, no. 6, pp. 26–54, November 2004.
- [64] —, "Timing Ultra-Wideband signals with dirty templates," *IEEE Trans. on Communications*, vol. 53, no. 11, pp. 1952–1963, November 2005.
- [65] Y. Yang and R. S. Blum, "MIMO radar waveform design based on mutual information and minimum mean-square error estimation," *IEEE Trans. on Aerospace and Electronic Systems*, vol. 43, no. 1, pp. 330–343, January 2007.
- [66] —, "Minimax robust MIMO radar waveform design," *IEEE Journal on Selected Areas in Communications*, vol. 1, no. 1, pp. 147–155, June 2007.
- [67] Y. Zeng, J. Cao, J. Hong, and L. Xie, "Secure localization and location verification in wireless sensor networks," in *Proceedings of IEEE International Conference on Mobile Adhoc and Sensor Systems*, Macau, November 2009.
- [68] S. Zhong, M. Jadliwala, S. Upadhyaya, and C. Qiao, "Towards a theory of robust localization against malicious beacon nodes," in *Proceedings of IEEE Infocom 2008*, 2008, pp. 2065–2073.